Interactions of Vegetation and Climate: Remote Observations, Earth System Models, and the Amazon Forest

Gregory R. Quetin

A dissertation
submitted in partial fulfillment of the
requirements for the degree of

Doctor of Philosophy

University of Washington

2017

Reading Committee:

Abigail L. S. Swann, Chair

Dennis L. Hartmann

Christopher S. Bretherton

Program Authorized to Offer Degree:
Atmospheric Sciences

University of Washington

Abstract

Interactions of Vegetation and Climate: Remote Observations, Earth System Models, and the Amazon Forest

Gregory R. Quetin

Chair of the Supervisory Committee:
Chair Abigail L. S. Swann
Atmospheric Sciences

The natural composition of terrestrial ecosystems can be shaped by climate to take advantage of local environmental conditions. Ecosystem functioning, e.g. interaction between photosynthesis and temperature, can also acclimate to different climatological states. The combination of these two factors thus determines ecological-climate interactions. The ecosystem functioning also plays a key role in predicting the carbon cycle, hydrological cycle, terrestrial surface energy balance, and the feedbacks in the climate system. Predicting the response of the Earth's biosphere to global warming requires the ability to mechanistically represent the processes controlling ecosystem functioning through photosynthesis, respiration, and water use. The physical environment in a place shapes the vegetation there, but vegetation also has the potential to shape the environment, e.g. increased photosynthesis and transpiration moisten the atmosphere. These two-way ecoclimate interactions create the potential for feedbacks between vegetation at the physical environment that depend on the vegetation and the climate of a place, and can change throughout the year.

In Chapter 1, we derive a global empirical map of the sensitivity of vegetation to climate using the response of satellite-observed greenness to interannual variations in temperature and precipitation. We infer mechanisms constraining ecosystem functioning by analyzing how the sensitivity of vegetation to climate varies across climate space. Our analysis yields

empirical evidence for multiple physical and biological mediators of the sensitivity of vegetation to climate at large spatial scales. In hot and wet locations, vegetation is greener in warmer years despite temperatures likely exceeding thermally optimum conditions. However, sunlight generally increases during warmer years, suggesting that the increased stress from higher atmospheric water demand is offset by higher rates of photosynthesis. The sensitivity of vegetation transitions in sign (greener when warmer or drier to greener when cooler or wetter) along an emergent line in climate space with a slope of about 59 mm/yr/°C, twice as steep as contours of aridity. The mismatch between these slopes is evidence at a global scale of the limitation of both water supply due to inefficiencies in plant access to rainfall, and plant physiological responses to atmospheric water demand. This empirical pattern can provide a functional constraint for process-based models, helping to improve predictions of the global-scale response of vegetation to a changing climate.

In Chapter 2, we use observations of vegetation interaction with the physical environment to identify where ecosystem functioning is well simulated in an ensemble of Earth system models. We leverage this data-model comparison to hypothesize which physiological mechanisms - photosynthetic efficiency, respiration, water supply, atmospheric water demand, and sunlight availability - dominate the ecosystem response in places with different climates. The models are generally successful in reproducing the broad sign and shape of ecosystem function across climate space except for simulating generally lower leaf area during warmer years in places with hot wet climates. In addition, simulated ecosystem interaction with temperature is generally larger and changes more rapidly across a gradient of temperature than is observed. We hypothesize that the amplified interaction and change are both due to a lack of adaptation and acclimation in simulations. This discrepancy with observations suggests that simulated responses of vegetation to global warming, and feedbacks between vegetation and climate, are too strong in the models. Finally, models and observations share an abrupt threshold between dry regions and wet regions where strong positive vegetation

response to precipitation falls to nearly zero in places receiving around 1000 mm/year.

In Chapter 3, we investigate how ecoclimate interactions change across seasons in the Amazon basin. We use observations of solar induced fluorescence from the Orbiting Carbon Observatory 2 (OCO2) to statistically analyze the sensitivity of fluorescence to synoptic variations in temperature and precipitation. In addition to studying the sensitivity of vegetation to climate across seasons, we use OCO2 measurements of total column water vapor (TCWV) and CO_2 concentration (XCO_2) to investigate the influence of the Amazon basin vegetation on the CO_2 concentration and water vapor of the atmosphere leaving the basin. Our analysis determines the seasonal importance of vegetation activity on the outflow of CO_2 from the Amazon basin, while providing evidence that transpiration is primarily driven by variations in temperature during the dry season, rather than photosynthesis. We establish a statistical relationship between fluorescence (as a proxy for vegetation photosynthesis), temperature, and precipitation, as well as the difference between the outflow of atmospheric water vapor from the inflow water vapor, basin fluorescence, temperature, and precipitation.

TABLE OF CONTENTS

LIST OF FIGURES

GLOSSARY

AVHRR: Advanced Very High Resolution Radiometers

CERES-SYN: Clouds and the Earth's Radiant Energy System Synoptic

CMIP5: Coupled Model Intercomparison Project 5

DJF: The season December January February

EVI: Enhanced Vegetation Index

GLDAS: Global Land Data Assimilation System

GPCP: Global Precipitation Climatology Project

GPM: Global Precipitation Measurement

GPP: Gross Primary Productivity

JJA: The season June July August

LAI: Leaf Area Index

MAM: The season March April May

MODIS: Moderate-Resolution Imaging Spectroradiometer

NDVI: Normalized Difference Vegetation Index

OCO2: Orbiting Carbon Observatory 2

PET: Potential Evapotranspiration

SON: The season September October November

SRB 3.1: Surface Radiation Budget 3.1

TCWV: Total Column Water Vapor

TRMM: Tropical Rainfall Measuring Mission

XCO2: Atmospheric CO2 concentration

ACKNOWLEDGMENTS

The author wishes to express sincere appreciation to the Ecoclimate Lab: Marysa Lague, Elizabeth Garcia, Marlies Kovenock, and Jennifer Hsiao for their constant support and scientific feedback. To my advisor Abigail Swann for being a supportive mentor and colleague. The work was partially conducted while GRQ was supported by the University of Washington Program on Climate Change Fellowship. We would also like to acknowledge the Keck Institute for Space Studies at the California Institute of Technology who hosted GRQ during part of this work. Finally, the authors wishes to acknowledge the numerous people involved in collecting data, and building and running Earth system models that were used in this work.

DEDICATION

To my parents, Robin Ross and Langdon Quetin, for sharing their passion for science and the natural world.

Chapter 1

INTRODUCTION

Some form of vegetation covers nearly the whole land area of Earth, only held in check by freezing temperatures and scorching deserts. In every climate on Earth, vegetation is attempting to solve the same general problem - how to turn sunlight into useful sugars through photosynthesis. The climate in every location presents a different challenge that shapes the type and success of vegetation in an ecosystem; some places are warm but lack water, while others have so much water there are frequent clouds blotting out the sun. In return, vegetation shapes both local and global climate through the water cycle, carbon cycle and the surface energy budget [Friedlingstein et al., 2006, Schlesinger and Jasechko, 2014, Jasechko et al., 2013, Ghimire et al., 2014]. Changes in how much carbon vegetation absorbs, or how much water vegetation transpires into the atmosphere has the potential to alter the course of global warming and the regional climates of where humans live [Friedlingstein et al., 2013]. In addition, changes in the distribution of vegetation can alter the general circulation of the atmosphere across the whole planet [Swann et al., 2012]. The key role of vegetation in these broader climate processes, and the potential for feedbacks between changes in climate and changes in vegetation motivate my study of how different climates shape the function of vegetation, and what that tells us about climate constraints on vegetation.

In this thesis I use global observations and Earth system models to analyze the interaction of vegetation and interannual variations in climate and help answer the question: how does the climate in a place constrain vegetation?

1.1 Distribution of Vegetation Across Earth

Where plants exist on the Earth, what kind of plants, and why the plants are there, have been longstanding questions. Early efforts to explain the distribution of plants across Earth date back to 1900 (original mapping of climates by Koppen) and 1961 (update by Geiger) with the combined work commonly referred to as Koppen-Geiger climate classification [Kottek et al., 2006]. These early works took a biogeography approach, observing where particular types of ecosystems existed (for example tropical forest), and then using mean annual climate variables such as temperature and precipitation along with variations on the mean annual such as minimum and maximum season temperatures, the seasonality of precipitation. These works have been recently been updated with recent datasets [Peel et al., 2007b]. Underlying these climate classifications is the assumption that the climate of a place controls what plants and ecosystems exist there. This assumption is also present in Whittaker's notional climate space defined by mean annual temperature and precipitation [Whittaker, 1970] (Figure 1.1). We expand on this previous work that only observes the static ecosystems that result in a certain type of climate by observing ecosystem functioning: the interaction of vegetation with the physical environment. The systematic change of ecosystem functioning across a climate space that drives changes in that functioning provides insights into the processes and tradeoffs through which the distribution of plants on Earth is shaped. In addition, analyzing the ecosystem functioning, albeit a simple view of functioning, allows us to provide hypotheses on the biological and physical mechanisms that lead to the observed ecosystem functioning.

1.2 Water, Energy, Carbon, and Physiology

Plants connect water, energy, and carbon at the Earth's surface through photosynthesis. During photosynthesis, sunlight is absorbed in chlorophyll to combine CO_2 and H20 into sugars for use in plant growth. However, only a small fraction of the water is used in the photosynthetic chemical reaction itself. Instead, most of the water is lost from the leaves

through stomata, small valves in the leaf used to absorb CO_2 from the atmosphere. In this way, plants exchange water for CO_2. Vegetation can reduce how much water is lost by closing their stomata, but only by also reducing the amount of CO_2 absorbed. Our understanding of how vegetation controls stomata is captured in the quasi-empirical Ball-Berry equation for stomatal conductance (Equation 1.1):

$$\frac{1}{r_s} = g\frac{A}{c_s}\frac{e_s}{e_i}P_{atm} + g_o \tag{1.1}$$

Here r_s is stomatal resistance, A is photosynthesis (a function of soil moisture, shortwave radiation and temperature), c_s is the concentration of CO_2, $\frac{e_s}{e_i}$ is relative humidity, P_{atm} is the pressure of the atmosphere, and g and go are plant specific constants. Our primary take-away from this equation is that stomatal resistance is proportional to the inverse of photosynthesis, while the scaling of the proportionality is controlled by the concentration of CO_2 in the atmosphere, and the relative humidity of the atmosphere. Put more simply, photosynthesis requires energy (sunlight) and CO_2. For a given amount of sunlight, the stomata have to be opened enough to match the flux of CO_2 into the leaf with the demand provided by the sunlight. However, CO_2 is exchanged for H20, with the rate of exchange set by the difference between concentration of CO_2 in the leaf and in the atmosphere, and the difference of concentration of H20 in the leaf and in the atmosphere (represented in the Ball-Berry equation by the relative humidity). The stomata controls the level of transpiration as well, and thus the latent heat cooling of leaves, however there is no evidence that stomata dynamics are frequently driven for the purpose of thermoregulation of the vegetation canopy.

It is often assumed that the airspace in the interior of the leaf is fully saturated with water vapor at the temperature of the leaf. This assumption is used to define a vapor pressure deficit between the leaf's full saturation and the partial saturation of the atmosphere at the temperature of the atmosphere. The vapor pressure deficit for a fixed relative humidity increases as an exponential function of increased temperature following the Clausius-Clapeyron relationship, which makes the exchange rate of CO_2 to H_2O (often referred to as the water

use efficiency) worse at warmer temperatures. In addition to the warmer mean temperature leading to greater vapor pressure deficits, variations in temperature and greater mean temperatures will also cause increasingly larger variations in vapor pressure deficit. This sensitivity of vapor pressure deficit to variations in temperature is important to consider when interpreting interannual variations in temperature, particularly in the warm parts of the Earth. The combination of these factors serve to link water lost from plants through transpration with the temperature and saturation state of the atmosphere, carbon uptake, and shortwave radiation at the surface.

Water, sunlight and temperature are also linked at Earth's surface through the balance of energy at the surface. The portion of shortwave radiation absorbed at the surface is offset either by emissions of net longwave radiation from a hot surface into a cooler atmosphere, turbulent fluxes of hot air away from the surface (sensible heat), or turbulent fluxes of water vapor that have evaporated from the surface (latent heat). In addition, when vegetation is present the water lost in exchange for CO_2 also serves to cool the leaves, and air, through evaporation. The surface energy balance serves to set the temperature of the surface (or leaf, or canopy), as surface temperatures increase until net longwave radiation, sensible heat, and latent heat bring the surface into energy equilibrium.

In addition to the effects of temperature on vapor pressure deficit, temperature is important in driving the chemical reaction rates in photosynthesis and respiration (release of carbon through use of the photosynthetically created sugar to maintain the plant or microbial decomposition). Up to a point, higher temperatures mean faster rates of photosynthesis, along with modest increases of respiration, for an overall gain in sugars for the plant. The photosynthesis of a plant has been observed to have a concave performance curve with temperature (Figure 1.2). At low temperatures, chemical reactions are sluggish and performance is low. Performance increases with increasing temperature up to an optimal temperature. before decreasing rapidly for temperatures higher than optimum. At a plant scale, recent research has suggested that a temperature performance curve combines two mechanisms. The first, chemical reaction rates due to temperature, primarily operates at the cold end of

the curve, and then flattens off at warmer temperatures. Second, at extreme temperatures, greater than 40 °C, performance drops precipitously as proteins used in photosynthesis begin to denature. However, in the mid-range, it has been proposed that the performance of photosynthesis is primarily driven by the exchange of CO_2 for water, and thus by the increasing vapor pressure deficit.

In describing our observations of the interaction of vegetation with the interannual variation of temperature and precipitation we often invoke the concept of a performance curve. For both variations in temperature and precipitation we consider the relationship between increased temperature or precipitation and the performance of the vegetation as sampling the slope of the performance curve for that place. For example, if in a hot dry place increases in temperature lead to decreases in plant greenness this would suggest that the plant is beyond the optimum temperature, and on the downside of the performance curve where increased temperatures hurt performance. In 2003, Nemani used simple models of what these performance curves looked like to create a map of climate constraints on vegetation [Nemani et al., 2003] (Figure 1.3). Their modeled performance curves predicted that temperature was the primary climate limitation in the high latitudes, while sunlight was the primary limitation in the tropics due to high cloudiness (and plenty of precipitation and warm temperatures). Our work seeks sample these performance curves using observations to create a more detailed and empirical map of climate constraints on vegetation.

1.3 Tools for Investigating Ecosystem Function

In our research we use a mix of observations, reanalysis, and model output. When using observations, our philosophy was to keep as close to an observed product as possible, rather than numerous products derived through models. Though we accept that nearly every observation contains some model, even if just a model of the instrument used to make an observation, we expect that the fewer layers of models containing how people think a part of the world should work, allows for greater ability to be surprised and informed by observations. We used satellite remote sensing observations in order to analyze a broad array of

climates (global scale observations in chapter 1 and chapter 2), or regions of the world that are not well monitored (the Amazon in chapter 3). Where the satellite observations were not available, primarily for two-meter temperature, we used reanalysis, the fusion of data and atmospheric models, as the best estimate of observations. Finally, we compared observations to a set of Earth system models with active carbon cycles from the archive of the Coupled Model Intercomparison Project 5 (CMIP5) to identify where ecosystem function is well modeled in comparison to observations. These Earth system models contain the community's best guess for the interactions between global vegetation and climate variations. In addition, our work helps to target specific areas for improving the ecosystem function in these models which will improve their projections of future climates and carbon cycles.

1.3.1 Satellite Observations

The remote sensing of vegetation depends on observing how different wavelengths of light interact with the vegetation canopy. In our work we use three different products that remotely measure different aspects of vegetation. The first product is the Normalized Difference Vegetation Index (NDVI). NDVI is a simple ratio of visible light and a near infrared band of light. This ratio of the wavelengths of light measures the 'greenness' of the vegetation and has a long time record dating back to when the instrument was first launched in 1979. We generally interpret increases in greenness as increased vegetation performance - more leaves, which took more carbon to make, which have the potential to produce more photosynthesis.

A related product to NDVI is Leaf Area Index (LAI), or the ratio of leaf area to the area of the ground beneath them. LAI is estimated in a number of ways, the most advanced is to run a radiative canopy model to recreate the reflectance observed from satellite across a number of wavelengths. Where the radiative canopy model cannot converge, a statistical relationship between NDVI and LAI is used to fill in. Finally, a neural network was used to extend the dataset of LAI back in time before the MODIS satellite. In general, LAI appears to be very similar to NDVI. We chose to use LAI in chapter 2 in order to match outputs available from the Earth system models in the CMIP5 archive.

In Chapter 3 we utilize the newly available fluorescence observations from the Orbiting Carbon Observatory 2 (OCO2). Fluorescence is emitted during photosynthesis and is thought to relate more directly to photosynthesis than other remote observations of vegetation such as NDVI.

Finally, we use a number of satellite observations for measurement of precipitation, total column water vapor, concentration of CO_2, surface pressure, and shortwave radiation. For precipitation we use both the Global Precipitation Climatology Project (GPCP), which includes information from Tropical Rainfall Measuring Mission (TRMM), and the relatively new Global Precipitation Measurement (GPM). In Chapter 3, we use OCO2 for total column water vapor, the concentration of CO_2, and surface pressure in addition to fluorescence. Finally, in Chapter 1, we use the Clouds and the Earth's Radiant Energy System Synoptic (CERES-SYN) dataset to construct an aridity index as the ratio of precipitation to the amount of energy available to evaporate water. The length of time record for overlap of observation of climate and vegetation was often limited by both, with high resolution precipitation data limiting how far back in time we had data for, and observations of vegetation limiting more recent time periods to when there was up to date vegetation data available.

1.3.2 Reanalysis

We use the ERA-Interim reanalysis dataset. These are models of the global general circulation that incorporate observations to improve the fidelity of the model with the real world. In concept, it is similar to interpolation between observations, but rather than with statistics; a dynamic model that includes all the appropriate physical processes is used to estimate where no observations are available. We used the ERA-Interim dataset due to a positive reputation in the community and ease of access to the data. From ERA-Interim we primarily used two-meter temperature, and surface winds.

1.3.3 Earth system models

Earth system models combine the dynamics of the atmosphere and ocean, with the dynamics and biology of a terrestrial biosphere in a numerical simulation of the whole Earth. Though these models do not include all the process relevant to vegetation interaction with climate, they are some of our best models of the whole system. Indeed, by comparing the ecosystem functioning in the Earth system models with observations, we are able to propose both which processes might be missing or poorly represented in models, as well as improve our understanding of what processes are at work in the real world.

1.4 Summary of Chapters

In this thesis we set out to quantify how the different climates on Earth change how vegetation interacts with its physical environment. In the first chapter we use the interannual variability of temperature and precipitation, along with greenness measured from space, as a natural experiment to investigate in which climates vegetation gets greener when it is warmer (or wetter). We quantify the climate boundaries between four distinct regions of the Earth's climate apparent in the sensitivity of vegetation to interannual variation in temperature and precipitation. From cold to warm the regions are: (1) a cold region where vegetation is greener during warmer years and drier years, (2) a transition region where vegetation is greener during warmer years and wetter years, (3) a dry hot region where vegetation is greener during cooler and wetter years, and finally (4) a hot wet region where there is a more mixed response, but vegetation is generally greener when warmer, and weakly greener when drier. The transition region separates the cold region from the hot dry region, as well as the hot dry region from the hot wet region. The boundaries of the transition region define two lines proportional to mean annual temperature and precipitation, illuminating a consistent trade-off in the function of vegetation in the amount of water available to the vegetation, and how hot a place is.

In the second chapter we investigate how vegetation interacts with its physical environ-

ment in Earth system models with active carbon cycles and prognostic leaf area. Earth system models represent our best attempt at reproducing the global vegetation, global climate, and their interactions through modeled processes. We compare the vegetation interactions with interannual temperature and precipitation across Earth system models, along with a derived observational product of leaf area. All comparisons are conducted in a climate space defined by mean annual temperature and precipitation. We find that the sensitivity of vegetation is generally stronger in the models, and that in changes with the mean annual temperature of a place too strongly. We hypothesize that the lack of an adaptation or acclimation mechanism in the models is consistent with the over sensitivity, and too strong change with mean annual temperature. In addition, we highlight that most models produce vegetation in the tropics that is greener when it is cooler in the tropics in contrast to observed vegetation that is generally greener when warmer in the tropics. We suspect that this discrepancy is due to different concomitant changes in clouds with variations in temperature in the models compared to observations. We note, that the strength and sign of the vegetation interaction with climate in these regions is generally very uncertain in both Earth system models and observations.

Finally, in chapter three we investigate the interaction of vegetation with climate in the Amazon basin using the recently launched Orbiting Carbon Observatory 2 to observe fluorescence, light emitted during photosynthesis, as a strong proxy for the photosynthetic rate. In addition, we provide evidence for strong influence of the vegetation in the Amazon basin on the carbon dioxide leaving the Amazon basin. We determine that strong positive sensitivity of vegetation to precipitation (more photosynthesis after rain events) in the transition from the wet season through the dry season, coupled with strong positive influence of photosynthesis on the carbon dioxide in the atmosphere in the same season creates the potential for a feedback between Amazon basin vegetation and the atmosphere over the basin and downwind of it. In this feedback, precipitation draws water vapor from the atmosphere, and stimulates the absorption of more carbon dioxide from the atmosphere through photosynthesis. This means that active and healthy vegetation in the Amazon basin is important for

to removing carbon dioxide from the atmosphere. It also demonstrates the importance of precipitation to this region, even though there is a large amount of rainfall overall.

1.5 Future Work

The broad question I am trying to answer is how does climate constrain life on Earth? In my thesis I have analyzed interactions of vegetation and climate variations as a window into how particular climates may be constraining vegetation through limits of water, temperature, and light.

In the near term, I would like to find different observational data to apply to vegetation interactions with climate variation. In particular, I think there is a lot of potential to use observations of leaf temperature, either from satellite or from infrared cameras based on towers, to more directly observe the energy balance occurring in the vegetation canopy. Leaf temperature connects with many of the biological and physical processes discussed in this thesis. Direct sunlight provides a large amount of energy to plants, while only a small fraction can be used for photosynthesis, the rest of the energy has to be dissipated in a way that doesn't damage the biological machinery of the plant (can't get too hot, or too cold), or waste the limited water resources of the plant. How this energy can be dissipated is also strongly tied to the stability and dryness of the atmosphere interacting with the vegetation. Observations of leaf temperature through with infrared cameras, particular at very high resolution (leaf scale?) would allow for a detailed view of how the energy balance in a canopy evolves over a day, or across seasons.

As a small aside, one challenge I came across in my thesis work was being able to find concomitant observations of both biological data (e.g. leaf area) and physical data (e.g. temperature). Though not a future question on its own, in pursuit of my scientific goals I would like to promote combining biological and physical observations more often so that interactions between the two can be more completely diagnosed. The separation of data is a problem for modeling efforts, as well as observational campaigns, as model intercomparison projects often leave out archiving some variables critical to diagnosing interactions (e.g. leaf

temperature). There are valid technical and scientific challenges in combining biological and physical data, but I hope to encourage the value of it from the perspective of diagnosing interactions between vegetation and climate.

In the long term, I intend to develop an idealized, and purely physical representation of vegetation on Earth. Still focused on the question of 'how does climate constrain life on Earth?' except replacing 'life' with 'work' in the thermodynamic sense, so 'how does the climate constrain work on the surface of the Earth?' One part of this puzzle, is that plants appear to capture only a negligible fraction of the sunlight reaching the surface through photosynthesis compared with what is possible thermodynamically []. In addition, the question is partially motivated by discussions about whether or not the increasing concentration of CO_2 in the atmosphere, and subsequent global warming is 'bad for life on Earth'. Certainly the dire consequences for the ecosystems and human civilizations adapted to the last 10,000 years of relatively stable climate are clear. However, so much of our knowledge about plants and ecosystems are drawn from empirical studies, and quasi empirical theories developed in our relatively stable climate to date, that it is hard to use them as a starting point to determine whether a wildly different climate than today's climate would be better or worse. However, by reducing the problem to one of thermodynamics, where plants are replaced by energy conversion cycle (e.g. a Carnot Cycle) it should be possible to build up some ultimate constraints on what climates would be able to sustain the work that necessarily underpins life.

Though highly idealized, reducing life to a (relatively) simple thermodynamic problem allows for a more concrete analysis of climates that we have limited or not empirical observations for. Beyond likely future Earth climates under global warming scenarios, this idealized framework would be applicable to questions surrounding paleoclimate, and the potential for life on extrasolar planets. Finally, once we have constructed the simplest model possible to explain the thermodynamic limits of work in a particular climate, we can experiment by adding processes back to the model. For example, how does adding the requirement to absorb CO_2 from the atmosphere, in exchange for water alter the ability to generate work in

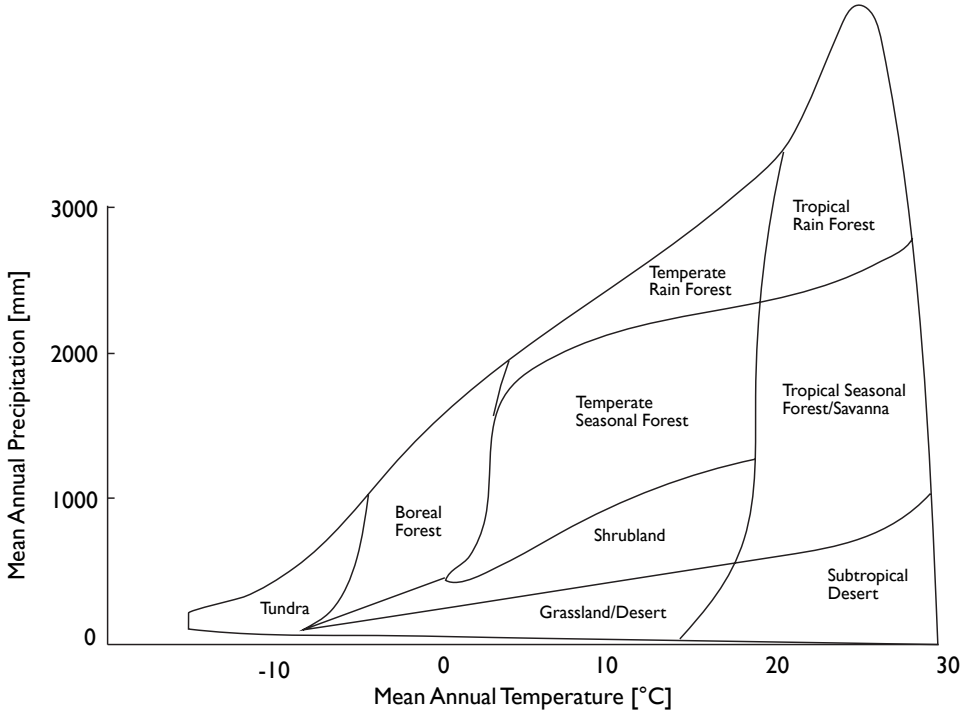

Figure 1.1: Reproduction of the Whittaker plot, using mean annual temperature and precipitation to define biomes.

a particular climate? How might this necessary exchange, change how the work generated at the surface of an atmosphere change that atmosphere?

Finally, combining this idealized approach, with the previously discussed observational, or empirical approach, I can help determine what parts of the climate constraints we observe are driven primarily by constraints from physics, and which are more tightly tied to unique limitations of the biological systems.

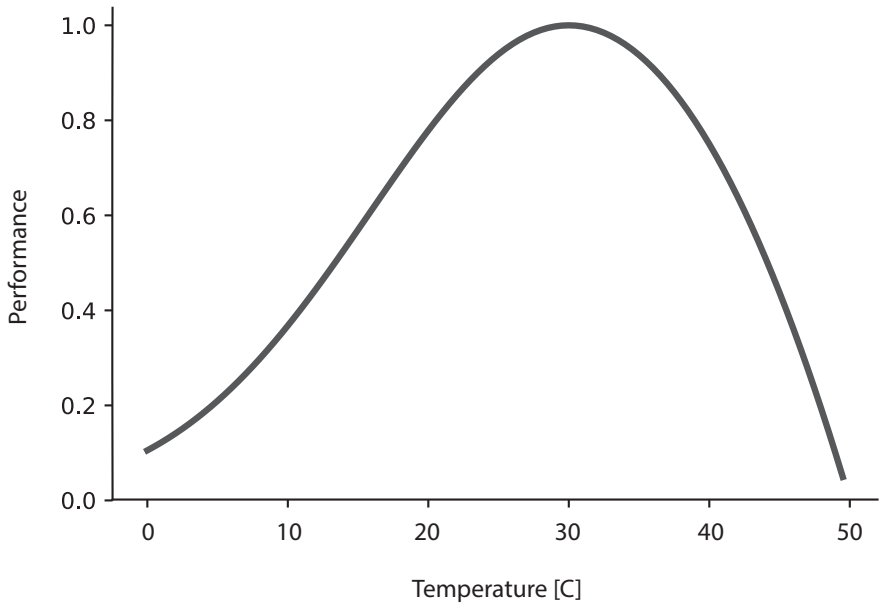

Figure 1.2: Simplified example of a general concave performance curve with temperature

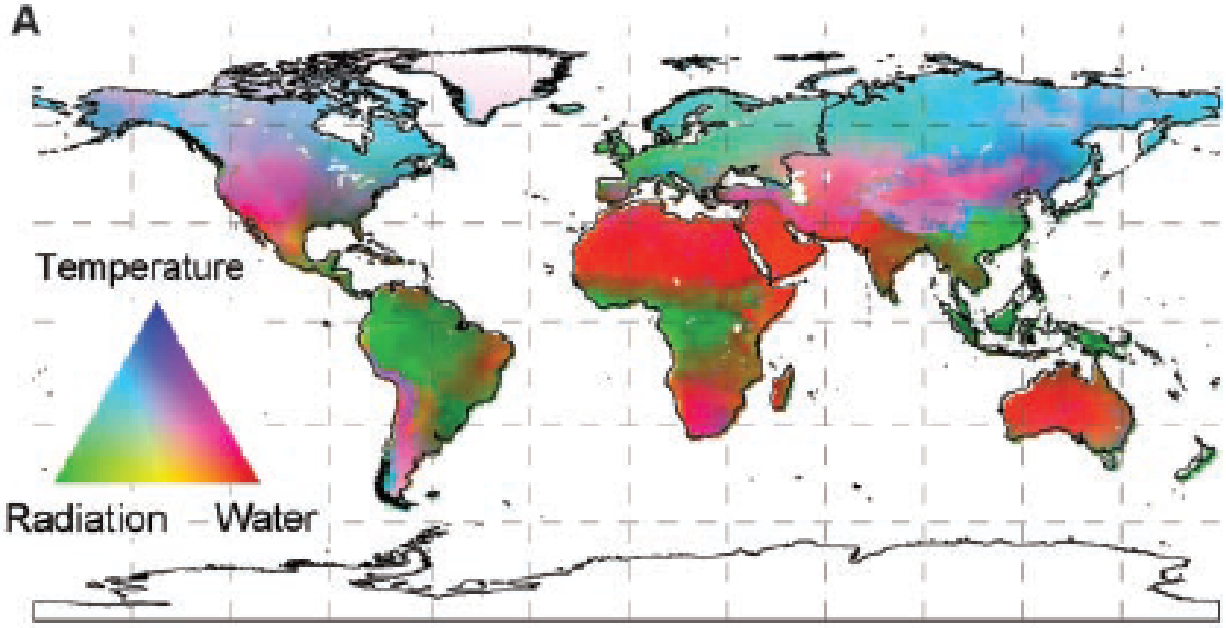

Figure 1.3: Reproduction of the Nemani 2003 plot showing how different climate resources limit vegetation.

Chapter 2

EMPIRICALLY DERIVED SENSITIVITY OF VEGETATION TO CLIMATE ACROSS GLOBAL GRADIENTS OF TEMPERATURE AND PRECIPITATION

2.1 Abstract

The natural composition of terrestrial ecosystems can be shaped by climate to take advantage of local environmental conditions. Ecosystem functioning, e.g. interaction between photosynthesis and temperature, can also acclimate to different climatological states. The combination of these two factors thus determines ecological-climate interactions. A global empirical map of the sensitivity of vegetation to climate is derived using the response of satellite-observed greenness to interannual variations in temperature and precipitation. Mechanisms constraining ecosystem functioning are inferred by analyzing how the sensitivity of vegetation to climate varies across climate space. Analysis yields empirical evidence for multiple physical and biological mediators of the sensitivity of vegetation to climate at large spatial scales.

In hot and wet locations, vegetation is greener in warmer years despite temperatures likely exceeding thermally optimum conditions. However, sunlight generally increases during warmer years, suggesting that the increased stress from higher atmospheric water demand is offset by higher rates of photosynthesis. The sensitivity of vegetation transitions in sign (greener when warmer or drier to greener when cooler or wetter) along an emergent line in climate space with a slope of about 59 mm/yr/°C, twice as steep as contours of aridity. The mismatch between these slopes is evidence at a global scale of the limitation of both water supply due to inefficiencies in plant access to rainfall, and plant physiological responses to atmospheric water demand. This empirical pattern can provide a functional constraint for

process-based models, helping to improve predictions of the global-scale response of vegetation to a changing climate.

2.2 Introduction

The structure and productivity of vegetation across the world is coupled to climate through environmental variables such as light, water, and temperature. Structure and productivity of vegetation are also controls on the terrestrial carbon cycle [Friedlingstein et al., 2006], the terrestrial hydrological cycle [Schlesinger and Jasechko, 2014, Jasechko et al., 2013], and the surface energy budget [Ghimire et al., 2014]. To understand how global vegetation will be altered under climate change, we must understand how ecological-climate interaction operates at large spatial scales, and thus across global climate gradients. In our work we have chosen mean annual temperature and precipitation as climate gradients with historical context in studying vegetation (e.g. Whittaker 1979), related to environmental resources important for vegetation function and with strong variation across the globe [Whittaker, 1962, Kottek et al., 2006, Metzger et al., 2013]. There is evidence that an important part of the way that vegetation and climate interact is through changes in phenology [Richardson et al., 2010, 2013]. Though our analysis aggregates across the seasonal cycle of vegetation and climate, we still observe these changes as interannual variation in the annual means (e.g. a longer growing season is a greener year).

Three common approaches have previously been used to study how vegetation is controlled by the climate of a region and to predict how it will change in the future: a) climate-biome classification - treating the current boundaries between biomes as determined by climate [Peel et al., 2007a, Kottek et al., 2006, Smith et al., 2002, Metzger et al., 2013], b) simplified models of climate constraint - based on physiological constraints on net primary productivity [Churkina and Running, 1998, Nemani et al., 2003, Jolly et al., 2005, Running et al., 2004], and c) global process-based models - extending plant or plot scale research to global scales through process based numerical global models [Oleson et al., 2010, Boisvenue and Running, 2006, Levis, 2010].

Our analysis serves to bridge the static geographical observational (a) and modeling approaches (b, c) by empirically quantifying the sensitivity of vegetation to interannual variations in environmental variables across the globe. By analyzing theses sensitivities across climate space we can diagnose how ecosystem function varies across annual climate and hypothesize mechanisms that could explain the observed pattern. We define ecosystem function here as the integrated environmental modulation of both plant-scale physiological (photosynthesis, respiration, transpiration, hydraulic stress) and population-scale ecological (demography, disturbance, competition) processes measured at a coarse spatial scale (100 km x 100 km). We do not discriminate grid points based on plant type or human influence. Differences in the growth cycle of vegetation that extend into the interannual variations of the vegetation are treated as additional error in our analysis. Our study captures broad patterns of ecosystem functioning across the global range of two environmental conditions (mean annual temperature and precipitation) and allows us to identify major climate constraints on remotely sensed vegetation.

The effect of climate on vegetation is evident from observations of how vegetation is distributed across the globe, and is explicit in efforts to classify biomes and the use of climate envelopes to predict the movement of biomes due to climate change [Koven, 2013, Rubel and Kottek, 2010]. However, the way that ecosystem function varies across climate, rather than just vegetation distribution, has not been empirically investigated at a global scale. In this study we combine the concept from climate classification that climate shapes vegetation with our calculation of the interannual sensitivity of vegetation to climate from remotely sensed vegetation and observations and reanalysis of climate data. This allows us to identify emergent functional constraints measured at the scales and resolutions required to make global predictions about vegetation. Analyzing the sensitivity of vegetation across climate space expands on other work and enables us to find the underlying pattern of ecosystem function across global climate gradients [Seddon et al., 2016, Wu et al., 2015]. Here our concept of binning across climate space is similar to the common practice in climate science of calculating the zonal mean of a variable, with latitude replaced with temperature and

precipitation (See Methods) (Figure 2.1, Figure 2.3A and 2.3B).

2.3 Methods

2.3.1 Empirical Sensitivity of Vegetation to Climate

We create an empirical estimate of the sensitivity of vegetation to climate at global scales by combining the satellite record of the Normalized Difference Vegetation Index (NDVI) with globally gridded estimates of temperature and precipitation. NDVI represents the longest global time series available to study vegetation response at a scale commensurate with global carbon cycling and ecological-climate feedbacks [Pinzon and Tucker, 2014]. NDVI has frequently been used to study temporal trends in vegetated land cover, e.g. [Chen et al., 2014], and has been correlated with environmental variables across biomes and regions to demonstrate the connection between the physical environment and surface greenness [Wu et al., 2015, Zhou et al., 2003, 2001, Goward et al., 1991, Asner et al., 2000, Xu et al., 2014, Myneni et al., 2002]. Though a simple metric of vegetation, observations of NDVI have the longest continuous global time series and relates strongly to leaf area, fraction of absorbed photosynthetically available radiation, plant fluorescence, gross primary productivity, and more advanced vegetation indices [Myneni et al., 2002, Frankenberg et al., 2011, Guanter et al., 2012, Glenn et al., 2008, Huete et al., 2002]. As the time series of MODIS Enhanced Vegetation Index (less saturation in dense vegetation) and targeted measurements of Solar Induced Fluorescence (a remote observation thought to be proportional to GPP) concurrent with climate observations grow longer we hope to be able to further test many of the hypotheses presented in this paper [Huete et al., 2002, Frankenberg et al., 2014, 2013, 2011, Guanter et al., 2012]. In addition to remote sensing, individual flux tower locations can make more direct measurements of carbon and water fluxes [Baldocchi, 2014]. However, global products derived from these site-level observations (e.g. [Jung et al., 2011, Beer et al., 2010, Xiao et al., 2011]) also depend heavily on similar satellite observations.

Here we use the globally observed NDVI as a direct observation of greenness to create a

metric of ecological-climate interaction. Our analysis uses a multilinear least squares regression between the interannual percentage anomalies in NDVI ($\%\Delta_{NDVI}$) and the interannual time series of temperature (T) in °C and precipitation (P) in mm/year to determine the sensitivity of greenness to climate at each vegetated grid point of the globe (Matlab function regress.m)(Equation 2.1).

$$\%\Delta_{NDVI} = T\beta_{TEMP} + P\beta_{PRECIP} + \beta_0 \tag{2.1}$$

We interpret the resulting β_{TEMP} and β_{PRECIP} for each grid point as the sensitivity of vegetation to interannual variation of climate. The β terms are expressed as a percent change in the mean NDVI from 1982 - 2012, with units of %NDVI/°C and %NDVI/mm respectively. Due to the assumed linear relationship between climate and vegetation implicit in a multilinear regression the coefficients β_{TEMP} and β_{PRECIP} can be interpreted as linearized metrics of ecosystem function. Ecosystem function is not necessarily linear in time or space, but at the limit of the interannual variation and the extent of each bin a linear fit is a useful approximation. In addition, we note that observations of greenness relate most directly to processes and structure of the vegetation canopy. A positive β shows positive sensitivity of vegetation to climate (i.e. greener in a warmer or wetter year) while a negative β shows negative sensitivity of vegetation to climate (i.e. greener in a cooler or drier year).

We chose a simple linear model with two predictors in order to learn about ecosystem-climate interactions from the variation of a metric that reflects ecosystem-climate interactions across climate space. Rather than attempt to create the best linear model for NDVI at each pixel on the map, our regression model serves to linearize the effect of both temperature and precipitation consistently across the globe, and simplify interpretation of the results.

Collinearity between the predictor variables of the linear regression (temperature and precipitation) is present at various levels across the globe. However, levels of correlation were not found to exceed commonly cited thresholds that would damage a linear regression

at most grid points, and experiments that excluded high correlation values (>0.6) did not impact the results of the analysis (See Appendix A section d).

To examine the aggregated structure of β_{TEMP} and β_{PRECIP} across climate space we assign each geospatial point to a bin dictated by its climatological mean annual temperature and precipitation (Figure 2.1, Figure 2.2). The pattern of aggregated β_{TEMP} and β_{PRECIP} across climate contains information about climate and ecological-climate interactions allowing us to hypothesize what physiological mechanisms are responsible for how climate shapes each ecosystem. For example, β_{TEMP} is likely influenced by interannual variations in photosynthetic performance due to chemical rates [Berry and Bjorkman, 1980], the water demand of the atmosphere [Day, 2000], and the increased costs of respiration at higher temperatures [Sprugel et al., 1995]. Alternatively, β_{PRECIP} will be influenced by a range of factors depending on the climatology of a region - from interannual variations in snowpack, water supply driven hydrologic stress, and light limitation from thick cloud cover during relatively high rainfall years. Based on the sign of β_{TEMP} and β_{PRECIP} we quantify where transitions occur between different ecological-climate interactions, suggesting how the growing season, the balance between the water demand of the atmosphere, water supply from precipitation, and the effects of clouds on solar radiation can each play a role in determining the ecosystem function in different climates. We expect ecosystem function to be determined by a myriad of time scales, so that processes that operate at a sub-annual scale but offset other processes will be less visible in our analysis. This is a possible explanation for the number of bins in the hot wet climates with high uncertainty, where less seasonality provides less structure for leaf drop and flushing. We note that both the analysis of the patterns of weak β_{PRECIP} and the uncertainty in both β_{TEMP} and β_{PRECIP} suggest that there could be offsetting or less coherent processes operating in these climates. Future investigation into the seasonal structure of β may help differentiate processes in areas of uncertainty.

2.3.2 Uncertainty

To quantify the uncertainty in the aggregate bins of β_{TEMP} and β_{PRECIP} we use a Monte Carlo technique on both the regression and the binning process, randomly choosing half the points (i.e. half the years for regression, and half the points in a bin for averaging) and running the calculation 10,000 different times. This creates a regression robust to outliers and characterizes the uncertainty for β in time and climate space (Figure 2.4). Our approach is similar to the concept of bootstrapping a distribution for uncertainty determination [Efron, 1979]. Additionally, we completed our analysis with alternative datasets and found that the results are robust to the choice of dataset for both climate, using the CRU TS3.21 gridded dataset (precipitation and temperature, [Jones and Harris, 2013]) and NDVI, using the MODIS NDVI product [Solano et al., 2010]. We do see some differences between results using alternate datasets, primarily while using the shorter MODIS NDVI dataset. The analysis performed with MODIS NDVI has a generally stronger β, and shows some change in sign in the warmer end of the transition zone for β_{TEMP}. The differences are partly due to the different time period covered by MODIS NDVI, the overall pattern is qualitatively similar across different time periods, environmental data and NDVI, differences are discussed further in Appendix A (Figure A1).

2.3.3 Environmental Data

We perform the analysis on the 16 year time series (1997 - 2012) of 1°x 1°latitude-longitude resolution observations where complete years of global observations of NDVI from NDVI3g [Pinzon and Tucker, 2014], near-surface air temperature from the two-meter ERA-Interim Reanalysis [Dee et al., 2011], and precipitation from the Global Precipitation Climatology Project (GPCP) [Adler et al., 2003] are concurrently available. We used the monthly surface temperature estimates from the two-meter ERA-Interim Reanalysis to represent the environmental temperature experienced by vegetation [Dee et al., 2011]. We calculated a monthly precipitation dataset by summing daily precipitation from the Global Precipitation

Climatology Project (GPCP) 1°x 1°latitude-longitude resolution global dataset [Adler et al., 2003]. The GPCP dataset is a combination of satellite and gauge data interpolated across the globe available at 1°x 1°degree from 1996 to 2012, with data for a complete year starting in 1997. Gridded data sets were interpolated to a common spatial grid with the Matlab function interp2.m.

To calculate the regression of shortwave radiation and temperature we use shortwave downward surface radiation from the Surface Radiation Budget 3.1 (SRB 3.1) a 1°x 1°latitude-longitude monthly dataset (Figure 2.7) [Zhang et al., 2013]. To create a radiatively based PET estimate we use surface net downward shortwave radiation from CERES-SYN from 2001 - 2012 [Smith et al., 2011](Appendix A, Equation A.1)(Figure A2B). Additional inter-annual environmental data for temperature, precipitation and PET from CRU TS3.21 was used to ascertain the robustness of the analysis to choice of environmental data [Jones and Harris, 2013]. Additional datasets of PET from MODIS and Global Land Data Assimilation System (GLDAS) were compared to ascertain the certainty of the P/PET estimate (Figure A2A) [Mu et al., 2007, Feng and Fu, 2013].

2.3.4 Remotely Sensed Vegetation

We chose Normalized Difference Vegetation Index (NDVI) as an observation of vegetation because of its global coverage and the availability of relatively long time-series. The NDVI 3g time series is an improved global NDVI dataset from the Advanced Very High Resolution Radiometers (AVHRR) [Pinzon and Tucker, 2014]. The dataset has a 1/12°latitude-longitude resolution and global coverage of 15-day global maximum composites. Processing the datasets into maximum composites reduces the effects from clouds and the satellite viewing angle [Holben, 1986]. To create a common time step we created monthly maximum composites from the NDVI 15-day composites before calculating an annual mean time series from 1983 - 2012. We interpolated the data to 1°by 1°spatial resolution prior to analysis, and shorten the NDVI time series to 1997 - 2012 to match the spatial scale and temporal

range of the environmental data.

In this study we will interpret NDVI as a proxy for the surface greenness and chloroplast density and use it to calculate the interannual variation of vegetation. NDVI is calculated by normalizing the difference between the visible channel and near-infrared channel from the AVHRR instruments by the sum of the channels. Vegetation absorbs strongly in the visible band, distinguishing it from soils and other non-vegetated surfaces. Though not directly used here, NDVI also relates to leaf area index and fraction of absorbed photosynthetically active radiation [Myneni et al., 2002], thus we consider the signal from NDVI as primarily related to the leaves of vegetation and their potential to fix sunlight into sugars. We assume here that the greening of an ecosystem relative to the climatological mean signals that it is advantageous for the plants to deploy more chloroplasts in an attempt to fix more carbon. On an annual basis, we use an increase in greenness as a metric for a positive sensitivity of vegetation to climate that correlates with increased net primary production [Myneni et al., 1995].

The launch of satellites with instruments that measure additional spectral bands has allowed for the creation of new vegetation indices and remote observations of vegetation. For example, observations from the Moderate-Resolution Imaging Spectroradiometer (launched in 1999) are used to generate an improved NDVI product with less interference from water vapor as well as the Enhanced Vegetation Index (EVI) that uses a blue measurement channel to reduce the effects of aerosols [Solano et al., 2010]. In general, both NDVI and EVI from MODIS have been shown to have larger seasonal amplitudes than NDVI from AVHRR, and EVI in particular does not saturate over high biomass areas as much as NDVI has been shown to [Huete et al., 2002]. There is also the exciting new development of solar induced fluorescence as a more direct observation of the photosynthetic activity, and thus gross primary productivity (GPP) [Frankenberg et al., 2014]. Though NDVI has been shown to relate to GPP, it is not completely proportional and can show markedly different relationships between different vegetation types [Frankenberg et al., 2011, Guanter et al., 2012]. Exploration of the measurement of solar induced fluorescence are just getting under-

way using observations from Greenhouse Gases Observing Satellite (GOSAT) and Orbiting Carbon Observatory-2 (OCO2), and do not yet have long enough time series to investigate the interannual ecological-climate interactions.

2.3.5 Standardization

We chose to standardize the NDVI time series in order to show the magnitude of the interannual change compared to the average NDVI of the pixel (Equation 2.2).

$$\%\Delta_{NDVI} = \frac{(NDVI - \overline{NDVI})}{\overline{NDVI}} \tag{2.2}$$

Where $\%\Delta_{NDVI}$ is the interannual percent change of NDVI, NDVI is the full time series (1983 - 2012) and $\overline{NDVI}$ is the average of the full time series (1983 - 2012). We chose not to alter the predictor variables of Temperature and Precipitation so that our analysis produced a metric that is consistent across the globe (%/°C or %/mm), rather than being standardized by a local effect (e.g. by environmental mean or interannual standard deviation).

2.3.6 Removing Non-Vegetated Terrestrial Grid Points

Our analysis considers only vegetated terrestrial grid points by removing ocean and non-vegetated land grid points (Figure 2.1). We removed ocean grid points using the water mask included in the NDVI 3g data files. We determined a grid point to have a non-vegetated year when the three months with maximum NDVI values either had a minimum monthly value less than 0.1, or the mean of the three months that was less than 0.3, as adapted from Zhou et al. [Zhou et al., 2001] (Figure 2.1). If a pixel was non-vegetated in any of the 30 years between 1983 and 2012 it was removed from further analysis. This filtering results in the removal of 3,726 points of the possible 14,693 land points (25%) and can be visualized in Figure 2.2. Defining vegetated points in this way is likely removes some points that are vegetated at some point during the time series. For example, removing points with vegetation recovering from bare ground (e.g. afforestation) or where vegetation has been

removed to bare ground (e.g. deforestation, fire). Removing non-vegetated grid points with this threshold also removes particularly low $\overline{NDVI}$. This removes the danger of dividing by zero in the standardization and creating falsely high sensitivity with no real ecological significance.

2.4 Results and Discussion

2.4.1 Broad Pattern of β_{TEMP} and β_{PRECIP}

Aggregated β_{TEMP} and β_{PRECIP} vary systematically across global climate gradients (Figure 2.3A and 2.3B). Large values of β highlight areas where ecosystem greenness generally responds strongly, and predictably, to interannual changes in the climate (temperature or precipitation in this study), without being limited by other resources required for greenness. The pattern of β_{TEMP} and β_{PRECIP} bin-aggregated in the climate space of mean annual temperature and mean annual precipitation explains a large portion of the pixel by pixel global variation of β_{TEMP} (26%) and β_{PRECIP} (37%) (Figure 2.3A and 2.3B). Considering the diversity of factors influencing the sensitivity of vegetation greeness to climate, the substantial amount of variance explained by the annual climate of temperature and precipitation suggest mean annual temperature and mean annual precipitation are strong controls on ecosystem function. The systematic variations of ecosystem functioning across mean annual temperature and precipitation supports why these climate variables have traditionally been included in biogeographic explanations of biomes. The remaining unexplained variance in β_{TEMP} and β_{PRECIP} may be due to other climate variables (e.g. solar radiation, or the climate seasonality), local controls (such as soil structure, or successional history), unidentified stochastic processes (such as storm damage, or multi-year effects of fire), strong gradients not represented by the coarse aggregation, or measurement noise.

We observe inflections between positive and negative β_{TEMP} and β_{PRECIP} extending as lines across a large range of average climates (Figure 2.3A and 2.3B). The linearity of the inflection lines suggest that ecosystem performance near $\beta = 0$ is determined by the pro-

portional amount of average precipitation relative to the average temperature of a location. It is notable that both of the inflection lines (β_{TEMP} or $\beta_{PRECIP} = 0$) are approximately parallel (slope of 62.5 to 59 mm/year/°C), as they highlight different aspects of ecosystem functioning, but offset by 7.9 °C (mean annual temperature intercept of 1.1 °C for β_{TEMP} and -6.8 °C for β_{PRECIP}) (Figure 2.3A and 2.3B). Near the inflection line, the ecosystem performance is dependent on both the average temperature and precipitation of a region. Thus there is equivalence between temperature and precipitation such that the performance cost of moving to a 1.7 °C warmer climate region can be offset by an additional 100 mm/year of rainfall.

We hypothesize that the proportional relationship between T and P is operating through the water balance of the vegetation. The evidence for the relation of the proportionality of T and P to water balance comes from three arguments: dependence of atmospheric water demand being a function of temperature, the presence of the proportionality across multiple datasets (see Appendix A) and the presence of the mechanism in previous work on plant hydraulics [McDowell, 2011, Grier and Running, 1977]. As temperature increases, the temperature driven increase in atmospheric demand for water increases potential evapotranspiration (PET), causing hydrologic stress. Hydrologic stress can then be offset for plants if more water is supplied through precipitation. Other aspects of the environment that we do not account for have the potential to exacerbate the annual imbalance (seasonality of water demand and supply leading to run-off) and soil water storage (helping balance offset of supply and demand) and matric water potential of soils (resisting vegetation in meeting the atmospheric demand) [Borchert, 1994]. With these additional mechanisms in consideration it is notable that though the proportional relationship between T and P spans a large range of climates, it is only observed as a proportional in a relatively narrow transition zone. A similarly sloped line between the max correlation of temperature and precipitation with gross primary productivity derived from flux towers is evident (but not discussed) in a paper from Jung et al. (2011) Figure 8 panel 'c' and 'f' [Jung et al., 2011]. Physiological experiments also provide evidence of temperature influencing plants through atmospheric water

demand. When the direct effects of temperature increases on vegetation are isolated from the temperature driven increase in vapor pressure deficit, the vapor pressure effects are large relative to the direct temperature effects at warmer temperatures [Day, 2000]. From this we expect increases in atmospheric water demand, in the form of vapor pressure deficit, to be the dominant constraint on vegetation in places with relatively warm temperatures (above 16 °C).

These observations of proportionality between temperature and precipitation also qualitatively agree with arguments that aridity (precipitation divided by potential evapotranspiration, P/PET) is a critical climate variable in shaping ecosystems (e.g. [Budyko, 1961, Lugo et al., 1999]). However, though contours of P/PET plotted across mean annual temperature and precipitation share the sign of the inflection contours, they have a slope (≈30 mm/year/°C) that is consistently half that of the inflection lines that we observe (Figure 2.3A and 2.3B, and Figure 2.5A). This consistent line of transition and mismatch with P/PET is evidence that vegetation either has access to a consistent fraction of precipitation, less than the total precipitation, across a wide range of climates or that vegetation is more sensitive to changes in potential evapotranspiration than can be explained by P/PET. The consistency of the tradeoff between temperature and precipitation for both β_{PRECIP} and β_{TEMP} suggests a fundamental relationship between plant physiology and climate. The broad climate range (-5 °C to 28 °C and mean annual precipitation of 200 mm/year to 2000 mm/year) across which the lines of inflection extend, suggest that there is a strong ability for ecosystems to adapt to their climate and account for the negative effects of increased PET (driven by temperature) with increases in net photosynthesis due to increased temperature [Berry and Bjorkman, 1980]. We find that the lower slope of P/PET isopleths compared to those of β_{TEMP} and β_{PRECIP} is robust across multiple datasets of potential evapotranspiration, though the magnitudes of the pixel by pixel P/PET values are uncertain due to a wide spread between datasets on the values of PET (See Methods and Figure A2A).

In the following sections we further discuss hypotheses for the mechanisms governing the climate-vegetation interactions consistent with the observed pattern of β_{TEMP}, β_{PRECIP},

particularly in regards to the combination of the their signs. We discuss regions where length of the growing season length, water, and solar insolation limits greenness.

2.4.2 Growing season limited: Temperature and snow cover

Vegetation is greener during both warmer and drier years in the coldest, driest vegetated areas of the globe, as well as places with annual mean temperatures up to relatively warm values of 15 °C where precipitation is also high (1500 mm/year) (Figure 2.5A). Places with these climates are primarily spatially located at high latitudes, and experience a large seasonality in temperature and sunlight. These climate conditions lead to a growing season duration constrained by low temperatures and late snow cover melt [Takala et al., 2011] (Figure 2.3C and 2.3D, and Figure 2.5B). We hypothesize that the main driver of variability on annual greenness is the duration of the growing season. Thus, we expect to see this mechanism acting mainly in the months at either end of the growing season rather than during months of peak greenness. In addition, these months are favored by atmospheric patterns of blocking and ENSO variation that might suggest that the climate in these months is also critical to setting the length of the growing season [Lejens and kland, 1983]. Indeed, the months with the most variance in NDVI in cold (< -5 °C) Northern Hemisphere locations, are June (beginning of growing season) and September (end of growing season) (Figure 2.6). In places with a mean annual temperature below -5 °C there is very limited variance of NDVI during winter (November to April), including places with mean annual temperatures below -10 °C where the variance drops to zero in winter (Figure 2.6). Months with proportionally more variance in NDVI will most strongly influence the interannual NDVI variance. Therefore, for these very cold regions (< -5 °C) the shoulder months of the growing season primarily determine whether a year is greener or browner.

We hypothesize that the mechanism limiting vegetation greenness in these areas characterized by cold temperatures with both positive β_{TEMP} and negative β_{PRECIP} is a combination of temperature and snow; years with warmer average temperatures or drier years with less snow correspond to greener years. Warmer temperatures and an earlier snowmelt are

likely to correspond to more days during which conditions are favorable for growth. This mechanism is consistent with the hypothesis that the effects of the interannual variation in temperature and precipitation occur primarily in the shoulder months. In warmer climates the variance of NDVI becomes less concentrated in the shoulder months, and in places with an average temperature above 5 °C, the variance is more evenly spread across all months (Figure 2.6).

2.4.3 Water limited: hot and dry

Nearly all of the negative values of β_{TEMP} (greener in cooler years) occur in places with mean annual temperatures above 15 °C and precipitation less than 1000 mm/year (Figure 2.5A). The relatively large positive values of β_{PRECIP} suggest that greenness in drier years is driven by hydrologic stress from limited water supply. The combination of general greening during either cooler or wetter years shows that hydrologic stress is driven by both the supply of water and the atmospheric demand for water as discussed above.

Locations falling in the hot dry region are primarily clustered along the edges of non-vegetated deserts of the North American Southwest, the Sahel, South Africa, and Australia as well as Northeast Brazil and the rain shadow of the Chilean Coastal Range (Figure 2.3C and Figure 2.5D). Non-vegetated points in deserts have been explicitly eliminated from this analysis, but plants living in these places are presumably limited by water availability as well. Due to the extensive spatial extent of the hot dry region and deserts we hypothesize that low precipitation is the most common limitation on global vegetation. In climate regions with 0.2 to 0.5 P/PET, β_{TEMP} and β_{PRECIP} both weaken rapidly as the increased water supply relieves the hydrologic stress from the temperature-driven increase in atmospheric water demand (Figure 2.3A and 2.3B). As the climate becomes wetter, the signs of both β_{TEMP} and β_{PRECIP} change, becoming positive (greener when warmer) and negative (greener when drier) respectively. The certainty of β_{PRECIP} becomes limited in the hottest, wettests regions of the globe, while β_{TEMP} has stronger certainty (Figure 2.4).

2.4.4 Energy limited: interaction of clouds and sunlight

Areas with positive β_{TEMP} and negative β_{PRECIP} occur where rainfall is above 2000 mm/year and temperatures are above 20 °C, these areas include most of the Amazon basin and the Maritime Continent (Figure 2.5). To be generally greener during warmer years at these high temperatures, we hypothesize that plants must offset high respiration costs associated with warmer years with even larger increases in productivity (Figure 2.3A). To complicate matters, net photosynthesis measured experimentally at the plant scale shows a decrease at high temperatures, with a limit commonly seen around 30 °C, and this holds true even for those plant species adapted to high temperatures (optimum at 46 °C) [Berry and Bjorkman, 1980, Day, 2000].

One pathway that could explain generally increased greenness in warm years for these locations is for light limitation on photosynthesis to be relieved by additional insolation. Along a gradient of increasing P/PET, β_{TEMP} begins strongly negative (browner when warmer) at low P/PET but increases rapidly as P/PET increases in this relatively arid climate region ($<$ about 0.5) (Figure 2.7). β_{TEMP} transitions to positive values between P/PET values of 0.5 and 0.8, and then is generally positive along with a positive β_{PRECIP} above 0.8. Budyko hypothesized that a transition in the surface balance of water demand and water supply occurs from water limited evaporation conditions (more potential evapotranspriation than water available) to energy limited (more water available that insolation) as water availability increases. The shape of these observations is indicative of β responding to regions of water limitation ($<$0.5) and energy limitation ($>$0.8).

We also note that interannual increases in temperature are concomitant with greater increases in insolation in wetter climate regions (sunnier, less clouds when warmer)(Figure 2.7). We observe approximately a factor of two change in the concomitant change of insolation with temperature ($W/m^2/°C$) between P/PET values of 0.2 and 0.8 (Figure 2.7). Increased water availability changes the relationship of sunlight and temperature, diverting more of the surface energy flux through latent heat rather than sensible heat. Thus, the same increase

in photosynthetically active radiation does not lead to the same increase in air temperature as in drier regions. With a positive β_{TEMP} and negative β_{PRECIP} it is apparent that any hydrologic stress from the increase in water demand by a warmer atmosphere is being offset by ample water supply and concurrent increases in solar radiation, allowing for enhanced vegetation greenness during warmer years even at these high temperatures (Figure 2.7).

The response of ecosystem function in hot, wet regions to a changing climate may have strong implications for the terrestrial carbon cycle feedback on climate change. These hot-wet climate regions tend to have very large pools of above ground carbon storage [Simard et al., 2011, Saatchi et al., 2011], and encompass the tropical rainforests in South America, Africa, and Indonesia, as well as southeast China (Figure 2.3C and 2.3D, Figure 2.5B). Our results suggest that concomitant increases in shortwave radiation act as a mediator on the effect of warming on greening in these hot, wet regions. We hypothesize that these ecosystems would have a different sensitivity to warming if it occurred without increases in solar radiation (i.e. from greenhouse gasses). Ecosystems would also likely have different sensitivity to a multi-year decline in rainfall such as from an extended drought as opposed to interannual variability. These long-term changes would instead drive the whole ecosystem down the precipitation gradient out of the hot wet region towards positive β_{PRECIP} below 2000 mm/year (Figure 2.3C and 2.3D).

2.4.5 Climate Change Implications

Observations of β derived from greenness suggest that ecosystem functioning depends on multiple physical aspects of climate, as well as the coordinated changes among them. Predicting the future changes of some of aspects of climate is much more difficult (i.e. rainfall), which helps explain the uncertainty in current predictions of the carbon cycle [Friedlingstein et al., 2006]. In addition, climate change may not maintain the same concomitant changes that we can observe in interannual climate variations (e.g. temperatures damped response to sunlight in wetter climates). Predictions based on any one variable alone (e.g. temperature) will not do as well where these concomitant changes are strong drivers, with ramifications for

predictions ranging from global climate sensitivity to food supply [Friedlingstein et al., 2006, Battisti and Naylor, 2009]. In particular, temperature is likely to increase due to greenhouse gasses without an associated change in shortwave radiation. The strong implied effects of co-variation of temperature with shortwave radiation should motivate future research to investigate the interconnections between climate variables under climate change and take into account their location in climate space.

To aid in predictions of new climate regimes our empirical characterization of present-day relationships between ecosystem functioning and climate can also serve as an observationally-based constraints to improve process-based models [Luo et al., 2012]. Comparing our linear metrics of the sensitivity of vegetation to climate with model output probes the veracity of ecosystem-climate interactions directly rather than the final results of these interactions (e.g. sensitivity of vegetation to temperature, rather than solely the temperature or greenness of a particular region). This added constraint compliments and could possibly enhance other efforts to improve the representation of processes within global vegetation models. These observational constraints will improve simulations not only under current conditions, but also under novel conditions by improving the functional fidelity of the global vegetation model. Improved models can then make better predictions despite the differences between present-day observed variability and anthropogenic driven global warming of the next century.

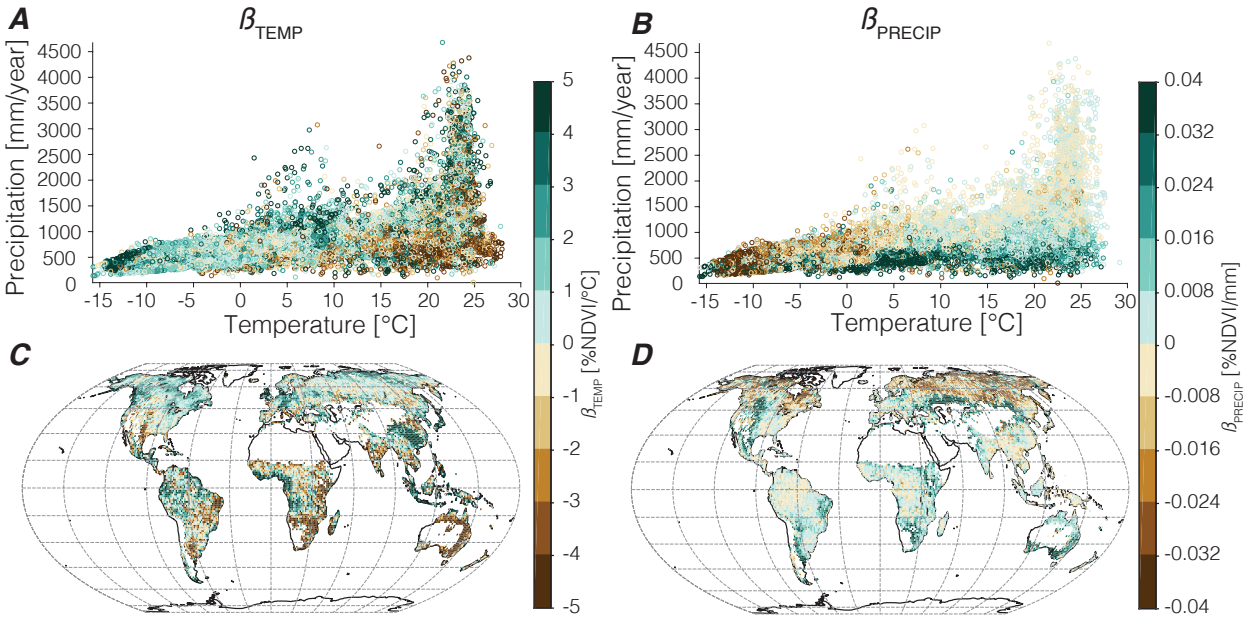

Figure 2.1: Sensitivity of vegetation to interannual variation in (**A**) temperature (β_{TEMP}) and (**B**) precipitation (β_{PRECIP}) calculated from robust regressions for years 1997 - 2012. Shades of green show positive sensitivity (generally greener vegetation when warmer (A) or wetter (B)). Shades of brown show negative sensitivity (greener vegetation when cooler (A) or drier (B)). A map of (**C**) β_{TEMP} and (**D**) β_{PRECIP}.

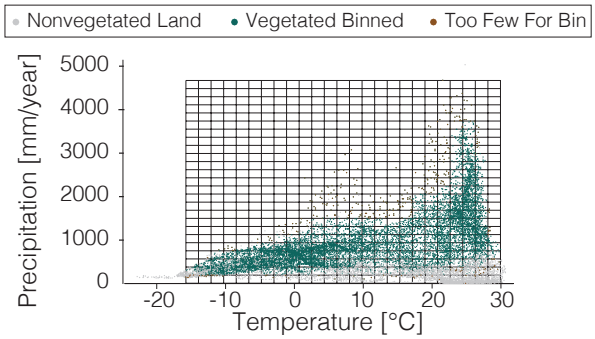

Figure 2.2: Spatial points plotted in climate space of Mean Annual Temperature and Mean Annual Precipitation. Non vegetated grid points (grey), Vegetated grid points used in analysis (Green) and Vegetated grid points where there were less than 10 in a bin (Brown)

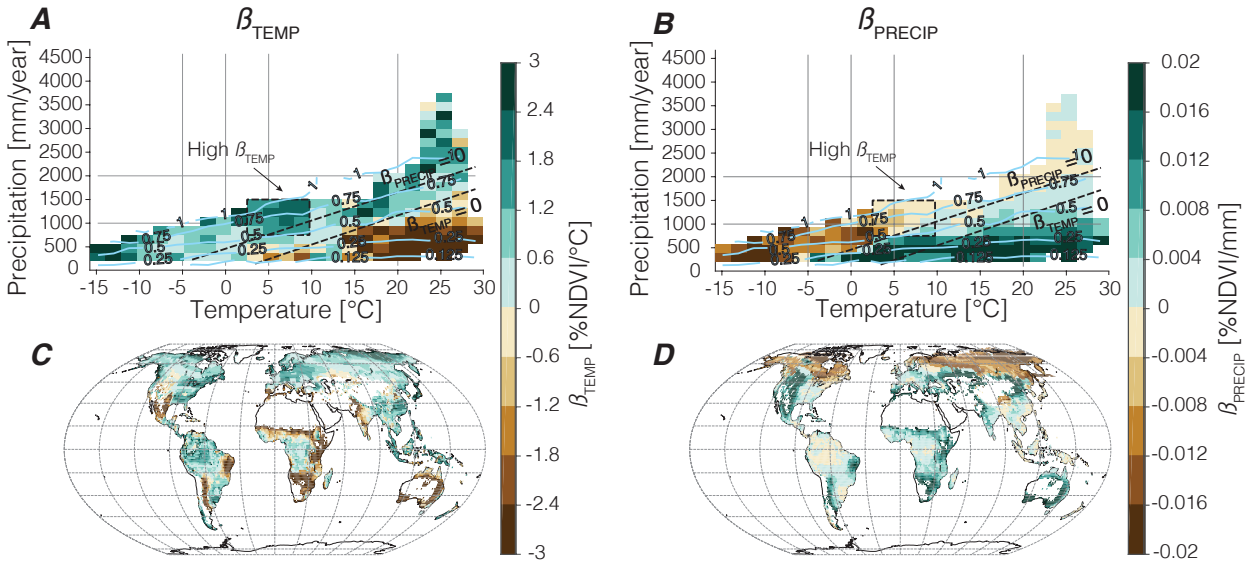

Figure 2.3: Sensitivity of vegetation to interannual variation from 1997-2012 in (**A**) temperature (β_{TEMP}) and (**B**) precipitation (β_{PRECIP}). Each pixel displayed is the average value of all spatial points found in locations with particular climatological mean annual temperature and mean annual precipitation. Shades of green (brown) show positive (negative) sensitivity (greener vegetation when warmer (cooler) (A) or wetter (drier) (B)). Blue contours in (A) and (B) are of P/PET derived from precipitation and shortwave radiation. The thick dashed black line marks the transition in sensitivity ($\beta_{TEMP} = 0$, $\beta_{PRECIP} = 0$). Boxes in (A) and (B) mark areas of particularly high β_{TEMP}. Light grey lines are for reference. A map of the average (**C**) β_{TEMP} and (**D**) β_{PRECIP} from each climate bin (as shown in A and B) is shown re-projected onto a spatial map.

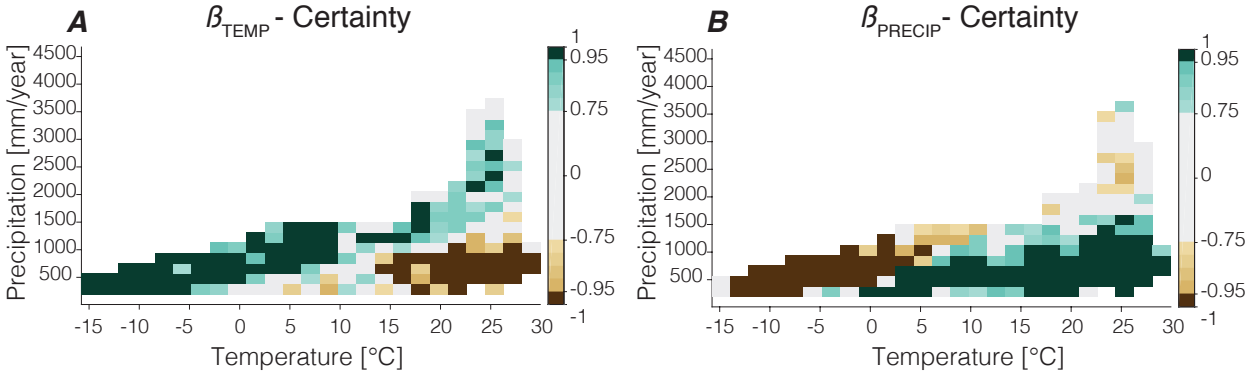

Figure 2.4: Combined temporal and spatial uncertainty for bins of **(A)** β_{TEMP} and **(B)** β_{PRECIP}. Dark colors show bins with 95% confidence that average is greater than (green) or less than (brown) zero. Gradient of colors show range of values greater than 75% certain.

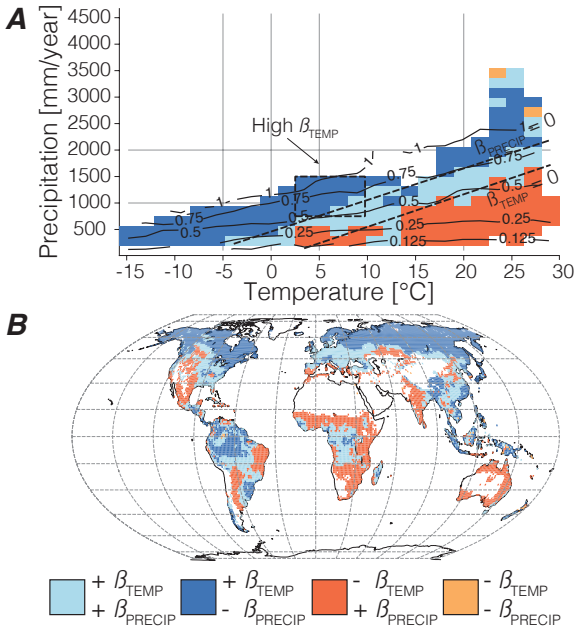

Figure 2.5: Comparison of the sign of β_{TEMP} and β_{PRECIP} is shown in (**A**) climatological mean annual temperature and mean annual precipitation space, and (**B**) projected onto a spatial map. Pixels are colored light blue where both β_{TEMP} and β_{PRECIP} are positive (warmer, wetter, greener), dark blue where β_{TEMP} is positive but β_{PRECIP} negative (warmer, drier, greener), dark orange where β_{TEMP} negative and β_{PRECIP} positive (colder, wetter, greener), and light orange where both negative (colder, drier, greener). Light grey lines in (A) are as described in Figure 2.3 and black contours of P/PET.

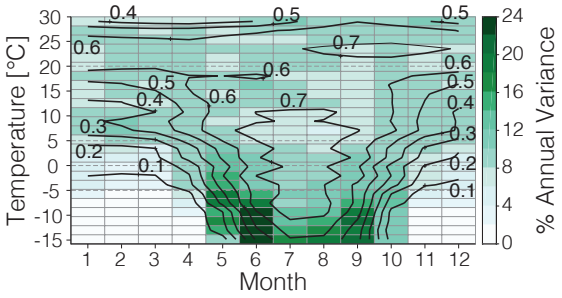

Figure 2.6: The variance for each month in NDVI divided by the annual sum of monthly variance, shown across a range of annual mean temperatures in the Northern Hemisphere. Months with higher percent variance (dark green colors) contribute more strongly to the annual mean variance. Contours show mean monthly NDVI values.

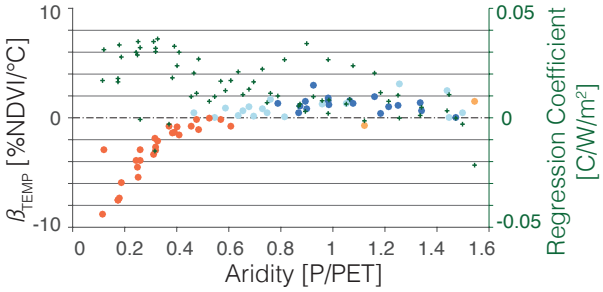

Figure 2.7: Variation of β_{TEMP} (filled circles, colors as in Figure 2.5, left axis) and regression coefficient of interannual temperature and shortwave radiation (green crosses, higher values show strong positive coupling between temperature and shortwave radiation, right axis) across places with different mean annual PET for locations with mean annual temperature greater than 20 °C.

Chapter 3

ECOLOGICAL-CLIMATE INTERACTIONS IN CMIP5 CARBON CYCLE MODELS

3.1 Abstract

The response of the biosphere to variation in climate plays a key role in predicting the carbon cycle, hydrological cycle, terrestrial surface energy balance, and the feedbacks in the climate system. Predicting the response of the Earth's biosphere to global warming requires the ability to mechanistically represent the processes controlling photosynthesis, respiration, and water use. This study uses observations of vegetation interaction with the physical environment to identify where ecosystem functioning is well simulated in an ensemble of Earth system models. This data-model comparison is leveraged to hypothesize which physiological mechanisms - photosynthetic efficiency, respiration, water supply, atmospheric water demand, and sunlight availability - dominate the ecosystem response in places with different climates. The models are generally successful in reproducing the broad sign and shape of ecosystem function across climate space except for simulating generally lower leaf area during warmer years in places with hot wet climates. In addition, simulated ecosystem interaction with temperature is generally larger and changes more rapidly across a gradient of temperature than is observed. We hypothesize that the amplified interaction and change are both due to a lack of adaptation and acclimation in simulations. This discrepancy with observations suggests that simulated responses of vegetation to global warming, and feedbacks between vegetation and climate, are too strong in the models. Finally, models and observations share an abrupt threshold between dry regions and wet regions where strong positive vegetation response to precipitation falls to nearly zero in places receiving around 1000 mm/year.

3.2 Introduction

In many places, the climate at the end of the century will be unlike any found on Earth today, and thus there exists no modern analog for either climate or ecosystems with which to compare [Williams et al., 2007]. Observational evidence suggests that increasing atmospheric CO_2 and the associated global warming has already led to changes in the biosphere and altered the carbon cycle [Zhu et al., 2016, Martin G. De Kauwe et al., 2016, Piao et al., 2014, Wang et al., 2014]. Because there is no analog ecological community to base predictions on, in order to project vegetation response to novel environments process based models must correctly predict ecosystem functioning: the interaction between vegetation and the physical environment. Observational constraints are critical for testing the fidelity of our ability to simulate ecosystem functioning both in present day climate and under a changing climate. Here we evaluate the ecosystem functioning of process-based models by comparing interactions of terrestrial vegetation with climate in simulations from the Coupled Model Intercomparison Project 5 (CMIP5) [Taylor et al., 2011] with observations. We focus on Earth system model simulations from the CMIP5 archive, which simulate both physical and biological Earth processes for the whole globe, along with the interactions between them. We compare Earth system models and observations of present-day ecosystem climate interactions as a functional constraint on the models to reduce persistent spread in predictions and to improve our understanding of the underlying mechanisms.

Earth system models show a significant spread in their predictions of future CO_2 concentration and thus global temperature at the end of the century [Friedlingstein et al., 2013]. The inclusion of an interactive carbon cycle increases the projected uncertainty and absolute value of global temperature, with most of the signal coming from uncertainties in land carbon uptake [Yu et al., 2016, Friedlingstein et al., 2013, Booth et al., 2012]. Vegetation plays a large role in absorbing CO_2 added to the atmosphere through anthropogenic emissions of CO_2 - currently absorbing approximately a quarter of emissions [Le Qur et al., 2015]. Though there has been an expansion of the biological and physical processes represented in

these models over time, the uncertainty in future CO_2 absorption by the terrestrial biosphere has stayed stubbornly consistent [Lovenduski and Bonan, 2017, Friedlingstein et al., 2013, 2006].

To simulate vegetation, models must use a number of simplifications to represent real world processes. This includes simplified physiological processes, omission of relevant processes, and representation of complex ecosystems with only a few plant functional types - simplified and static representation of the broad physiological characteristics of major plant groups. The realities of limited computational resources for numerical simulations also lead to calculations at coarse spatial resolution for both vegetation and climate processes in Earth system models. Simulation at course spatial scales will affect the climate that the biosphere is interacting with in addition to affecting the ecosystem functioning of the biosphere itself. Climate simulated by Earth system models can have biases in mean climate (e.g. mean annual precipitation) as well as biases in variation (e.g. high interannual variability in surface temperature) [Merrifield and Xie, 2016] which can have significant implications for the simulations of the ecosystems. This makes it difficult to separate the effects of biases in climate from the effects of a poor representation of vegetation processes. Our work specifically analyzes the interaction between vegetation and climate independent of spatial pattern to constrain and formulate hypotheses about the simulated ecosystem functioning compared to observations.

Prior studies have used satellite observations and up-scaled flux tower observations to analyze interactions between vegetation and climate [Quetin and Swann, 2017, Green et al., 2017, Martin G. De Kauwe et al., 2016, Chu et al., 2016, Rafique et al., 2016, Seddon et al., 2016, Wu et al., 2015, Piao et al., 2009, Jung et al., 2011, Beer et al., 2010, Xiao et al., 2011]. Through these various analyses it is clear that there is a strong interaction between vegetation and climate, that the relationship changes across the globe, and that it varies with the mean annual climate of a place. Our analysis also builds on analyses of the carbon cycle in Earth system model simulations from the CMIP5 archive [Anav et al., 2013b,a, Mahowald et al., 2016, Shao et al., 2013], and simulated interactions between climate and the carbon

cycle [Liu et al., 2017, 2016, Mahowald et al., 2016, Wang et al., 2014, Cox et al., 2013, Shao et al., 2013]. For example, it has been observed that leaf area simulated by Earth system models from CMIP5 is consistently larger on average and has larger variability compared to observations [Anav et al., 2013b,a]. Additionally, there is a relatively large spread of leaf area across the models [Mahowald et al., 2016, Shao et al., 2013]. Prior studies have also established that the observed interactions of climate and carbon cycle can be used to constrain carbon cycle forecasts [Cox et al., 2013].

3.2.1 Deriving Ecosystem Function from Observations

In Quetin and Swann (2017) we developed a metric for ecosystem climate interaction that can be used to compare the behavior of modeled ecosystems against observations. The metric is calculated by fitting a multilinear regression for the percent interannual variations in plant activity, using the interannual variations in temperature and precipitation (see Methods Equation 1). Our coefficients of interaction are then the regression coefficients of this equation. β_{TEMP}, the interaction of vegetation with temperature, is positive when there are more leaves in a warmer year. β_{PRECIP}, the interaction of vegetation with precipitation, is positive when there are more leaves during a wetter year. For this analysis, we calculate β_{TEMP} and β_{PRECIP} for observations of Leaf Area Index (LAI) derived from satellite, reanalysis of two meter air temperature, and observations of precipitation (see Methods). We then compare these observed values with β_{TEMP} and β_{PRECIP} calculated from LAI and climate variables simulated by Earth system models with active carbon cycles and prognostic leaf area.

3.2.2 Proposed Processes Driving β_{TEMP} and β_{PRECIP}

We hypothesize that the magnitude of β_{TEMP} and β_{PRECIP} result from a number of underlying processes that occur in nature and are simulated to various degrees in the Earth system models (Table 3.1). We expect that the primary drivers of β_{TEMP} (the change of leaves in response to warmer/cooler years) will be photosynthetic performance, respiration, and the

response of stomata to the dryness of the atmosphere through the temperature driven vapor pressure deficit. In contrast, we expect that the primary drivers of β_{PRECIP} (the change of leaves in response to wetter or snowier/drier years) will be the effects of snow in colder climates and how well the water supply matches the water demand of the environment. In addition to these direct drivers of β_{TEMP} and β_{PRECIP}, we note that both temperature and precipitation correlate with sunlight in different ways across the globe (e.g. increased sunlight in the tropics generally comes with lower rainfall and higher temperatures). These additional concomitant changes in sunlight with temperature or precipitation suggest other potential drivers of β_{TEMP} and β_{PRECIP} due to increases of sunlight driving more overall photosynthesis.

From empirical and theoretical studies in the literature we can develop an expectation for how different processes would influence the sign of β_{TEMP} independent of one another. The dependence of photosynthetic efficiency on temperature is often measured as a concave curve, increasing with temperature to some optimum and then decreasing for hotter temperatures beyond the optimum [Berry and Bjorkman, 1980, Day, 2000, Smith and Dukes, 2013, Way and Yamori, 2014, Yamori et al., 2014]. Given this shape, a plant living in an environment colder than the optimum temperature would have increased photosynthesis in warmer years and thus positive β_{TEMP}. Similarly, plants living in environments warmer than the optimum would have decreased photosynthesis in warmer years and thus a negative β_{TEMP}, while plants living near the optimum temperature would have only a weak response and a β_{TEMP} near zero. In contrast to photosynthesis, the metabolic costs of respiration generally increase with temperature so that a warmer year would lead to a negative β_{TEMP} across all temperatures. Finally, warmer years increase the vapor pressure deficit (assuming relative humidity is about the same), which increases the atmospheric demand for water from the vegetation. We expect this increased atmospheric demand for water to lead to a negative β_{TEMP} as the strategies that plants invoke to avoid hydraulic damage reduce carbon uptake.

Precipitation can fall either as snow or rain depending on the climate and season. In cold regions, where we expect that a large fraction of annual precipitation falls as snow, our

previous research found negative β_{PRECIP} with most of the variation in vegetation driving the β_{PRECIP} occurring at the beginning of the growing season [Quetin and Swann, 2017]. In these cold and highly seasonal climates, the mean annual leaf area is partly controlled by the length of the growing season. Thus increased precipitation is realized as increased snowfall that melts out later and can lead to a reduction in the length of the growing season. Without a large increase in maximum LAI during the summer, we expect the shorter growing season during a heavy snow year to have lower annual LAI and thus a negative β_{PRECIP} (more leaves during drier years). Conversely, where precipitation falls as rain it serves as the main water supply for most vegetation. We expect having less water available from rainfall would induce water limitation and lead to less photosynthesis, thus a positive β_{PRECIP} (more leaves during a wetter year).

We hypothesize that the concomitant change of cloudiness with annual changes in temperature and precipitation would impact both β_{TEMP} and β_{PRECIP}. Warmer years can be accompanied by more sunlight due to fewer clouds. We expect increases in sunlight to benefit vegetation and lead to a positive β_{TEMP} through the positive correlation between sunlight and mean annual temperature. Sunlight is also correlated with rainfall such that rainier years can be correlated with less sunlight due to increased clouds. We expect a reduction in sunlight to reduce photosynthesis and lead to less leaves and thus through the negative correlation with precipitation lead to a negative β_{PRECIP}.

In our analysis we us the values of β_{TEMP} and β_{PRECIP} to hypothesize which processes dominate in different climates. In addition, we quantify how β_{TEMP} and β_{PRECIP} change across climate in both observations and models. By comparing across models and observations we are able to hypothesize which processes lead to disagreements among models and observations.

3.3 Methods

In this study we compare vegetation activity across climate space between models and observationally-based estimates. We chose to use LAI to represent vegetation activity as

it can be derived from remote observations and is easily available as output from Earth system models. We use an ensemble of different Earth system model simulations from the CMIP5 archive, and choose a time interval that overlaps with observations. Analysis uses python and particularly depends on modules from numpy, scipy, scikit-learn, matplotlib and xarray [J. D. Hunter, 2007, McKinney, 2010, Pedregosa et al., 2011, S. van der Walt et al., 2011, Hoyer and Hamman, 2017].

3.3.1 Data

We use observationally-based LAI estimates derived from a combination of optical observations from the Moderate-resolution imaging spectroradiometer (MODIS) and the Advanced Very High Resolution Radiometer (AVHRR) [Zhu et al., 2013, Xiao et al., 2014, Liu et al., 2012] (the LAI3g, GLASS, and GLOBMAP datasets). In our primary analysis we use LAI from the LAI3g dataset. For observationally-based estimates of temperature we use 2m air temperature from ERA-Interim reanalysis and for observations of precipitation we use Global Precipitation Climatology Project (GPCP) [Dee et al., 2011, Adler et al., 2003]. We recognize that LAI estimates derived in this way are not direct observations of LAI and contain uncertainty in both the observations and statistical techniques used to derive LAI from optical observations. We refer to these observationally-based estimates as observations for the remainder of the paper.

3.3.2 Earth System Models from CMIP5

We use an ensemble of 10 fully coupled Earth system model simulations from the CMIP5 archive that have prognostic LAI (single realization r1i1p1). Included in each of these models is a terrestrial biosphere that models the flux of carbon, water etc. from the land surface [Taylor et al., 2011]. The Earth system model simulations that we analyze here are from fully coupled models, with the land and atmosphere (including atmospheric CO_2 concentrations) interacting with each other. The models used are detailed in Table 3.2 [Taylor et al., 2011]. Our analysis uses monthly mean model output of LAI, surface temperature, and precipitation

(variable names lai, tas, and pr respectively). We create a continuous dataset that includes recent years and has maximum overlap with observations by combining simulations of the historical period (simulation name esmHist) with the first 6 years of future simulations from the emissions scenario which best matches the actual carbon emissions for the time period 2006-2011 (simulation name esmRCP8.5).

3.3.3 Interpolation of Data

Observations of temperature and precipitation were both reported at the same spatial resolution however, the two grids did not match so we interpolated them both to a matching 1x1 degree latitude-longitude grid. In addition, we coarsened the high-resolution LAI data derived from observations to better match other observations and models by interpolating it to 1x1 degree grid using the python scipy interpolate interp2D function and then re-interpolating to the midpoint of the coarser grid - essentially doing an averaging across grid points [McKinney, 2010]. All models were analyzed on their native spatial grid (see Table 3.2).

3.3.4 Multilinear Regression

We create a metric of the ecosystem-climate interaction between leaf area and climate (both observed and simulated) by performing a multi-linear regression of the percent change in LAI (%LAI) interannual variation with the interannual variation of Temperature (T) and Precipitation (P) (Equation 3.1).

$$\%\Delta_{LAI} = T \cdot \beta_{TEMP} + P \cdot \beta_{PRECIP} + \beta_0 \tag{3.1}$$

The regression coefficients are metrics of interaction showing how the percent leaf area generally changes in warmer/cooler, wetter/drier years; β_{TEMP} has units of %LAI/°C and β_{PRECIP} has units of %LAI/mm.

We compute the multilinear regression at each grid point using the python function sklearn.linear_model.LinearRegression from the scikit-learn package [Pedregosa et al., 2011]. To test for the impact of temporal trends, we performed the regression both on the raw data as well as de-trended and data. We found that our analysis was not sensitive to the inclusion or emission of trends and therefore report the results without de-trending so as to preserve the full ecosystem-climate interaction. We performed regressions for the longest time series available (1997-2011), as limited by observations. The earliest available high-resolution precipitation data (at 1x1 degree lat-lon grid) is available starting in 1997 and the latest LAI observation (LAI3g) is available for 2011. We compare our metrics of ecosystem-climate interaction, β, across 10 Earth system models from the CMIP5 archive as well as a dataset of leaf area derived from observations.

3.3.5 Aggregating Across Climate

We aggregate our results in climate space by assigning vegetated terrestrial grid points from observations and models into climate bins defined by mean annual temperature and precipitation, and we calculate the average interactions for these climate bins. The climate space ranges from -20°C to 30°C temperature, and 0 to 5000 mm/year of precipitation and each bin extends 2°C by 200 mm/year. We accounted for water and non-vegetated points by discarding spatial points where the mean value of LAI fell below a threshold indicating little vegetation (less than 0.2 LAI) [Scurlock, 2002]. Each model generates a unique climate relative to each other and the observations. In the case of our analysis this means that not all climate bins represented in observations are represented by all of the models, and some models also create novel climates not seen in observations as discussed in section 3.4.1. We generally restrict out comparisons to bins (representing a climate) where there are vegetated land points present for each model and the observations.

3.3.6 Uncertainty in value of β for each climate bin

Each climate bin represents a number of spatial locations on Earth that share the same mean annual temperature and mean annual precipitation. Each spatial point thus contributes an estimate of β to that climate bin, from which we calculate the average value of β for that climate bin, as well as characterize the variability within a bin. The uncertainty in the value of β for each bin results from a combination of the uncertainty of the regression (temporal uncertainty) and the spread in β for each bin (spatial uncertainty). To account for both uncertainties, the standard errors of the regression coefficient for each spatial grid point and the standard errors of the distribution of regression coefficients from all spatial grid points in each bin were combined through a root mean square weighted by degree of freedom to create a standard error of the regression coefficient for each bin. We use this standard error to test if the values of β differ from zero using a student t distribution from Python's scipy package [McKinney, 2010]. We report the p-value of the student t distribution and mark the bins that have field significance at 95% using the method from Wilks 2016 [Wilks, 2016].

3.3.7 Comparison Across Models

We compared models to each other and to observations by analyzing the consensus as well as the outliers in the sign and amplitude of β. For consensus in sign, the number of models that agreed in sign was counted in each climate bin. When at least 8 models agreed in sign we identified outliers as any model that didn't agree with the rest. We tested the similarity in amplitude by using the standard error, where outliers were identified as models that fell outside two standard errors of the mean across models in any bin.

3.3.8 Systematic Change of β Across Climate Gradients

To better quantify and compare consistent features of the systematic change in β across climate we calculate fits to β within a sub-set of climate space. We focus our analysis on two climate gradients: changes in β_{TEMP} across temperature for places with precipitation

between 100 mm/year and 1000 mm/year, and changes in β_{PRECIP} across precipitation for places with mean annual temperature between 20°C and 30°C. We characterize the change in β in these domains using a linear fit where applicable and a smoothing technique where a predetermined function like a linear fit is less useful.

We fit a line to β_{TEMP} to quantify the slope of change and the temperature of transition from positive to negative β_{TEMP} using sklearn.linear_model.LinearRegression(). In addition, to check for the influence of outliers in the regression slope and intercept we also fit the points with a RANSAC fit which omits outliers using sklear.linear_model.RANSACRegressor(). Where the two solutions resulted in dramatically different answers it was noted in Table 3.3.

For β_{PRECIP}, we interpolated between binned values of β_{PRECIP} and then smoothed the resulting transition across mean annual precipitation to highlight the general shape of the systematic change. We interpolated using (scipy.interpolate.interP_{1d}) in order to use a butterworth filter (scipy.signal.butter, scipy.signal.filtfilt) to remove the higher frequency noise. The smoothed change across the gradient of mean annual precipitation is more representative of the systematic change to be quantified and compared across Earth system models and observations. The butterworth filter was set to $b, a = signal.butter(4, 0.03125)$ and applied through $signal.filtfilt(b, a, method = 'gust')$ [McKinney, 2010]. We used the similarity of shape of the systematic change between Earth system models and observations to quantify a maximum value of β_{PRECIP} and the mean annual precipitation at which β_{PRECIP} approached zero. We defined the approach to zero as the point where β_{PRECIP} drops below 0.01 %LAI/mm/year divided by the maximum β_{PRECIP} we calculated above.

3.4 Results

In the following section we present results detailing the difference between simulated climates and observed climates as well as the agreement between β_{TEMP}, and β_{PRECIP} derived from Earth system models and observations. We use βs calculated from LAI derived from Normalized Difference Vegetation Index (NDVI) in the LAI3g dataset to compare to observations [Zhu et al., 2013]. We focus on LAI from LAI3g but found that the mean LAI and

the derived β_{TEMP}, and β_{PRECIP} were broadly similar when calculated from either GLASS or GLOBMAP LAI (Figure 3.1, and 3.2). We focus on the form of the change in β_{TEMP} and β_{PRECIP} across climate gradients of mean annual temperature and mean annual precipitation respectively.

3.4.1 Contrasting Simulated Climates to Observed Climate

Before examining ecosystem functioning in climate space, we first examine the climate space itself. Each of the 10 Earth system models we analyzed simulates its own climate, and therefore can differ from the others in the mean annual temperature and precipitation at each spatial point. We find that the climate simulated by the 10 Earth system models do not capture the full breadth of joint temperature and precipitation space found in observations. In particular, a large majority of models fail to simulate high precipitation climate regions at all temperatures (Figure 3.3). This systematically low bias in precipitation results in particularly poor model coverage over climates observed in the deep Amazon and the maritime continent (Figure 3.4). In addition, all of the models fail to simulate very cold vegetated land areas (Figure 3.3). These vegetated places with low temperatures are primarily observed at high latitudes and along the Tibetan plateau (Figure 3.4). Previous work has also noted that the simulated interannual variance of LAI, temperature, and precipitation is larger than that of the observed interannual variance of those quantities [Merrifield and Xie, 2016, Anav et al., 2013a]. We observe something similar, mean LAI in models, though generally stronger, agree with observations, while the interannual variation of LAI, temperature and precipitation are much stronger than observed.

Outside of these extreme environments, the majority of observed vegetated land points fall within climate regions that are represented by all of the models. For the remainder of the paper we restrict our analysis of ecosystem functioning to climates common to both models and observations to avoid the confounding influence of ecosystem models operating in different climates.

3.4.2 Consensus in Simulated Ecosystem Function Across Climate Space: β_{TEMP}

All of the models agree with observations that very cold-regions (below 0°C) have positive β_{TEMP} (more leaves when warmer) (Figure 3.5, 3.7A). Above mean annual temperatures of 0°C, the consensus among models for a positive β_{TEMP} is dependent on mean annual precipitation. In places with more precipitation, regions of complete agreement among models on positive β_{TEMP} (more leaves when warmer) extend up to temperatures of 10°C (Figure 3.5, 3.7A). However, at lower precipitation, about half the models show disagreement on the sign of β_{TEMP} starting at 0°C. This transition from complete agreement among models on the sign of β_{TEMP}, to an even split between the models demarks the cold end of a climate region with little agreement among the models. The uncertainty of the sign of simulated β_{TEMP} occurs in climates where observations show a very weak positive β_{TEMP} changing to negative β_{TEMP} in warmer climates. When projected on to a map this region of uncertainty in models primarily consists of the Northern mid-latitudes (Figure 3.8A). The climates that are uncertain across models also includes areas of high β_{TEMP} uncertainty in each bin for many models and observations (Figure 3.9A). Where there is strong agreement in simulated sign of β_{TEMP} in cooler climates, there is also a strong agreement in the simulated amplitude of β_{TEMP} across models, with a standard deviation across the ensemble of less than 2 %LAI/°C for most of the climate space below 10°C (Figure 3.7C).

A strong consensus among models for a negative β_{TEMP} is evident at temperatures warmer than 10°C in dry climates, and warmer than 18°C in the wettest climates analyzed. In these warmer climates, the consensus is shared primarily between 8 models, sometimes reaching 9 models (Figure 3.5, 3.11B). Two models (MIROC-ESM and BNU-ESM) display the most climates with a disagreement in β_{TEMP} with other models compared with the overall model consensus on the sign of β_{TEMP} (Figure 3.10). These warmer climates also show a much larger spread across models of the amplitude of β_{TEMP}, generally having an across model standard deviation greater than 10 %LAI/°C and above 16 %LAI/°C in the driest/hottest climates (Figure 3.7C). Although the majority of models agree with one an-

other in simulating negative β_{TEMP} in hot climates, observations only concur with the model consensus of a negative β_{TEMP} in dry climates with precipitation below 1000 mm/year (Figure 3.5). In climates wetter than 1000 mm/year, there is model consensus but it disagrees with observations which show generally positive β_{TEMP} (more leaves when warmer) in all but a few climate bins above 1000 mm/year (Figure 3.5). In these wet climates most models and observations show large uncertainty in β_{TEMP} (Figure 3.9).

Using a linear fit of the change of β_{TEMP} across climate space we estimate the slope of change of β_{TEMP} across mean annual temperature to be 0.9 %LAI/°C/°C in observations and -0.84 to 0.9 %LAI/°C/°C in models. We estimate that the temperature of the transition from positive to negative β_{TEMP} is -5°C in observations and -2.5°C to +7°C in models (See Methods) (Figure 3.11A, Table 3.3). The modeled slopes of the change of simulated β_{TEMP} across mean annual temperature (units: %LAI/°C/°C), from positive β_{TEMP} (at cooler temperatures) to negative β_{TEMP} (at relatively dry high temperature), are more than 2x stronger than the observed slope (Table 3.3). In addition, models consistently transition from positive β_{TEMP} to negative β_{TEMP} at warmer temperatures, +1.7°C, compared to the transition in observations at -5.1°C (Table 3.3).

3.4.3 Consensus in Simulated Ecosystem Function Across Climate Space: β_{PRECIP}

Models and observations show broad agreement on the sign of β_{PRECIP} across climate space (Figure 3.6, Figure 3.7B). In hot and dry climates (greater than 0°C and less than 1000 mm/year) there is a consensus across models for strong positive β_{PRECIP} (more leaves when wetter) (Figure 3.7 B). A relatively high spread in the amplitude of model-derived β_{PRECIP} occurs in the driest climates (below 500 mm/year, above 0°C) (Figure 3.6, Figure 3.7D). In contrast to observations and other models, only one model (BNU-ESM) shows a large number of negative β_{PRECIP} bins in the hottest and driest climates (Figure 3.6 and 3.10). The consensus across models is that the amplitude of β_{PRECIP} sharply decreases below 0°C and above 1000 mm/year, becoming negative in the majority of models (7) below 0°C (Figure 3.7). This simulated consensus of a decrease in β_{PRECIP} concurs with an observed transition

from positive to negative β_{PRECIP} (below 0°C) and relatively weak β_{PRECIP} (above 1000 mm/year). Above 1000 mm/year of precipitation, and across a wide range of temperatures (0°C to 30°C), there is only a weak consensus among models that β_{PRECIP} is positive, but all of the models concur with observations that the strength of β_{PRECIP} is relatively weak in these wetter climates (Figure 3.6). These regions of weak β_{PRECIP} are primarily in the tropics and savannahs of the Amazon and Africa (Figure 3.8B). The uncertainty in β_{PRECIP} in both models and observations is broadly similar to the amplitude of β_{PRECIP}, with low uncertainty where β_{PRECIP} is large (Figure 3.12).

The transition from strong positive β_{PRECIP} in dry climates to weak β_{PRECIP} values in wet climates has a similar shape across most models (9) and observations for relatively warm climates above 20°C (See Methods) (Figure 3.11B). The magnitude of maximum positive β_{PRECIP} in dry climates is highly variable (observations: 0.05 %LAI/mm, model mean+/-standard deviation: 0.08 +/- 0.1 %LAI/mm). In contrast, the mean annual precipitation of the transition from strong β_{PRECIP} to relatively weak β_{PRECIP} is consistent across observations and models (observations: 1100 mm/year, model mean+/-standard deviation: 1000 +/- 250 mm/year) (Figure 3.11B, Table 3.3).

3.5 Discussion

In the following section we discuss the similarities and differences of modeled and observed ecosystem functioning. In particular, we discuss the disparity between models (strong negative β_{TEMP}) and observations (weak positive β_{TEMP}) in hotter (above 20°C) and wetter (above 1000 mm/year) climates and propose that the lack of real-world adaptation and acclimation in models is the mechanism driving the amplified change of β_{TEMP} across the global gradient of temperature. We also discuss the notable consistency across observations and models of the annual average precipitation at which β_{PRECIP} rapidly decreases, and the potential consequences of feedbacks driven by the highly variable strength of β_{PRECIP} in dry-hot climates.

We evaluate these ecosystem-climate interactions across climate space, defined by mean

annual temperature and precipitation in order to compare like climates in observations with like climates in models. In contrast to analyses that depend on the spatial location for comparison, our approach puts the Earth system models on a more equal climate footing and more specifically targets the modeling of the ecosystem climate interactions as opposed to the spatial patterns. Discrepancies between observations and models, and between models in particular climates can suggest which process may be in error and provides a functional constraint that can be used in efforts to model the ecosystem climate interactions.

3.5.1 Temperature Driven Processes Dominate Increases in Sunlight in Hot-Wet Climates

The most prominent difference in ecosystem functioning between observations and models is a model consensus for a strong negative β_{TEMP} (more leaves when cooler) in wet climates where only a weak positive β_{TEMP} is observed (Figure 3.5 and 3.7). Similar disagreements between observations and models have been shown in prior research with interactions of net biosphere productivity and net primary productivity with temperature [Liu et al., 2017, 2016]. These hot wet climate regions where models and observations disagree in the sign of β_{TEMP} encompass tropical forests and represent a large amount of global above ground carbon [Saatchi et al., 2011]. This climate region also shows high uncertainty in the mean value of β_{TEMP} in the bins for both models and observations, even though models have a strong β_{TEMP}. The simulated strong negative β_{TEMP} suggests that simulated tropical forests may be too sensitive to increases in temperature, and Earth system models are thus prone to predict worse outcomes for tropical forests in a warming climate than observations would suggest. These results are suggestive, but it should be noted that interannual variations in temperature occur with many other concomitant changes in environmental conditions and the same correlations may not hold under greenhouse gas-driven warming. Therefore interannual variations are a limited indicator of how vegetation will respond to the longer-term changes under climate change.

In hot climates, increased temperature has three costs for plants: increased respiratory costs, reduced photosynthetic efficiency since plants are likely to be living near or beyond

the thermal optimum for photosynthesis, and increased stress from high atmospheric water demand. In previous work we hypothesized that an increase in sunlight during warmer years in these very hot and wet climates offsets these three factors by increasing photosynthesis [Quetin and Swann, 2017]. In wet climates there is a large enough supply of water so that energy from the sun incident on the surface is largely dissipated through latent heat, rather than sensible heat or longwave radiation that requires the surface to heat up. In this way, ample water in the environment from precipitation allows for smaller increases in the cost to vegetation from temperature resulting in larger benefits from increased sunlight.

In hot wet places, models show a consensus on the sign of simulated β_{TEMP}, but disagree with observed β_{TEMP}. For the models to consistently disagree with observations, one of the three processes that we expect to cause a negative β_{TEMP} on its own - photosynthetic efficiency, respiration, or stomatal response to atmospheric water demand - must be stronger in the models compared with observations or the observed increase in sunlight during warmer years must be weaker. Simulating the wrong amplitude for any one, or combination, of these processes could result in an amplified negative β_{TEMP} even if some of the processes were correctly simulated. It is notable that despite disagreeing about the sign of β_{TEMP}, the models and observations all agree that β_{PRECIP} is relatively weak in these hot wet climates (Figure 3.6). Weak β_{PRECIP} in this wet climate suggests that the simulated vegetation is not water supply limited.

Though the weak β_{PRECIP} is suggestive of a lack of water supply limitation, we cannot rule out that atmospheric water demand is causing intermittent stress leading to negative β_{TEMP}. Even though plants may have ample soil water, atmospheric water demand during a warmer year could still cause hydraulic stress or stomatal closure without exhausting the water supply. Plants should have reduced carbon uptake in warmer years independent of their strategy to either endure or avoid stress during high atmospheric water demand (anisohydric, isohydric), creating another potential mechanism for negative β_{TEMP} in these hot wet climates. In addition, vapor pressure deficit increases exponentially with temperature due to the Clausius Clapeyron relationship for saturation pressure. Due to this exponential

increase we expect that a warmer year in warm to hot climates will have a much bigger negative influence on the vegetation than warm years occurring at cooler climates. Thus, it is possible that the vegetation in hot wet climates is not experiencing any limitation from water supply, but is experiencing limitations during years where there is more water demand that the physiology of the vegetation can keep up with leading to negative β_{TEMP}.

The timing of the seasonality of increased rainfall compared with the seasonality of increased temperature may effect the interannual ecosystem functioning observed through β. For example, warming during the dry season in the tropics would likely lead to negative β_{TEMP} (lack of water supply and increased atmospheric water demand), whereas warming during the wet season could be simultaneously associated with reduced cloudiness and increased sunlight allowing for higher rates of photosynthesis and a positive β_{TEMP}. Other work suggests that there is more seasonality to interactions with precipitation, rather than interactions with temperature [Liu et al., 2017].

3.5.2 Lack of Adaptation and Acclimation in Models Amplifies the gradient in Ecosystem Function

Adaptation and acclimation allow for physiological characteristics of plants (e.g. photosynthetic performance) to adjust to best match the environment in which the plant is growing. Adaptation operates through evolutionary changes of species over multiple generations. Acclimation happens within a single individual, and can operate on a range of time scales, from minutes to the plant's lifetime. Conceptually, adaptation and acclimation both provide vegetation with flexibility in responding to environmental change. We hypothesize that the generally high magnitudes of simulated β_{TEMP} (both negative and positive) and the amplified change of β_{TEMP} across mean annual temperature is due to models not simulating the ability of vegetation to adapt or acclimate to local climate conditions. Vegetation simulated with fixed responses to environmental factors is, by construction, unable to exhibit this responsive behavior.

While it is possible to represent acclimation and adaptation in models (e.g. Lombardozzi

et al. 2015, Smith et al. 2017), it requires defining how the processes occur, and observations are generally lacking to constrain the problem at global scales across many ecosystems [Lombardozzi et al., 2015, Smith et al., 2017]. Models generally represent species with only a few, plant functional types with fixed physiological characteristics [Box, 1996]. One way to change the physiological characteristics of an ecosystem is to change what plant functional types occur there. While Dynamic Global Vegetation Models can move plant functional types around the globe spatially, these changes occur slowly (i.e. generations of plants), and there is evidence of acclimation on short time scales (i.e. in a single plant down to minutes) in the real world [Berry and Bjorkman, 1980, Smith and Dukes, 2013, Way and Yamori, 2014, Yamori et al., 2014, Atkin and Tjoelker, 2003, Atkin et al., 2005].

Given that these Earth system models do not adjust the performance of simulated vegetation as a function of mean climate, we expect to see higher simulated β_{TEMP} compared with observations. For example, vegetation of the same species grown in a colder climate compared to a warmer climate has been observed to flatten and shift the optimum of its photosynthetic performance curve to colder temperatures [Berry and Bjorkman, 1980, Smith and Dukes, 2013, Way and Yamori, 2014, Yamori et al., 2014]. In this example, a warmer year would increase the performance less, and thus lead to a lower overall β_{TEMP}, because the performance curve is flatter. Though operating through difference mechanisms, any ability plants have to adjust physiology to match the environment should dampen the response of vegetation to changing climates.

We can use temperature at which the transition from positive β_{TEMP} in colder climates to negative β_{TEMP} in warmer climates occurs to help identify which processes drive the amplified change of ecosystem function across climate. The transition of β_{TEMP} in sign demarks the temperature at which benefits of a warmer year for improved photosynthetic performance are outweighed by the costs of increased respiration during a warmer year, and water stress from a drier atmosphere. Models represent this transition at warmer temperatures than observations (-5°C in observations and -2.5°C to +7°C in models). Either the positive benefits in models of a warmer year are too large for photosynthesis, or the costs are too

low for respiration and water stress. We hypothesize that the majority of the cause of the warmer transition is due to simulating too steep a photosynthetic performance curve due to a lack of simulated adaptation and acclimation, leading to a stronger than observed benefit in warmer years. This hypothesis is also in line with the overly strong β_{TEMP} at colder temperatures due to the lack of flattening of the photosynthetic performance curve through adaptation and acclimation [Berry and Bjorkman, 1980, Smith and Dukes, 2013, Way and Yamori, 2014, Yamori et al., 2014].

Without the flexibility of adaption and acclimation, the ecosystem functioning simulated by Earth system models changes more from climate to climate compared with observations. This lack of flexibility may have consequences for predicting the response of vegetation to global warming. If ecosystem functioning changes too strongly across climate gradients, it follows that the ecosystem functioning may be too sensitive to changes in the global climate. In this case, our predictions of vegetation changes in response to a warmer future using Earth system models would be too large. Indeed, in global warming experiments, adding temperature acclimation of photosynthesis and respiration to one Earth system model alters the carbon cycle and the biophysical response of the vegetation [Booth et al., 2012, Lombardozzi et al., 2015, Smith et al., 2017]. Without the addition of adaptation and acclimation, our results suggest the ecosystems simulated in these Earth system models will respond too strongly to changes in physical climate due to global warming.

3.5.3 Highly Consistent Precipitation Threshold for Ecosystem Functioning

The rapid transition from strong positive β_{PRECIP} to very weak β_{PRECIP} occurs at nearly the same annual precipitation in all models and observations. The uniformity of the precipitation level at which the transition occurs appears to demark a sharp threshold separating water-limited ecosystems (strong positive β_{PRECIP}: more leaves in a wetter year) from ecosystems with little response to interannual variation in precipitation (relatively weak β_{PRECIP}). The concept of a water-limited (not enough water) and energy-limited (more water than surface incident energy) region is common in literature [Budyko, 1961]. However, we do not have a

strong hypothesis for the consistency across multiple models and observations in the value of mean annual precipitation for this threshold. Our estimated threshold of approximately 1000 mm/year of precipitation separating water limited from energy limited regimes is similar to thresholds in previous studies [Swann et al., 2016, Guan et al., 2015, Malhi et al., 2009]. In addition, we note that the extent of these water-limited and energy-limited regions approximates the region described in Nemani et al. (2003) as light limited. In climates with temperatures above 20°C, precipitation correlates strongly with an aridity index derived from dividing precipitation by the potential evaporation from the shortwave energy incident on the surface [Quetin and Swann, 2017]. Though not explanatory, the threshold of 1000 mm/year concurs with an aridity index of approximately 0.5 (two times the potential energy to evaporate water as there is water from precipitation for evaporation). We note that the threshold in precipitation extends down to temperatures of 0°C for most models and observations. We lack an explanation at this time for the consistency of value for this threshold and suggest it as an avenue for future study.

3.5.4 Spread in Amplitude of β_{PRECIP} - Consequences for Feedbacks in Dry Climates

The broad pattern of β_{PRECIP} in climate space is very similar across models and observations but the amplitude of the maximum positive β_{PRECIP} (more leaves when wetter) in dry climates varies considerably. This variation in amplitude could determine the strength of ecology-climate feedbacks for a particular climate. For example, Charney (1975) proposed a feedback where a decrease of relatively dark (low albedo) vegetation results in decreased rainfall. The brightening of the surface causes the surface to cool due to absorbing less shortwave energy. The cooler surface then produces less uplift, resulting in less rainfall. In a dry climate with positive β_{PRECIP} (more leaves when wetter) this describes a positive feedback, as less rainfall will lead to fewer dark leaves and even less rainfall. However, the likelihood of being able to create this feedback with a large enough change in surface albedo will depend on how strong the change is leaf area is for a particularly dry year - i.e. the strength of β_{PRECIP}. From our analysis, half the models have larger values of β_{PRECIP}

than observations in dry climates and half have smaller values of β_{PRECIP}. We suggest that models with particularly high β_{PRECIP} in dry climates may have a larger feedback to natural or climate change induced changes in the annual rainfall than we would expect from observations.

The spread in the amplitude of β_{PRECIP} may also be related to acclimation and adaptation, similar to the gradient of β_{TEMP} across mean annual temperature. The representation of a varying stomatal conductance serves as a form of acclimation of the vegetation to vary water supply, and atmospheric dryness, but other adaptations and acclimations are not dynamic. It is possible that in the real world, vegetation is altering other hydrologic characteristics, such as the size of xylem, on a seasonal basis during growth. However, as there is a spread in the amplitude of β_{PRECIP} in the models that is both stronger and weaker than the observed, it is apparent that these missing processes do not provide a consistent effect on the β_{PRECIP}.

3.6 Conclusion

The majority of the 10 Earth system models we analyze here reproduce the broad pattern of ecosystem functioning: both the interaction of vegetation with temperature (β_{TEMP}) and precipitation (β_{PRECIP}) - across climate space. An exception to this general agreement is that the majority of models produce negative β_{TEMP} (more leaves when cooler) in hot-wet climates, where observations show a mild positive β_{TEMP}. This disagreement is particularly concerning for representing and predicting global carbon storage as these hot-wet regions contain a disproportionate amount of global above ground biomass [Saatchi et al., 2011]. This disagreement is not observed in β_{PRECIP}.

We hypothesize that the lack of representation of adaptation and acclimation of vegetation in models results in larger year-to-year variations in leaf area than occurs in the real world as well as the amplified change of ecosystem functioning across climate. Our analysis suggests that simulated photosynthetic performance curves are too steep, and thus simulated plants benefit too much from warmer years in cold climates and lose too much productivity

Table 3.1: Proposed mechanisms driving β.

Mechanism	*EffectonBeta*	*DependenceonClimate*
Photosynthetic Efficiency	(+) β_{TEMP} when colder than optimum	Concave across temperature
Photosynthetic Efficiency	(-) β_{TEMP} when warmer than optimum	Concave across temperature
Respiration	(-) β_{TEMP}	Increasing with temperature
Vapor Pressure Deficit	(-) β_{TEMP}	Exponentially increasing with temperature
Increased Snowfall	(-) β_{PRECIP}	Only occurs in cold climates
Increased Water Supply	(+) β_{PRECIP}	Potential Evaporation Increases with temperature and sunlight
Correlation of Temperature and Sunlight	(+) β_{TEMP}	Decreasing with increasing precipitation
Correlation of Rainfall and Clouds	(-) β_{PRECIP}	Increasing with increasing precipitation

in warmer years in hot climates. We find a strong agreement across models and observations for a threshold between water-limited ecosystems and energy-limited ecosystems at an annual precipitation of 1000 mm/year, as observed in β_{PRECIP}. Due to the strong agreement between observations and models on this threshold, more detailed analysis of the simulated mechanisms that control this threshold could help determine the real-world mechanisms behind it.

A stronger response of simulated ecosystem functioning to interannual variations of climate compared to observations leads us to suggest that estimates of the response of vegetation to physical climate changes due to increased atmospheric CO_2 may be too large. In particular, we have identified that additional research is needed to determine which process - high respiration costs, decreases in photosynthetic efficiency at high temperatures that are too large, high carbon costs of atmospheric water demand, or too little increased sunlight during warmer years - result in less leaves during warmer years in hot wet climates. Incorporating and improving process details - i.e. acclimation and adaptation - into Earth system models is critical for predicting the carbon cycle, hydrological cycle, and terrestrial surface energy balance in the sparsely observed regions of the globe and novel climates we expect from global warming.

Table 3.2: Summary of models.

Model	*Institute*	*LandModel*	*LandModelReference*	*MainReference*
canESM2	Canadian Center for Climate Modeling and Analysis, BC, Canada	CLASS2.7 and CTEM1	[Verseghy et al., 1993] and [Arora et al., 2011]	[Arora et al., 2011]
CESM1-BGC	National Center for Atmospheric Research Boulder, CO, USA	CLM4	[Lawrence et al., 2011]	[Gent et al., 2011]
GFDL-ESM2M	Geophysical Fluid Dynamics Laboratory, United States	LM3	[Dunne et al., 2012]	[Dunne et al., 2012]
HadGEM-ES	Met Office Hadley Center, Exeter, Devon, UK	JULES and TRIFFID	[Cox, 2001] and [Clark et al., 2011]	[Collins et al., 2011]
IPSL-CM5A-R	Institut Pierre Simon Laplace, Paris, France	ORCHIDEE	[Krinner et al., 2005]	[Dufresne et al., 2013]
MIROC-ESM	Japan Agency for Marine-Earth Science and Technology, Japan; Atmospheric and Ocean Research Institute, Japan	MATSIRO and SEIB-DGVM	[Sato et al., 2007]	[Watanabe et al., 2011]
MPI-ESM-LR	Max Planck Institute for Meteorology, Hamburg, Germany	JSBACH	[Knorr, 2000]	[Giorgetta et al., 2013]
NorESM1-ME	Norwegian Climate Center, Norway	CLM4	[Lawrence et al., 2011]	[Iversen et al., 2013]
bcc-csm1-1	Beijing Climate Center, China Meteorological Administration	BCC_AVIM1.0	[Ji et al., 2008]	[Wu et al., 2013]
BNU-ESM	Beijing Normal University Earth System Model	CoLM	[Ji and Dai, 2010]	[Ji et al., 2014]

Table 3.3: Systematic variation across climate gradients.

$Model/Obs$	$Slope(\%LAI/°C/°C)$	$Intercept(°C)$	r^2	$DiffSlopew/outliers$	$MaxValue(\%LAI/mm)$	$Threshold(mm/year)$	r^2
Observations	-0.14	-5.1	0.28	No	0.05114	1106	0.83
canESM2	-0.56	2.76	0.46	Yes	0.04430	1132	0.17
CESM1-BGC	-0.76	-0.71	0.52	No	0.01349	521	0.16
GFDL-ESM2M	-0.56	-2.05	0.24	Yes	0.08273	1067	0.28
HadGEM-ES	-0.32	0.72	0.18	No	0.07154	1027	0.46
IPSL-CM5A-R	-0.25	4.7	0.09	No	0.11506	1382	0.44
MIROC-ESM	0.9	-2.49	0.12	No	0.30583	1109	0.47
MPI-ESM-LR	-0.32	6.95	0.76	No	0.12696	765	0.54
NorESM1-ME	-0.84	0.14	0.38	No	0.02303	876	0.09
bcc-csm1-1	-0.3	1.44	0.69	No	0.03173	980	0.59
BNU-ESM	-0.66	5.3	0.18	No	-0.05296	1171	0.36

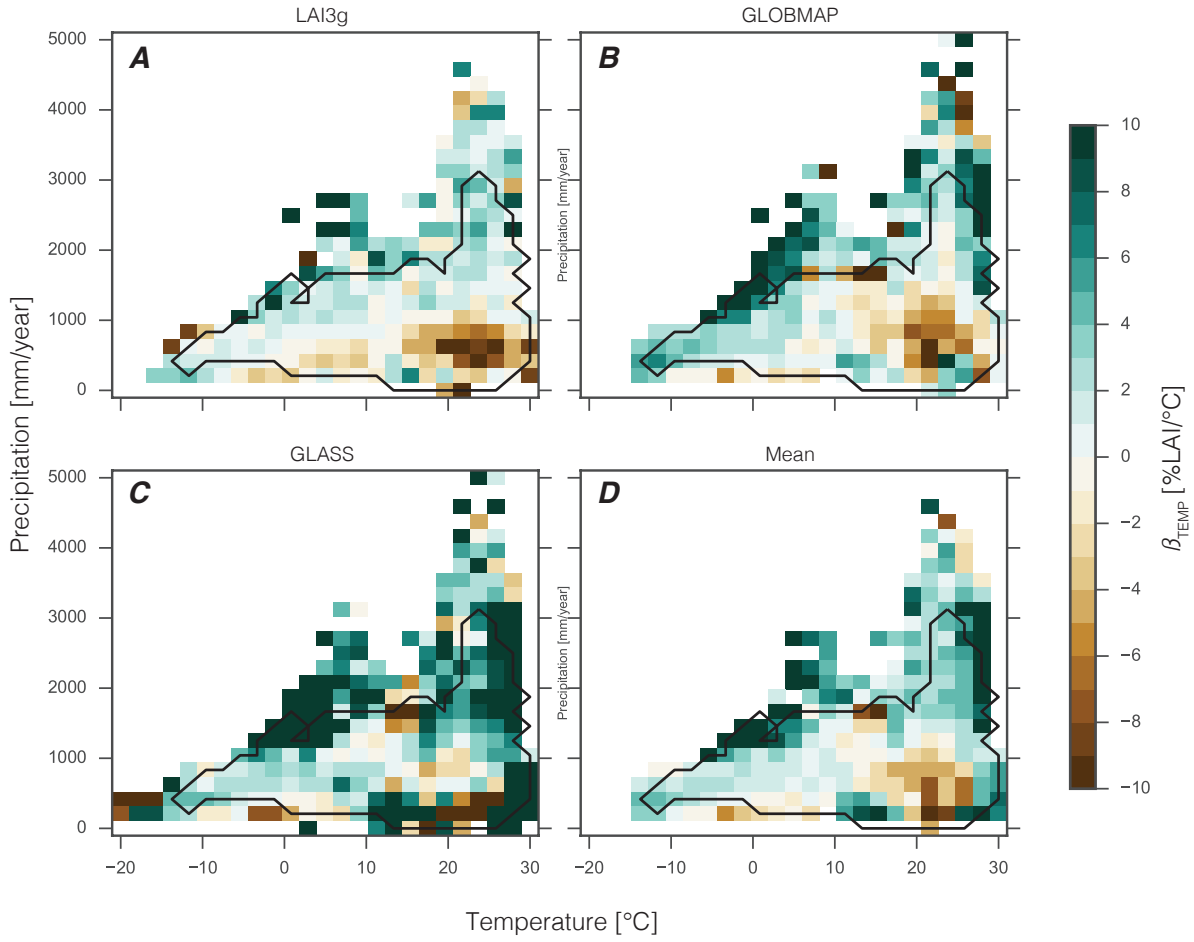

Figure 3.1: β_{TEMP} aggregated in climate space derived from LAI from (**A**) LAI3g, (**B**) GLOBMAP, and (**C**) GLASS, and (**D**) the mean of all three.

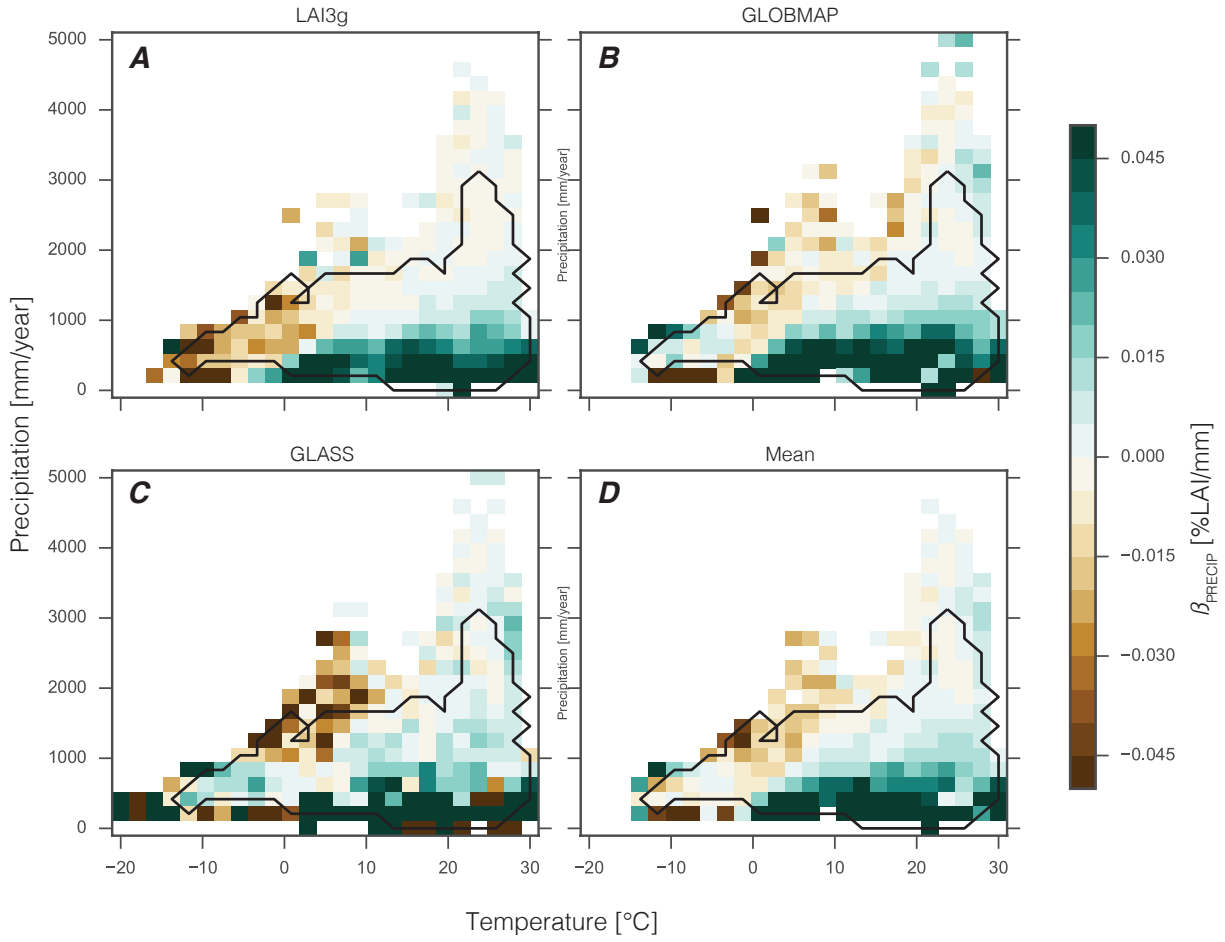

Figure 3.2: β_{PRECIP} aggregated in climate space derived from LAI from (**A**) LAI3g, (**B**) GLOBMAP, and (**C**) GLASS, and (**D**) the mean of all three.

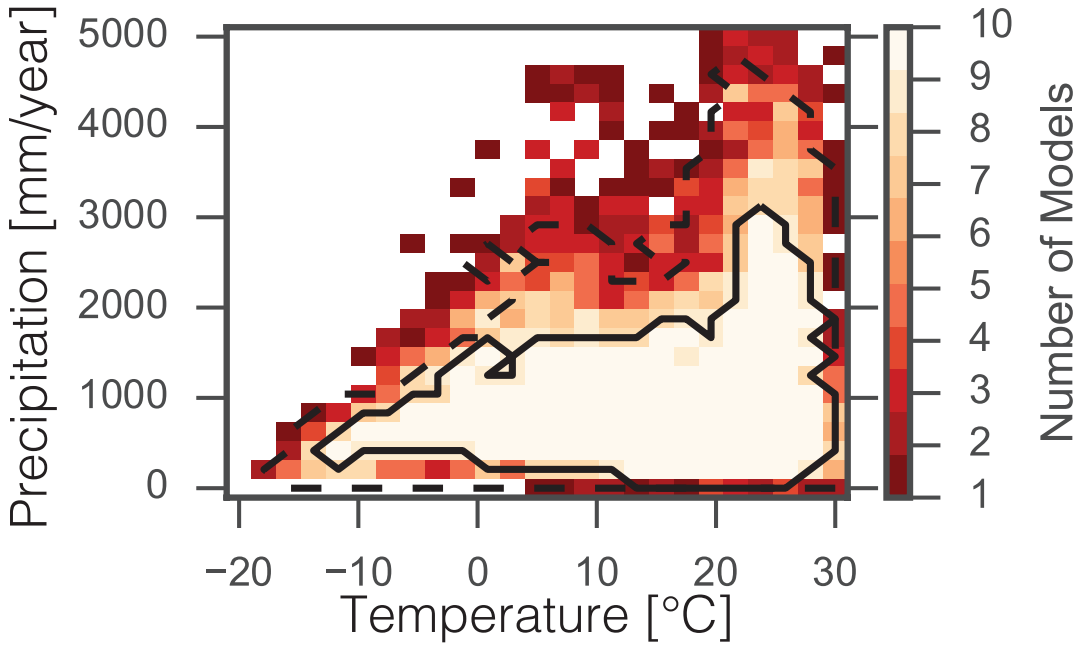

Figure 3.3: Number of models, out of 10, that represent each binned space in Mean Annual Temperature and Mean Annual Precipitation Space. Black contour shows the maximum extent of climate space in observations.

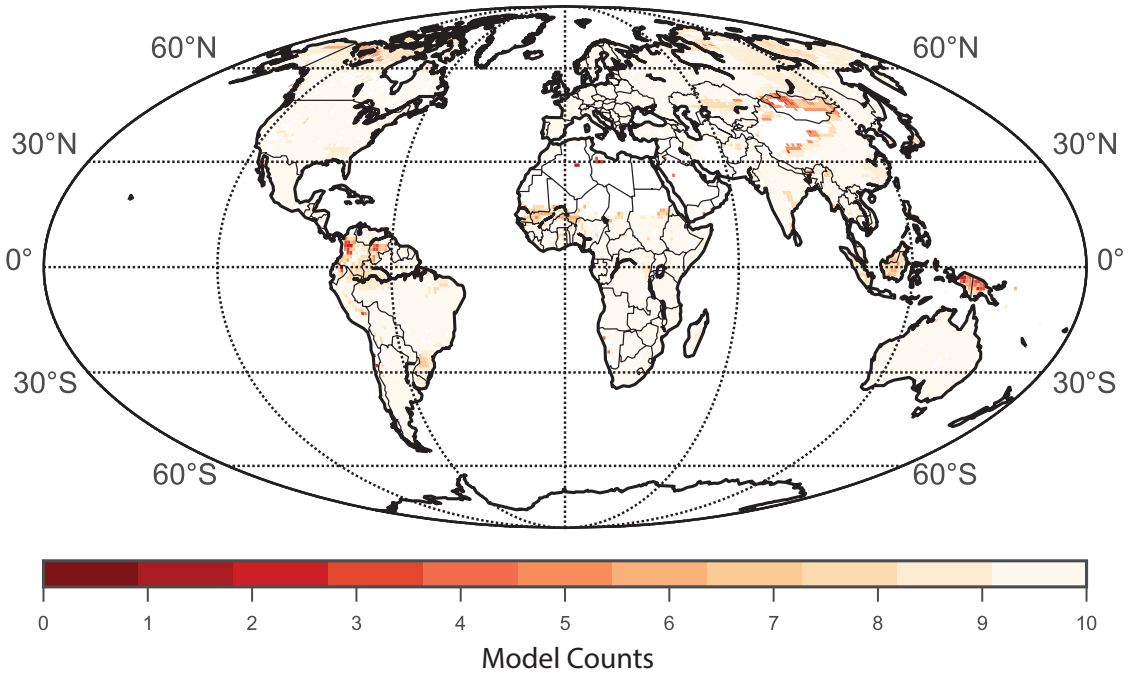

Figure 3.4: Number of models, out of 10, that represent each binned space in Mean Annual Temperature and Mean Annual Precipitation Space. Projected on to a spatial map using observed values of Mean Annual Temperature and Mean Annual Precipitation.

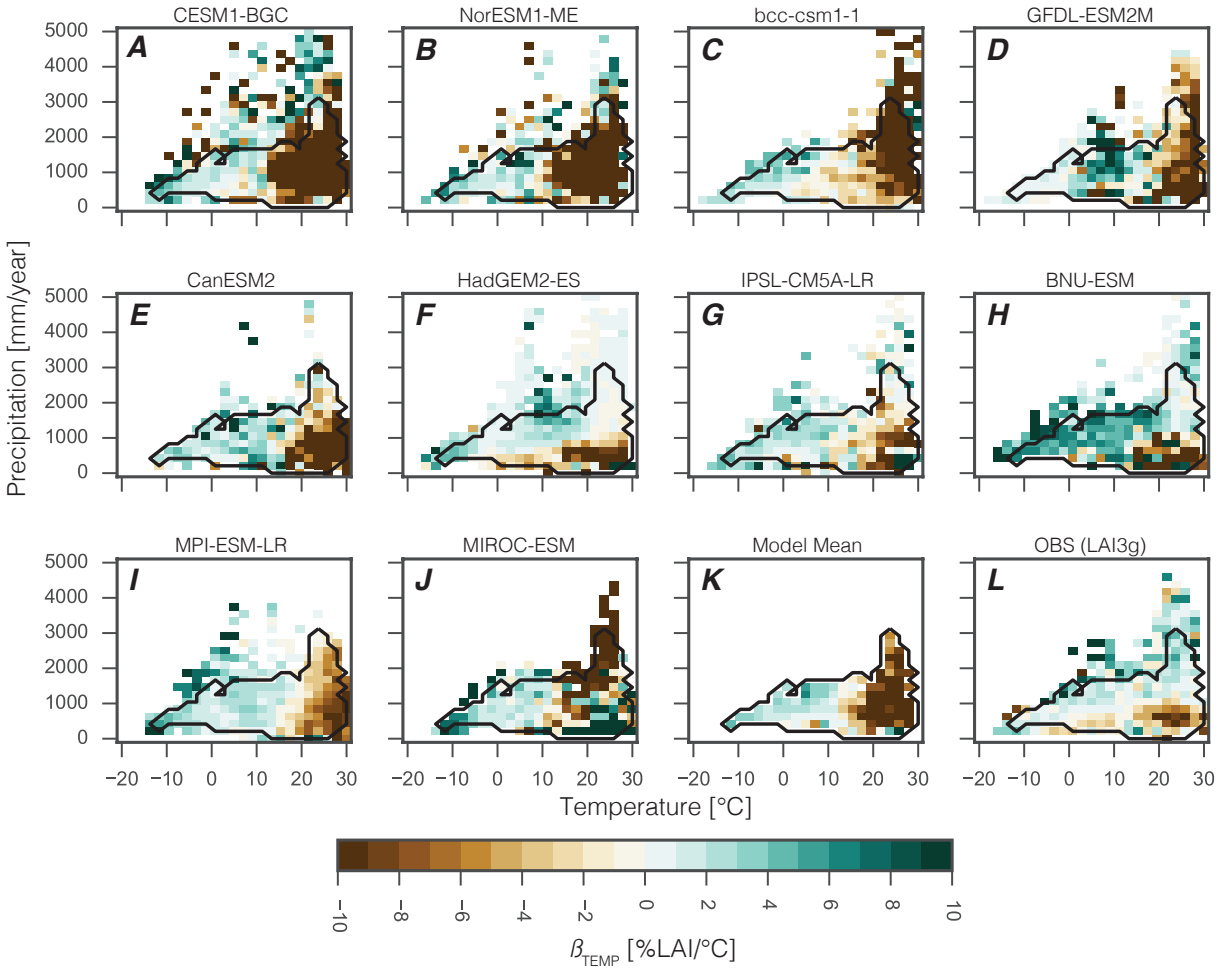

Figure 3.5: β_{TEMP}aggregated in climate space for (**A-J**) CMIP5 models, (**K**) the mean of those models, and (**L**) LAI3g observations. Contours represent the extent of observations (black line) and climate space represented in all models (dashed black line).

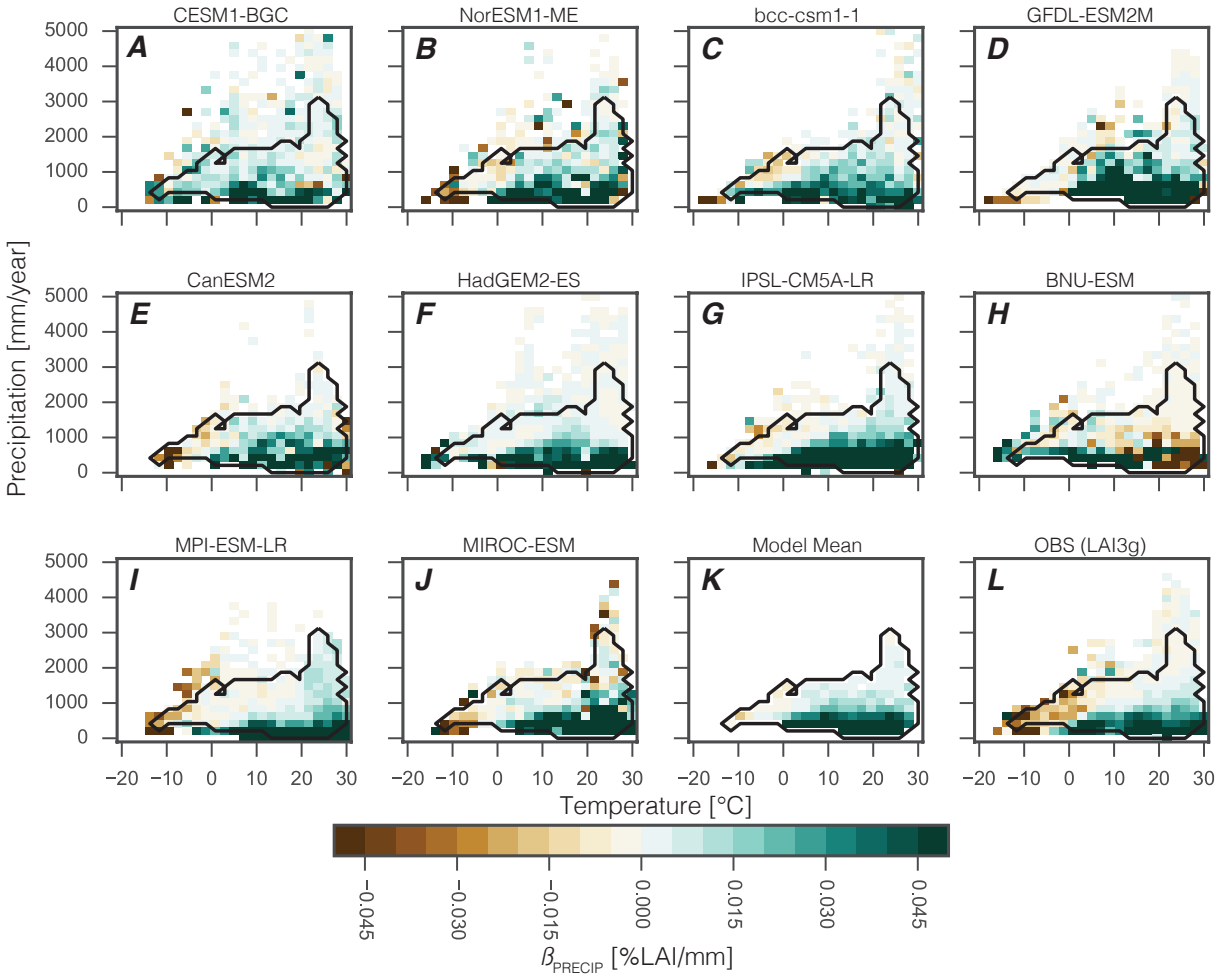

Figure 3.6: β_{PRECIP} aggregated in climate space for (**A-J**) CMIP5 models, (**K**) the mean of those models, and (**L**) LAI3g observations. Contours represent the extent of observations (black line) and climate space represented in all models (dashed black line).

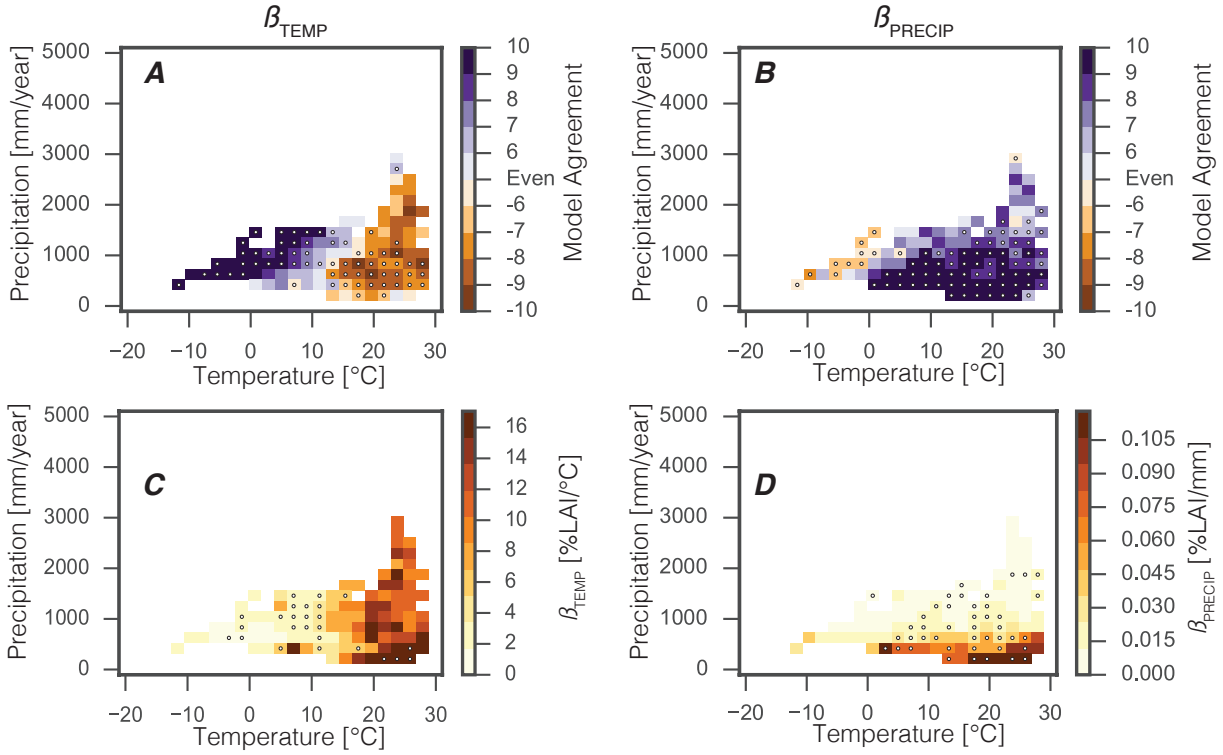

Figure 3.7: The number of models that agree in sign for (**A**) β_{TEMP} and (**B**) β_{PRECIP}. The standard deviation across models for (**C** β_{TEMP} and (**D**) β_{PRECIP}. Where the majority of models have a negative Beta colors are brown, where positive β colors are purple (A,B). Dots indicates majority of models agree in sign with observations (A,B) and the observations are included with two standard errors of the models (C,D)

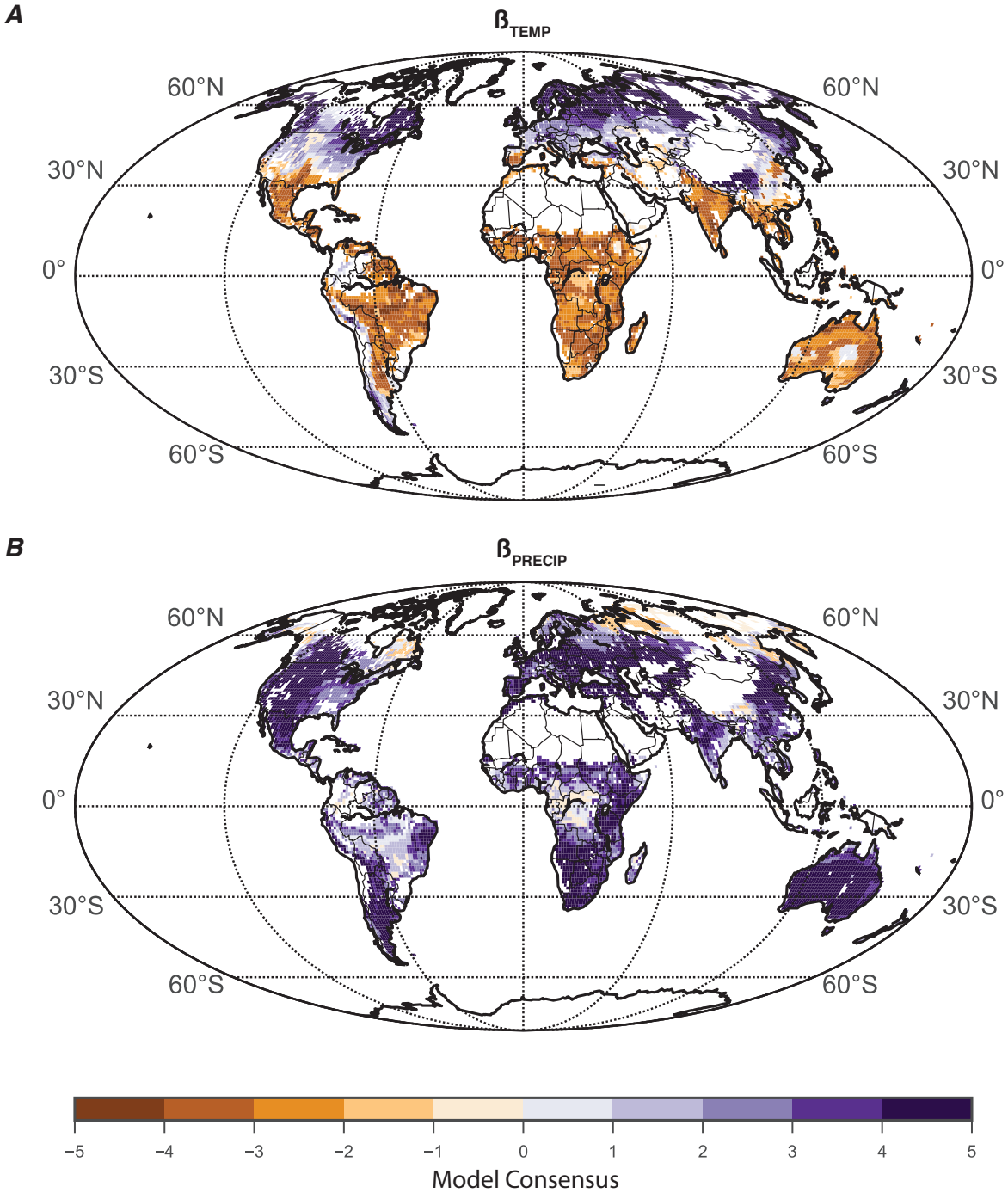

Figure 3.8: The number of models that agree in sign for (**A**) β_{TEMP} and (**B**) β_{PRECIP}. Where the majority of models have a negative Beta colors are brown, where positive β colors are purple (A,B). Projected on to a spatial map using observed values of Mean Annual Temperature and Mean Annual Precipitation.

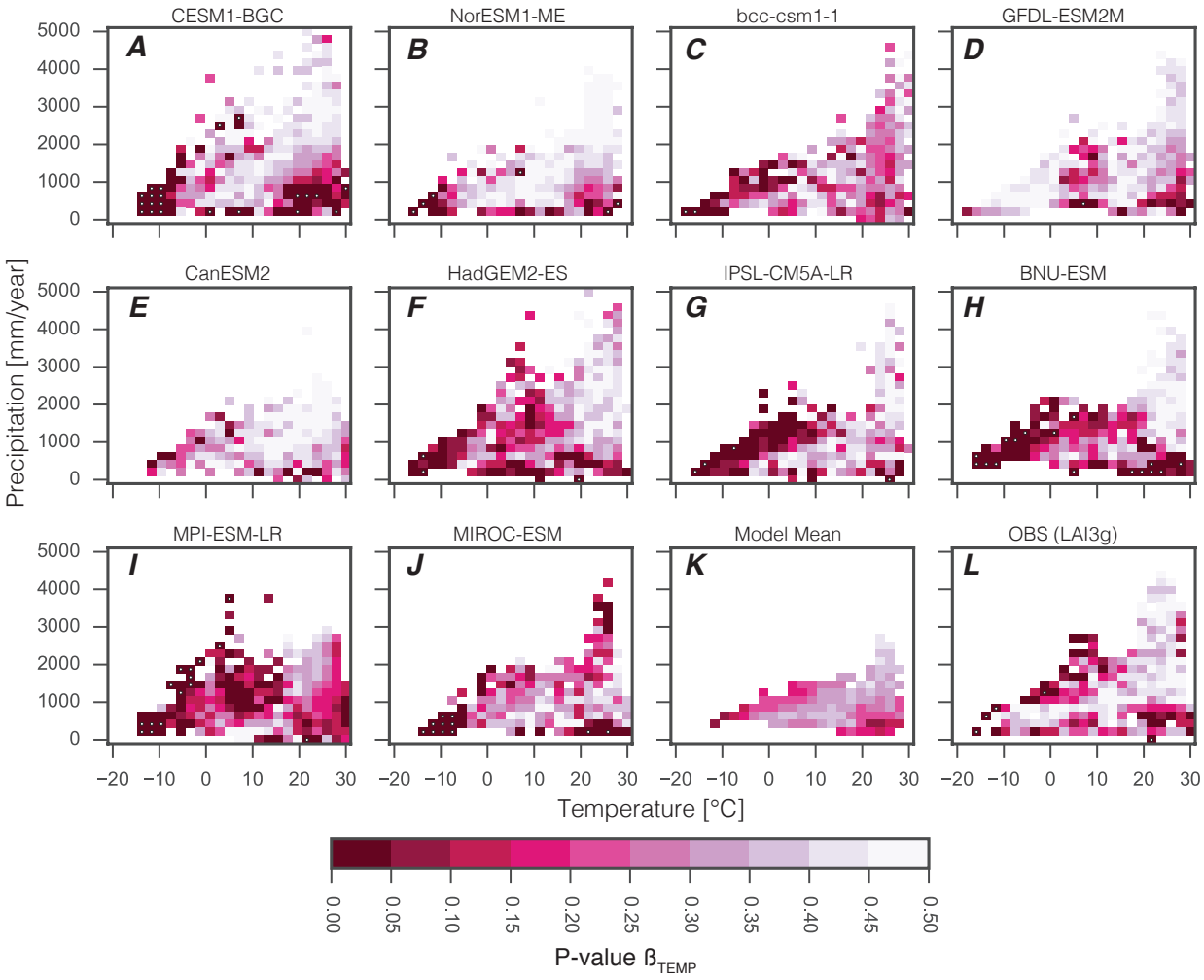

Figure 3.9: P-value of mean β_{TEMP} of each bin in climate space for (**A-J**) CMIP5 models, (**K**) the mean of those models, and (**L**) LAI3g observations. Dots signify field significance per Wilks 2016.

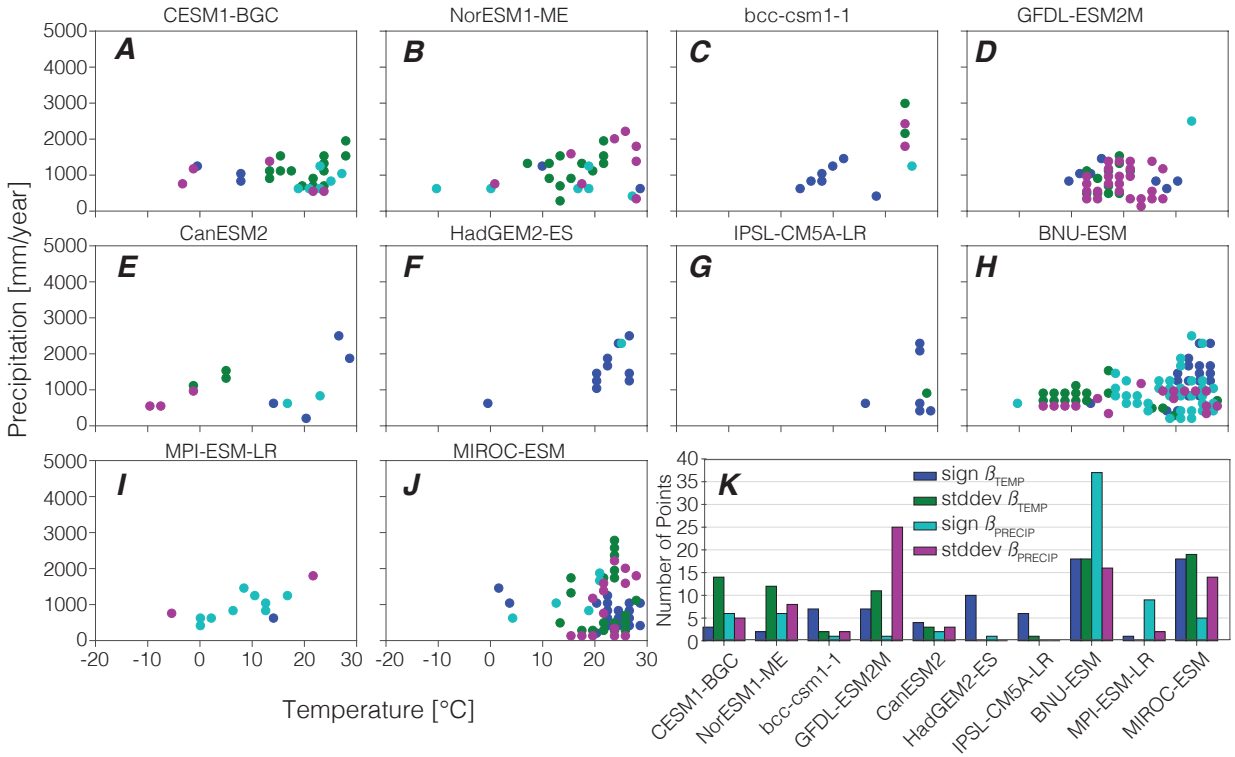

Figure 3.10: Mean annual temperature and Mean annual precipitation bins that are outliers in the sign (disagree with 8 or models in sign) and the standard deviation (outside two standard deviations of the mean) of β_{TEMP} and β_{PRECIP}. (**A-J**) CMIP5 models, (**K**) Summary of number of bins outliers. Colors per the legend. Points jittered for clarity.

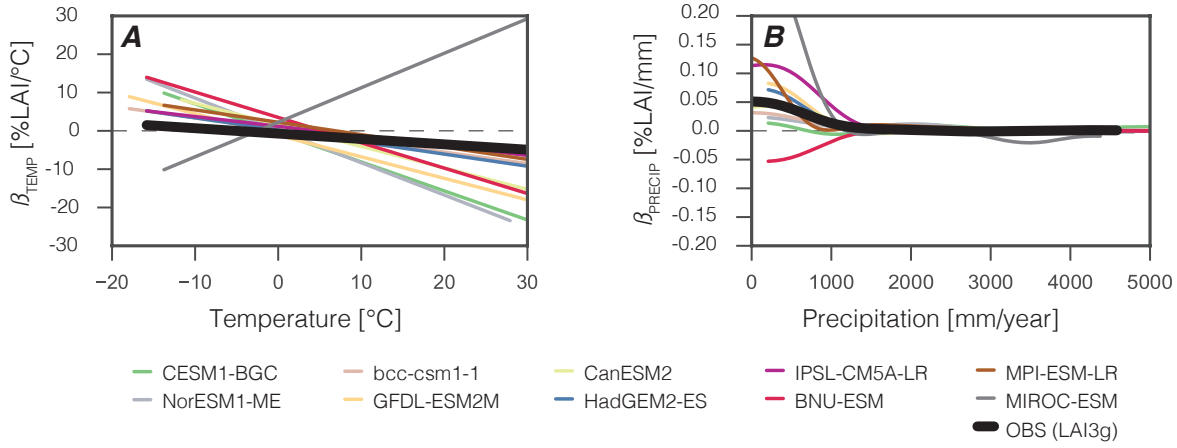

Figure 3.11: (**A**) A linear fit of the climate bins between 100mm/year and 1000mm/year across the global gradient of temperature for 1997-2011 β_{TEMP}. (**B**) An interpolated and smoothed line of the climate bins between 20C and 30C across the global gradient of precipitation for β_{PRECIP} 1997 - 2011. Each line is a different model (see legend). LAI3g observation (black line).

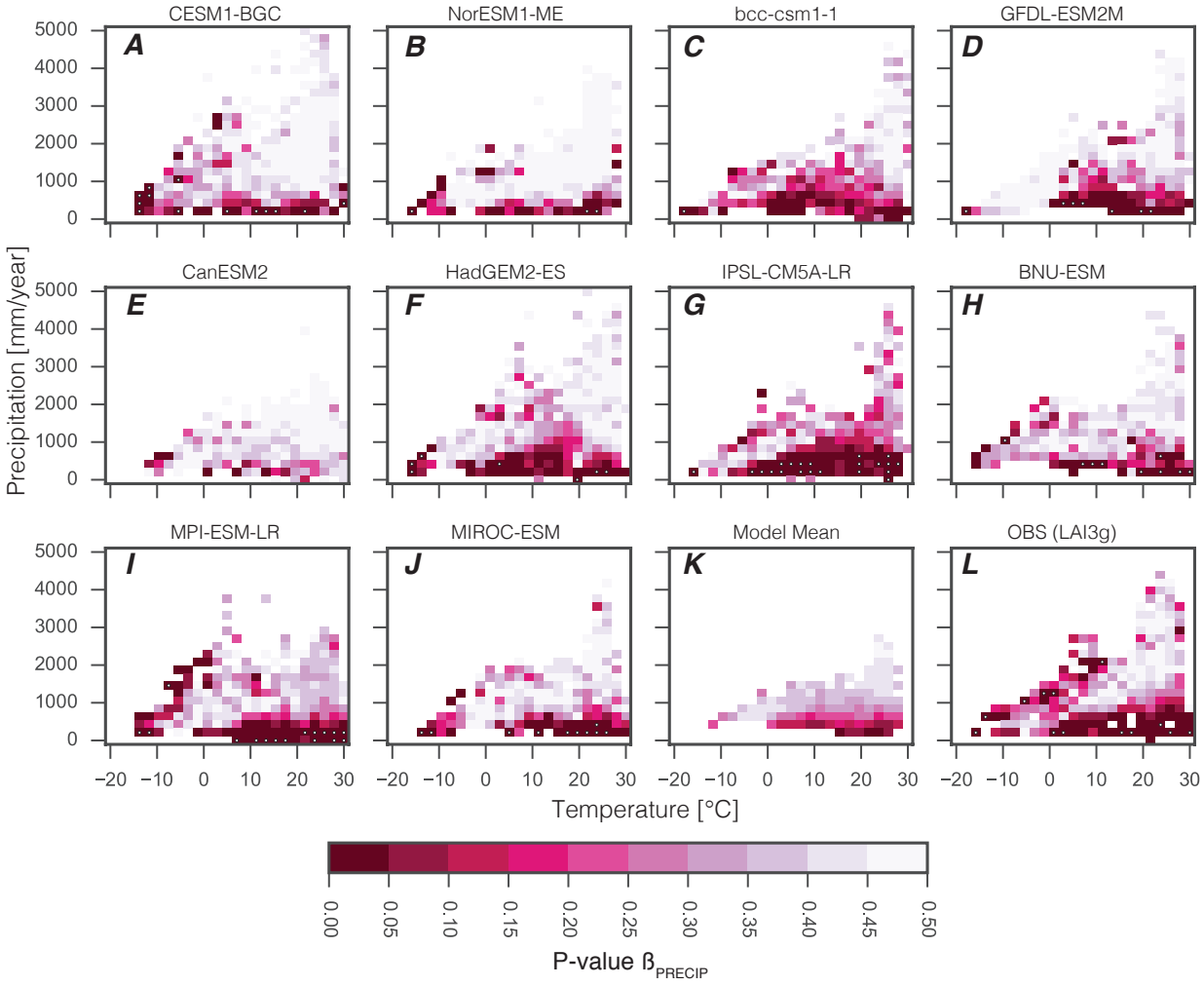

Figure 3.12: P-value of mean β_{PRECIP} of each bin in climate space for (**A-J**) CMIP5 models, (**K**) the mean of those models, and (**L**) LAI3g observations. Dots signify field significance per Wilks 2016.

Chapter 4

FEEDBACK BETWEEN SURFACE AND ATMOSPHERIC WATER VAPOR DRIVEN BY TEMPERATURE IN THE DRY SEASON IN THE AMAZON

4.1 Abstract

The physical environment in a place shapes the vegetation there, but vegetation also has the potential to shape the environment, e.g. increased photosynthesis and transpiration moisten the atmosphere. These two way interactions create the potential for feedbacks between vegetation at the physical environment. In this chapter we investigate how ecoclimate interactions-the influence of the climate on vegetation and the influence of vegetation on the climate-change across seasons in the Amazon basin. We use observations of solar induced fluorescence from the Orbiting Carbon Observatory 2 (OCO2) to statistically analyze the sensitivity of fluorescence to synoptic variations in temperature and precipitation. In addition to studying the sensitivity of vegetation to climate across seasons, we use OCO2 measurements of total column water vapor (TCWV) and CO_2 concentration (XCO_2) to investigate the influence of the Amazon basin vegetation on the CO_2 concentration and water vapor of the atmosphere leaving the basin [Eldering et al., 2017, Nelson et al., 2016]. Our analysis identifies a weak control of vegetation activity on the outflow of water vapor from the Amazon basin within the limits of these observations, and the preeminence of temperature in driving the surface flux of water into the atmosphere during the dry season. We establish a statistical relationship between fluorescence (as a proxy for vegetation photosynthesis), temperature, and precipitation, as well as the difference between the outflow of atmospheric water vapor from the inflow water vapor, basin fluorescence, temperature, and precipitation.

4.2 Introduction

The physical climate and the biosphere are coupled together at the Earth's surface through exchanges of energy, momentum, water, and, among other molecules, CO_2. In locations where there is strong coupling in both directions, the biosphere to the climate, and the climate to the biosphere, there is the potential for ecoclimate feedbacks. For example, in the Amazon basin, previous work has shown that a large fraction of precipitation over land is considered recycled. Water evaporates from the ocean, precipitates over the Amazon basin and is then returned to the atmosphere through evapotranspiration to precipitate again. Thus recycling enhances precipitation amounts. Plants require this precipitation to grow and the observations of precipitation recycling provide evidence that the plants play a strong role in mediating how much water is returned to the atmosphere. The water recycling in the Amazon basin is critical to maintaining inland humid forests in the Amazon. Estimates show that evapotranspiration from the Amazon basin is responsible for between 30% and 50% of the rainfall in the Amazon and up to 70% of the rainfall in the La Plata basin region in Brazil [Drumond et al., 2014, van der Ent et al., 2010, van der Ent and Savenije, 2011, Satyamurty et al., 2013, Eltahir and Bras, 1994, Dominguez et al., 2006].

Photosynthesis and surface water fluxes are coupled by plant regulation of transpiration rates through stomatal control. Thus, we expect that as water recycling is related to evapotranspiration, recycling will also be related to photosynthesis through the exchange of water for CO_2 from the atmosphere. Previous work has estimated the amount of additional precipitation due to recycling of evapotranspiration in the Amazon basin through reanalysis, but has not explicitly shown the relationship between photosynthetic activity and increased water vapor in the atmosphere, or resolved variations across seasons [Drumond et al., 2014, van der Ent et al., 2010, van der Ent and Savenije, 2011, Satyamurty et al., 2013, Eltahir and Bras, 1994, Dominguez et al., 2006]. The evidence of strong water recycling in the Amazon basin is also suggestive that there should be strong ecoclimate feedbacks on carbon cycle through the exchange of water and CO_2 in photosynthesis.

In this chapter we analyze variations in atmospheric water vapor, atmospheric CO_2, and Amazon basin photosynthesis to determine the ecoclimate interactions in the Amazon forest. We address how the seasonal change in mean climate shapes the interactions, and when there is a potential for ecoclimate feedback. We focus on the Amazon basin for two reasons. First, there is a strong expectation of ecoclimate feedbacks in the hydrological cycle due to the role of recycled precipitation. Second, changes to the Amazon forest have large consequences for the global carbon cycle, being both a large sink of CO_2 from the atmosphere, as well as storing a large amount of carbon in above ground biomass [Baccini et al., 2017, Saatchi et al., 2011]. Any changes in the functioning of the Amazon as a carbon sink and a region of carbon storage will alter the concentration of atmospheric CO_2 globally. A better understanding of interactions and feedbacks between climate and vegetation will help provide information to constrain our understanding of carbon storage in the Amazon and how it might change under climate change.

Previous work, including my own, using both observations and models, has shown that the sensitivity of vegetation to climate changes with the change in mean annual climate across the globe [Quetin and Swann, 2017, Green et al., 2017, Martin G. De Kauwe et al., 2016, Chu et al., 2016, Rafique et al., 2016, Seddon et al., 2016, Wu et al., 2015, Piao et al., 2009, Jung et al., 2011, Beer et al., 2010, Xiao et al., 2011]. Generally these studies analyze observed variations in the sensitivity of vegetation to climate across the whole globe or global climatic gradients, and are limited to interannual variations in vegetation [Quetin and Swann, 2017, Seddon et al., 2016, Wu et al., 2015].

In this chapter, we focus on the sensitivity of vegetation to synoptic variations in temperature and precipitation, and how these relationships vary between seasons in the Amazon basin. We analyze observations of fluorescence, a remote sensing observation related to photosynthesis, from the Orbiting Carbon Observatory (OCO2). The advantage of using observations from OCO2 is that the data has a low noise measurement of fluorescence, and has a relatively high spatial resolution compared to many other data sources. Retrievals of fluorescence are only possible under cloud free conditions, making the Amazon basin a

challenging location to retrieve data. High spatial resolution sampling increases the number of observations available by increasing the probability of cloud-free pixels. Thus, our analysis provides a detailed look at the sensitivity of vegetation in a region with a limited number of in situ measurements, and frequent clouds blocking satellite remote observations [Schimel et al., 2014].

Plant fluorescence is as an emission of light in particular wavelengths that occurs during photosynthesis, and is presumed to be proportional to photosynthetic rates. Thus it provides an observation that has a direct functional relationship with photosynthesis. As photosynthesis converts sunlight into sugars, a small part of that absorbed energy is emitted as fluorescence with wavelengths between 660nm and 850nm for chlorophyll a [Sun et al., 2017]. There is still uncertainty about how directly fluorescence relates to photosynthesis across environments and biomes, but it has been measured to correlate with photosynthetic rates and Gross Primary Productivity (GPP) [Sun et al., 2017, Porcar-Castell et al., 2014]. For this work, we will generally interpret fluorescence as proportional to photosynthesis and GPP.

The Amazon ecosystem is fed by moisture that flows in off of the Atlantic Ocean, transverses the Amazon basin exchanging moisture with the surface through precipitation and evapotranspiration, and then exits the Amazon basin to the South [Drumond et al., 2014, Satyamurty et al., 2013]. In addition to measuring fluorescence, the primary measurement of OCO2 is the measurement of XCO_2, and a related measurement of TCWV. With these measurements we can measure how processes of precipitation, temperature, and photosynthesis alter the CO_2 and water vapor content of the air as it passes over the Amazon basin.

The exchange of CO_2 and water during photosynthesis, as well as the observations of high rates of water recycling in the Amazon basin provide mechanisms and evidence for a strong influence of the vegetation on the atmosphere over the Amazon basin [van der Ent et al., 2010]. Air flow over the Amazon basin is relatively constrained and predictable, providing a direct link between the atmosphere leaving the basin, and processes occurring in the basin [Satyamurty et al., 2013]. Previous work has estimated the hydrological cycle in the Amazon

basin as well as the season origin and flow of water vapor over the Amazon basin [MARengo, 2006]. In this chapter we expand on previous work that studies the seasonality of CO_2 flux in the Amazon [Alden et al., 2016, Parazoo et al., 2013]. Our work establishes a statistical link on the seasonality of ecological interactions and the potential for feedbacks between changes in the atmosphere and vegetation.

4.3 Methods

We combine satellite observations of fluorescence, precipitation, atmospheric CO_2, and atmospheric water vapor, along with reanalysis of winds and two-meter temperatures to investigate the interaction of vegetation and the atmosphere over the Amazon basin. We use fluorescence as a proxy for photosynthesis and create multi-linear models relating synoptic variations in photosynthesis to variations in temperature and precipitation. We then use dominant season wind patterns to relate changes in atmospheric CO_2 and to TCWV to synoptic variations in the fluorescence, temperature, and precipitation over the Amazon basin.

4.3.1 Atmospheric Water Budget

Our statistical models are based on the concept of the atmospheric budget for water or CO_2. The budget is based on the idea that air enters the basin from a prescribed region, air is altered by exchanges with the land surface as it passes over the Amazon basin, and then leaves the basin in a prescribed region (Equation 4.1 and 4.2). This is a highly idealized view of the dynamics of water vapor and CO_2 across the Amazon basin, but will serve as the basis of a first look at how the Amazon basin alters the atmosphere transiting across it. Using the available observations we generate a water budget based on the follow assumptions. First, we assume that all water transverses the basin in the same time. Second, the spatial distribution of OCO2 sampling is representative of the mean for upwind, downwind and Amazon basin. Third, the area of the upwind and downwind sampling is representative of the amount of water (CO_2) fluxed into and out of the basin along each boundary. And fourth, air only

enters the basin along the upwind boundary and only exits along the downwind boundary. Using these assumptions we can write a budget as if water and CO_2 can only enter and leave through convection, or through processes contained in the basin, yielding Equation 4.1 and Equation 4.2:

$$TCWV_{out} * A_{out} = TCWV_{in} * A_{in} - P * A_{basin} * dt + ET * A_{basin} * dt + error \quad (4.1)$$

$$CO2_{out} * A_{out} = CO2_{in} * A_{in} - GPP * dt * A_{basin} + Respiration * dt * A_{basin} + error \quad (4.2)$$

In these equations, A is the area of observation for downwind regions (A_{out}), upwind regions (A_{in}) and area of Amazon basin (A_{basin}), dt is the lag between 'in' and 'out' atmospheric columns. For the water budget, precipitation (P) removes water from the atmosphere, while evapotranspiration (ET) returns water to the atmosphere. For the carbon budget, Gross Primary Productivity (GPP) removes CO_2 from the atmosphere, while Respiration (R) returns CO_2 to the atmosphere. Our model makes the assumption that all air parcels enter the basin in a prescribed region, exit the basin in a prescribed region, and take the same time to traverse the basin for a given season (dt). In reality, the possibility of each air parcel taking much different paths across the Amazon basin makes constraining an estimate of the water budget from the perspective of the atmosphere difficult. However, the connections from the water budget create testable hypotheses about how different observable aspects of the Amazon basin, and downwind air should relate.

4.3.2 Data

Orbiting Carbon Observatory 2

Soundings from the Orbiting Carbon Observatory 2 (OCO2) were used as observations of atmospheric CO_2 concentration (dataname: 'xCO_2', units: ppm), surface pressure (dataname: 'psurf', units: hPa), 757 nm fluorescence (dataname: 'fs', units: W/m2/um/sr) and total column water vapor (dataname: 'tcwv', units: kg/m2) from version 7 'OCO2_LtCO2' files from https://oco.jpl.nasa.gov/science/OCO2DataCenter/.

Global Precipitation Measurement

Daily observations of precipitation (dataname: precipitationCal, unit: mm/day) gridded at 0.1 degree by 0.1 degree resolution from the NASA Global Precipitation Measurement (GPM) were used [Hou et al., 2013]. We used data from version 04 '3B-DAY.MS.MRG.3IMERG' and downloaded files from https://pmm.nasa.gov/data-access/downloads/gpm.

ERA-Interim

ERA-Interim (ERA) reanalysis dataset gridded at 0.75 degree by 0.75 degree used for two-meter temperature (dataname: 't2m', units: Kelvin) and surface winds (dataname: u10, v10, units: m/s) [Dee et al., 2011].

World Resource Institute Watersheds

The World Resource Institute (WRI) map of watersheds was used to collect data over the humid forest of the Amazon basin. Data was downloaded from:

http://www.fao.org/geonetwork/srv/en/metadata.show?id=30914&currTab=simple.

Global Land Analysis and Discovery Tropical Biomes

The Global Land Analysis and Discovery (GLAD) biomes map was used to identify the boundaries of the humid forest inside of the Amazon basin. Data was downloaded from:

http://www.glad.umd.edu/dataset/gfm/globaldata/global-data.

4.3.3 Data Aggregation

All data were collected into three regions: the humid forests of the Amazon basin, the area upwind of the Amazon (inflow), and the area downwind of the Amazon (outflow) (Figure 4.1). The upwind and downwind regions were roughly sized with the distance air would travel in the five day sampling period, but are fixed in time, while the average wind speed is variable by season (Figure 4.2). The humid forest of the Amazon was defined as the humid forest biome that falls within in the Amazon watershed. The upwind region was defined as an area where winds (derived from ERA Interim) pointed into the Amazon watershed on average through out the year. The collection regions were made approximately as far across as the distance traveled by an air parcel in five days at the mean wind speed of the region. The downwind region was similarly defined for the part of the Amazon basin where the wind was out of the basin.

OCO2 data were aggregated into pentad averages by taking the mean of all satellite soundings (soundings occur at 13:30 local time) over five days of collection time. Five days was chosen as the amount of time necessary to retrieve soundings with sufficient spatial coverage across the basin. We were able to generate 181 pentad averages for the three regions (upwind, downwind and over the amazon basin) from 2014-09-08 to 2017-02-24, nearly 2.5 years of data. The beginning of the time series is limited by the launch of OCO-2, while the end date is limited by the availability of processed precipitation data from GPM. In our model of the sensitivity of vegetation we use climate data sampled by collecting variables from the same day of the OCO2 sounding that were closest in latitude and longitude to the OCO2 sounding, and then aggregating these values into pentad averages. In our model of the sensitivity of the atmosphere water vapor and CO_2 to the Amazon basin we used all of the points in the three regions, but removed pentads with limited numbers of observations in them, each pentad had to have more than 100 soundings for the upwind region, more than 200 for the Amazon basin, and more than 50 for the downwind region. The threshold of

soundings, which we deemed to be insufficient data coverage, was roughly based on the area of each region.

4.3.4 Filtering datasets

The data was filtered to separate the slow changing seasonal cycle from more synoptic scale variation in climate and vegetation. To perform the filtering we first linearly interpolated the data across removed or missing pentads and then performed a forward and back filter with a 2nd order butterworth filter 0.08 of the Nyquist frequency (in this case a period of 125 days). We used the python signal processing tool kit, scipy.integrate, scipy.signal.

4.3.5 Sensitivity of Vegetation to Climate Variability

We create a model of the sensitivity of vegetation to climate variations by using a multi-linear statistical model. We use climate observations that are closest in space to the OCO2 observation. We aggregate the observations into a time series of five-day means (pentads). We then use the high-pass filter on the timeseries to remove seasonal variation in the multi-linear statistical model. In our model fluorescence is the independent variable (Fs) and we determine the regression coefficients for the high frequency variations of two-meter temperature the day of each OCO2 observation (T_{1d}), and the mean of precipitation for the 10 days before the observation in fluorescence including the day of the observation (P_{10d}) (Equation 4.3):

$$Fs = \beta_o + \beta_{T1d} T_{1d} + \beta_{P10d} P_{10d} \tag{4.3}$$

We performed the multi-linear regression for the entire time series, as well as independently in each season: December-January-February (DJF), March-April-May (MAM), June-July-August (JJA) and September-October-November (SON). We calculated the variance explained by the entire model, as well as the uncertainty of each regression coefficient using

statsmodel.py, with 95% certainty bounds plotted at two times the standard error . The regression coefficients represent the sensitivity of photosynthesis (as observed through fluorescence) to five day variations in the climate. For example, a positive β_{T1d}, would be more photosynthesis over five days during warmer five day periods.

4.3.6 Regression Partitioning of Variance in downwind TCWV and xCO_2

We also build a model of the outflow of water vapor and CO_2 from the Amazon basin. Similar to the approach above, we used a multi-linear statistical model with down wind total column water vapor ($TCWV_{out}$) or atmospheric CO_2 concentration ($xCO2_{out}$) as the independent variable. In this case, our goal is to determine how much of the variance in outflow of water or carbon is explained by each predictor variable, so we removed the means and standardized all of the time series (by dividing by the standard deviation). We include a time lag between the inflow and outflow quantities (water vapor and CO_2) based on an estimate of the time it would take upwind air to travel across the basin for the average wind speed for that season. The lags used are: 15 days - full year, 10 days DJF, 20 days MAM, 10 days JJA, and 25 days SON. The appropriate travel time across the basin is an area of uncertainty, however, we tried different lags and found that they only changed the amplitude of the results modestly. The predictor variables are spatial averages over the Amazon basin and temporal averages over the period of time between the lag of the inflow and outflow. In this way, the predictors are averages of the basin values during the time the atmosphere is assumed to be over the basin. For example, for a 10-day lag, the 10 days of fluorescence after the time of the inflow would be averaged together. In this way, the $TCWV_{in}$ (or $xCO2_{in}$) comes before $TCWV_{out}$ (or $xCO2_{out}$) in time, while the Amazon basin fluorescence (fs), precipitation (Precip) and temperature (TEMP) are averages that approximate the amount of time the air is over the basin. The multi-linear model predicting $TCWV_{out}$ is represented by Equation 4.4, while the model predicting $xCO2_{out}$ is represented by Equation 4.5.

$$TCWV_{out} = \beta_{wvo} + \beta_{wvtcwv} TCWV_{in} + \beta_{wvprecip} Precip + \beta_{wvfs} fs + \beta_{wvtemp} TEMP \quad (4.4)$$

$$xCO2_{out} = \beta_{CO2o} + \beta_{CO2CO2} xCO2_{in} + \beta_{CO2fs} fs + \beta_{CO2temp} TEMP \quad (4.5)$$

The regression coefficients were calculated on the high pass time series independently for the full year, as well as for each season (DJF, MAM, JJA, SON). Larger regression coefficients represent greater importance for the variance of atmospheric characteristics downwind of the Amazon basin. For example, a large $\beta_{wvprecip}$ suggests that increases in rainfall results in less water in the atmosphere downwind. Uncertainties for each regression coefficient are estimated as described above.

4.4 Results

4.4.1 Hydrological Cycle Over the Amazon

Water laden air generally enters the humid forest of the Amazon Basin from the Northeast and exits in the South. Escape of water vapor to the West is primarily blocked by the Andes (Figure 4.1). We quantify our analysis of vegetation activity using three collection regions: the first is the area of inflow North of the Amazon basin, second is the humid forest in the Amazon basin, and the third is the outflow to the South (Figure 4.1). Over the Amazon basin itself there is a seasonally varying surface wind that coincides strongly with seasonal temperature and precipitation. The winds are relatively high in the wet season (DJF) when there is a large amount of precipitation and cooler temperatures (Figure 4.2, Figure 4.3). The winds are also high during the dry season (JJA) when the precipitation is at a minimum and temperatures are the hottest. Finally, between these two extreme seasons there are three months of relatively weak winds during the transition from wet season to dry season (MAM) and the transition from dry season to wet season (SON). The fluorescence in the Amazon basin generally follows the precipitation (Figure 4.3). The surface winds are descriptive of

the circulation across the Amazon basin, however a more appropriate description of flow in future work would be the water vapor or CO2 weighted winds. These weighted winds more faithfully describe the dynamics steering the flux of water vapor and CO2 across the basin.

The wet-cool season (DJF) is weakly related to stronger fluorescence observed by OCO-2 (Figure 4.3). Our observations show two relatively different seasonal cycles of fluorescence between 2015 and 2016. In 2015 fluorescence is similarly strong in both in the wet season (DJF) and the dry season (JJA), whereas compared to a stronger seasonal cycle in 2016, the wet season has relatively stronger fluorescence than 2015, and the dry season has relatively weaker fluorescence than 2015. With only 2.5 years of data it is hard to generalize our results beyond these particular years, which also occur during a strong El Nio from early 2014 through most of 2017 per the Nino 3.4 index.

In addition to seasonality in precipitation, temperature, and vegetation activity over the Amazon basin, there is a strong seasonal cycle in the total column water vapor (TCWV) at both the inflow and the outflow of the Amazon basin that generally mirrors the seasonality of precipitation (Figure 4.3, Figure 4.5). There is a consistent difference the TCWV at the inflow (higher) compared to the outflow (lower) during the hot-dry season (JJA) (Figure 4.5 A).

The concentration of CO_2 over the Amazon basin does not have a clear regular seasonality when detrended (Figure 4.3 B). There is a lot of high frequency variance around the seasonal signal of the concentration of CO_2. At the inflow and outflow of the basin, the temporal trend in CO_2 is clear, along with a few ppm annual cycle in the difference between upwind CO_2 and downwind CO_2 that roughly mirrors the seasonality of fluorescence (larger drop in CO_2 across the basin when fluorescence is high) (Figure 4.5 B).

4.4.2 Observing Forests in the Amazon Basin

Cloud conditions in the Amazon basin vary over the seasons, impacting the ability to successfully retrieve observations from the Amazon basin using OCO2. This seasonality of successful retrievals is evident in the density of observations across the Amazon basin by season (Figure

4.4). During the wet season (DJF) and the transition from the wet season to the dry season (MAM), there is wide area that has low observation counts, particularly in the Northwest of the basin (Figure 4.4 A and B). By contrast, during the dry season (JJA), particularly away from the Northwest, there are many thousands of retrievals (Figure 4.4 C). During the transition from the dry season to the wet season, the number of observations are somewhat biased towards the more mountainous West side of the basin where there are fewer clouds (Figure 4.4 D). Finally, the Southern edge of the Amazon basin has the most successful retrievals for all seasons, but particularly for the dry season (JJA) and the transition from the dry season to the wet season (SON) (Figure 4.4).

4.4.3 Sensitivity of Fluorescence to Precipitation and Temperature

We calculate the sensitivity of fluorescence, a proxy for photosynthesis in the Amazon basin, to variations in temperature and precipitation, all collected into five-day averages with low frequency variations removed (see Methods). The coefficients of the multi-linear regression represent the sensitivity of vegetation to variations in temperature and precipitation. Where the coefficient is positive there is generally more fluorescence when it is warmer the day of the observation (T_{1d}), or rained in ten days prior to the observation (P_{10d}).

We find that the regression coefficients are relatively consistent in sign and magnitude across seasons - though the overall multi-linear regression model explains the most variance in the transition from wet season to dry season (MAM) (36%), while the transition from dry season to wet season (SON) (6%) and the full year (12%) explain a small amount of the overall variation in fluorescence (Figure 4.6). There is more fluorescence during warmer pentads (positive T_{1d}) in every season except for the wet season (DJF) where T_{1d} is relatively small. The rain on the day of the measurement of fluorescence (P_{1d}) has been omitted from the model because it has a small, non-statistically significant effect on fluorescence, while mean precipitation over the last 10 days has a consistent positive effect on fluorescence (P_{10d}). The mean temperature over the last 10 days was omitted has it has a strong correlation with T_{1d} (Figure 4.7). The sensitivity of fluorescence to precipitation is strongest during

the dry season (JJA), and weakest during the wet season (DJF). Regression coefficients for precipitation (P_{10d}) are statistically significant for the full year, as well as in each season except SON, but the uncertainty is too large to statistically distinguish differences in values of P_{10d} between seasons. The regression coefficients for temperature (T_{1d}) are only significant for the full year, while each season are not statistically significant (Figure 4.6).

There are a few notable cross correlations between climate variables that may affect the interpretation of these results. In particular, during JJA, T_{1d} correlates negatively with P_{10d}, such that cooler temperatures occur when there is more rain in the previous 10 days (R2 =-0.36) (Figure 4.7). T_{1d} similarly negatively correlates with P_{1d}. However, JJA is the only season in which P_{1d} and P_{10d} are positively correlated; other seasons show a nearly zero correlation. It would be interesting to investigate the interaction terms between temperature and precipitation, which we leave for future work.

4.4.4 Partitioning Variance of Water Vapor Outflow

The general pattern of wind and total column water vapor flux into the Amazon basin enters from the Northeast (inflow) and exits in the South (outflow). We test the hypothesis that vegetation activity in the Amazon basin has a significant effect on the water vapor in the outflow. To do so, we create a multi-linear regression of precipitation, temperature, fluorescence, and outflow surface pressure to explain the outflow total column water vapor (see Methods). The relative strength of the regression coefficients pertain to the amount of variance explained by each physical process. In addition, the overall variance explained shows in which seasons this linear model is applicable.

The multi-linear model explains an appreciable amount of the variance of downwind TCWV in each season, from MAM (24%) to JJA (61%), while the explanation across the whole year is relatively small (14%) (Figure 4.8). There are a number of statistically significant regression coefficients in the models: upwind TCWV in JJA (positive β_{wvtcwv}), and SON (negative β_{wvtcwv}), precipitation in SON (negative $\beta_{wvprecip}$), fluorescence in DJF (negative β_{wvfs}), temperature in JJA (positive β_{wvtemp}). During the dry season (JJA), increased water

vapor upwind of the Amazon basin is associated with larger outflows of water vapor from the Amazon basin. In addition, increased temperature in the Amazon basin is also associated with increases in the outflow of water vapor from the Amazon basin (Figure 4.8). During the transition from dry season to wet season (SON), larger TCWV upwind of the Amazon basin is associated with reduced outflows of water vapor from the Amazon basin (negative β_{wvtcwv}), while increased precipitation decreases outflows of water vapor (negative $\beta_{wvprecip}$). Finally, in the wet season, increased fluorescence is associated with reduce outflows of water vapor from the Amazon basin (negative β_{wvfs}). During the wet season (DJF), fluorescence also has a negative correlation with the upwind TCWV, downwind TCWV, and basin wide precipitation (Figure 4.9). The transition seasons (MAM, SON) are the only seasons during which upwind TCWV is negatively correlated with downwind TCWV (Figure 4.9).

4.4.5 Partitioning of the variance in xCO_2 outflow

We also identify factors that explain the variance of CO_2 leaving the Amazon basin. We test the hypothesis that the variation in concentration of outflow of CO_2 is due to vegetation activity. To do so, we compare the regression coefficients from a multi-linear regression model including the inflow of CO_2, fluorescence in the Amazon basin, and temperature in the Amazon basin (see Methods). The model explains an appreciable amount of the high frequency variance in CO_2 downwind of the Amazon basin for the wet season (DJF, 48%), the dry season (JJA, 49%), and the transition from dry season to wet season (SON, 20%) (Figure 4.10). Across all seasons increased fluorescence is associated with decreases in down wind CO_2 concentrations (negative β_{CO2fs}) (Figure 4.10). In addition, increases in upwind CO_2 concentrations are also associated with increases in downwind CO_2 concentrations, though it is only relatively large during the dry season (positive β_{CO2CO2}). Finally, increases in temperature are associated with increases downwind CO_2 concentrations (positive $\beta_{CO2temp}$) in the wet season (DJF) and the dry season (JJA).

4.5 Discussion

4.5.1 Consistent Ecosystem Functioning Across Most Seasons

Observations of vegetation behavior across environments generally show that photosynthesis and overall vegetation performance, follows a concave curve across a gradient in an environmental variable[Berry and Bjorkman, 1980]. For a particular environmental condition, increases in, say, temperature are a benefit to vegetation performance (for example, photosynthesis) up to some maximum threshold, after which performance suffers [Berry and Bjorkman, 1980, Day, 2000]. We interpret the regressions coefficients of the multi-linear model of the sensitivity of fluorescence to short term changes in temperature (β_{T1d}) and precipitation (β_{P10d}) along this curve. For example, a positive β_{T1d} is the result of a general increase in fluorescence during a warmer pentad (or in the case of β_{P10d}, a general increase in fluorescence when it has been wetter in the previous 10 days). A positive sensitivity suggests that the vegetation is in an environment that places it to the left of its optimal temperature (or precipitation); otherwise we would expect to see no sensitivity or a negative sensitivity. The lack of response of vegetation to same day precipitation (no statistical significance in P_{1d}) suggests that it takes time for the water from precipitation to become available to vegetation.

We observe that both β_{T1d} and β_{P10d} are consistent in sign (both positive, more fluorescence when warmer or wetter) for every season except the wet season for β_{T1d} (very small), and the transition from the dry season to the wet season for β_{P10d}, where the multi-linear regression doesn't capture very much of the variance in fluorescence. The positive sensitivity of fluorescence to warmer and wetter pentads for most seasons suggests that, even in this hot and wet environment, no season in the Amazon basin is too hot or too wet for vegetation. In most seasons the plants are able to increase photosynthesis given warmer temperatures or wetter conditions, and it is never a detriment. The consistent amplitude of β_{T1d} suggests that the slope of the performance curve is similar across seasons. This way, even though the average temperature of the season is warmer or cooler, variations of temperature around

that mean result in similar sensitivity.

In contrast, the amplitude of β_{P10d} increases with decreasing precipitation from the wet season (DJF), through a transition season (MAM) to the dry season (JJA) (Figure 4.6). This suggests, that the longer it has been since heavy rains, the steeper the performance gets (larger increases in fluorescence for the same amount of precipitation). It is uncertain whether increasing temperatures (and associated sunlight) allow for a greater response of vegetation to the same amount of water, or if during the drier seasons the vegetation photosynthesizes more when water is available. From these observations we can conclude that the optimal temperature and precipitation for the Amazon basin's ecosystem is at least greater than about 29 °C and 9 mm/day.

During the dry season (JJA), when it is relatively hot and dry, β_{P10d} is at its highest relative to other seasons. We hypothesize that β_{P10d} is high because there is little precipitation, and the soil moisture available to vegetation is becoming limited. The loss of the stored moisture in the soil results in any precipitation that does occur driving a strong response from the vegetation. Additionally, the dry season has fewer clouds blocking sunlight compared to any other season (Figure 4.3, Figure 4.4). The relatively warm seasonal temperatures could indicate that vegetation is approaching an optimal temperature where performance is unconstrained by temperature. Although, there is no indication that T_{1d} is decreasing, as we would expect if approaching an optimum in the performance curve. If temperature is not influencing performance, or there is increased sunlight, this could lead to relatively higher β_{P10d} in the dry season. In other seasons, the limits on vegetation are more equally balanced between temperature and water supply, so that the sensitivity to either is muted.

The combination of increasing temperatures, and strengthened β_{P10d} during the relatively hot and dry season could also indicate increased limitations from water stress on the vegetation driven by vapor pressure deficit. On a warmer day, holding relative humidity constant, vapor pressure deficit increases as an exponential function of the temperature. This increase in vapor pressure deficit then increases the atmospheric demand for water from vegetation for the same amount of photosynthesis. Thus, hotter temperatures will increase demand for

water, just as the seasonal precipitation is decreasing. It is notable that β_{T1d} is relatively consistent in amplitude and positive. This suggests that the positive effects of temperature (faster rates of photosynthesis under higher temperatures) offset the expected negative effects of increased temperature through vapor pressure deficit stress even for the dry season when we expect it to have the most influence.

Previous work has suggested that vegetation in the Amazon basin should be light limited, as growing conditions are favorable at most times in temperature and precipitation, but cloudiness in the basin limits light in the wet season [Nemani et al., 2003]. OCO2 overpasses are at 13:30 each day, and fluorescence data is not retrieved on cloudy days. Thus our analysis of OCO2 fluorescence data observations is constrained both in time of day and the cloudiness of that day. Due to only observing photosynthesis on sunny days, it is unlikely that our analysis would show the effects of concomitant changes in sunlight with precipitation (often less sunlight due to cloudiness) and temperature (increased temperatures associated with increased shortwave energy). However, it is notable that, even though seasonally temperature is the lowest during the wet season (DJF), there is almost no sensitivity of fluorescence to temperature in the wet season (DJF). At these cooler temperatures we would expect the vegetation to be most constrained by low temperatures leading to a positive sensitivity. The low T_{1d} is consistent with the vegetation being primarily constrained by another resource such as sunlight. We note that fluorescence is highly dependent on how much incoming sunlight there is due to the light response curve. OCO2 is only observing fluorescence during clear sky conditions, but any variation in sunlight during observations may also be altering the observed fluorescence. We propose is future work to investigate these sensitivities using fluorescence normalized by incoming sunlight as a way separate the effects of temperature and incoming sunlight on photosynthesis.

4.5.2 Incomplete Observation of Amazon basin Photosynthesis

OCO2 observations of fluorescence over the Amazon basin are incomplete due to clouds. If a large amount of photosynthesis occurs in regions where it is not possible to observe flu-

orescence, it is possible to have a large bias in the time series of photosynthesis across the Amazon basin. The largest likely contributor to this would a region with thin clouds that allow for strong photosynthesis but no retrieval of fluorescence. We propose future work to identify the distribution of sunlight across the basin during observation to more clearly describe the potential for bias. A combination of the distribution of sunlight (energy for photosynthesis at the leaf level) and vegetation (scaling factor for the leaf level photosynthesis) across the basin will allow for a more complete estimation of the possible bias present in our estimation of basin wide photosynthesis. In addition to the sparse spatial sampling of photosynthesis, fluorescence is going to be strongly driven by sunlight. Particularly in the case of predicting downwind TCWV, this is a confounding effect due to our expectation of increase evaporation, and transpiration when there is more sunlight. In future work we intend to address this by including sunlight as a predictor in the multi-linear regression.

4.5.3 Photosynthesis and the Atmosphere

During photosynthesis, vegetation exchanges water for CO_2 through the stomata in their leaves. Because photosynthesis and evapotranspiration are tightly linked through stomatal opening, we expect photosynthesis to be linked with the amount of CO_2 and TCWV in the atmosphere. We expect increased photosynthesis to remove CO_2 from the atmosphere (negative β_{CO2fs}) and return water to the atmosphere (positive β_{wvfs}). The consistent negative β_{CO2fs} across seasons is consistent with the absorption of CO_2 during photosynthesis (Figure 4.10. However, the large negative β_{wvfs} during the wet season (DJF) is inconsistent with photosynthesis providing a significant amount of water vapor to the atmosphere (Figure 4.8).

The magnitude of the exchange of CO_2 and water will be moderated by how much photosynthesis there is, what the difference between the atmosphere and the internal leaf concentrations of CO_2 and water are, and what the difference is water vapor pressure is between the leaf and the atmosphere. For CO_2, it is thought this gradient is maintained at a nearly constant difference for biochemical reasons, so that the small changes in CO_2 over our study period should not modify the exchange the water for CO_2 (citation). By

contrast, in most cases the internal leaf water concentration is at 100% saturation at the temperature of the leaf, while the atmospheric water vapor concentration varies, producing a vapor pressure deficit between the leaf and the atmosphere. This vapor pressure deficit is particularly sensitive to temperature through the exponential Clausius-Clapeyron equation, such that for a given relative humidity the vapor pressure deficit is always larger when it is hotter. Due to this relationship, if photosynthesis were held constant, we would expect increases in temperature to return more water to the atmosphere (positive β_{wvtemp}). This is consistent with the significant positive β_{wvtemp} during the dry season (JJA), though other seasons consistently show a weaker negative β_{wvtemp} (Figure 4.8).

We find that the relative importance of variations in upwind TCWV and Amazon basin precipitation, fluorescence, and temperature varies across season. We suggest two possible reasons for why some seasons don't show much response. First, other sources of variance may be larger, so that the atmosphere does not change much from the variables in our multi-linear model. Or, second, that the explanatory variables do not exhibit much dynamic range. For example, if photosynthesis were fluxing a small amount of water compared to the overall change of water in the atmosphere we would not expect a strong regression coefficient.

4.5.4 Photosynthetic Activity Linked to Decreased Downwind Water Vapor During Wet Season

We aim to quantify the contributions to variations in total column water vapor as air passes over the Amazon basin. To do so we partition the drivers of total column water vapor variance on the downwind side of the Amazon basin 4.4 into contributions from temperature, precipitation, and fluorescence. We attempted to account for the variation in the time a parcel of air spends over the Amazon basin by sampling the Amazon basin for a variable amount of time in each season determined by the change in average wind speed over the basin (see Methods). However, this is an imperfect method, as in reality the air parcels entering the Amazon basin do not take the same path (or same time) to cross the basin as is apparent in the wind fields. In addition there is uncertainty from the sparse and spatially varying

sampling of fluorescence over the Amazon basin, CO_2, and TCWV from OCO2 (Figure 4.1).

There are statistically significant effects on total column water vapor variance from upwind TCWV, precipitation, fluorescence, and temperature during different seasons. The negative regression coefficient for precipitation (negative $\beta_{wvprecip}$, less TCWV in the outflow when there is more precipitation) during SON suggests a simple water budget relationship as follows: increased precipitation is responsible for removing more water from the atmosphere, leaving less to exit from the basin downwind. This is in contrast to other seasons where there is weak positive relationship between total column water vapor and precipitation (positive $\beta_{wvprecip}$, more TCWV in the outflow when there is less precipitation), though not statistically significant. The weak and positive response of total column water vapor to precipitation does not match our expectation, and is a motivation for future work applying this statistical analysis to a close water budget from ERA-Interim analysis to improve our mechanistic expectations (see Future Work). For precipitation to increase total column water vapor in the atmosphere, there would need to be a source of water to the atmosphere that is larger than the water lost during precipitation. We hypothesize that increased precipitation could make water stored in the soil more available to the atmosphere. For this to occur, precipitation would have to either increase evaporation from the soil or stimulate transpiration. Though speculative, we propose the following mechanisms: (1) a large amount of the precipitated water is intercepted by leaves and evaporated directly from the canopy, reducing the water deficit from the atmosphere; (2) precipitation wets the top layer of the soil, serving to reconnect capillary action in the soil that had be stopped due to a dry surface soil layer, this has the effect of allowing moisture deeper in the soil to evaporate into the atmosphere; (3) finally, it is possible that vegetation would respond to increased soil moisture with greater transpiration that could liberate more water from deep in the soil than fell as precipitation. We do not find the observations presented here as convincing of these mechanisms, but suggest that looking for increased transpiration and soil evaporation after a precipitation event would be an interesting topic for future research.

We hypothesize that the negative relationship between fluorescence and downwind TCWV

(negative β_{wvfs}) during the wet season (DJF) is due to the bias of OCO2 sampling due to clouds. A strong negative β_{wvfs} is not consistent with an increase in transpiration due to an increase in photosynthesis. In addition, it is plausible that increased precipitation could stimulate photosynthesis, thus leading to a relationship where photosynthesis was increased, and downwind TCWV was reduced due to precipitation. However, β_{wvfs} from the multilinear regression model is calculated 'as if precipitation was held constant'. We propose that downwind TCWV is related to cloudiness, and thus the spatial sampling of the Amazon basin during the wet season (DJF). During the wet season, much of the Amazon basin cannot be sampled due to clouds (Figure 4.4). We propose that high total column water vapor results in clouds over the wettest most productive (high potential fluorescence) parts of the basin. When that water vapor decreases, there are fewer clouds over the relatively wet and productive parts of the Amazon basin. With less clouds due to less water vapor, that pentad sampling of the Amazon basin results in more measurements over more productive vegetation. Thus, when water vapor is relatively low, there is a higher mean fluorescence because of where in the basin is being measured, rather than a measurement of the basin as a whole having strong fluorescence. This measurement bias towards higher fluorescence during lower water vapor days during the wet season is consistent with the observed strong negative β_{wvfs} (Figure 4.8).

Finally, the positive regression coefficient between total column water vapor and temperature (β_{wvtemp}) during the dry season (JJA) matches our expectation for the interaction of temperature with TCWV while (statistically) holding fluorescence, and precipitation constant. We would expect a positive β_{wvtemp} if temperatures, and thus vapor pressure deficits, were higher for the same photosynthesis. The increased vapor pressure deficit should force more water into the atmosphere for the same amount of photosynthesis. The relative strength of β_{wvtemp} during the dry season is also consistent with increased temperatures, as the effect of temperature increases exponentially with temperature. The dry season also has relatively low TCWV, such that smaller fluxes of water from the land could have a larger impact on the variance of the down wind TCWV. Finally, a strong β_{wvtemp}, without a large β_{wvfs}, suggests

that temperature and vapor pressure deficit is driving transpiration during the dry season, rather than photosynthesis.

4.5.5 Photosynthetic Control on Downwind CO_2 Concentrations during MAM

We expect CO_2 to be removed from the atmosphere through photosynthesis over the Amazon basin, and CO_2 to be returned to the atmosphere through respiration. We do observe a seasonal cycle for the drop in CO_2 across the Amazon basin from the inflow region to the outflow that is consistent with increased photosynthesis absorbing more CO_2 from the atmosphere during the wet season (DJF) (Figure 4.5). Additionally, the gradient of CO_2 across the Amazon basin is weakly reversed during the warmest part of the year (JJA), which is consistent with increase respiration (releasing CO_2) due to increased temperatures. On a sub-seasonal time scale, we find that upwind CO_2 concentration, temperature, and fluorescence explain the most variance during the wet season (DJF), and the dry season (JJA) (Figure 4.10).

The influence of fluorescence on outflow CO_2 (β_{CO2fs}) is consistently negative across seasons, with the largest negative regression coefficient during the dry season (JJA). The value of β_{CO2fs} is statistically significant for all seasons except for the transition from the wet season to the dry season (MAM). We hypothesize that the significant negative relationship between CO_2 and fluorescence (negative β_{CO2fs}, less atmospheric CO_2 when there is higher fluorescence) is evidence of photosynthesis removing CO_2 over the Amazon Basin. We suggest that the prominence of this mechanism during the dry season (JJA) is due to relatively broad spatial sampling due to reduced clouds resulting in a fluorescence time series that is strongly representative of the whole Amazon basin. If the relative strength of β_{wvfs} during the dry season is due to sampling bias, it does suggest that a large portion of the photosynthesis in the Amazon basin in other seasons is being missed due to the difficulty of observing the whole basin (Figure 4.4).

In order to increase downwind CO_2, respiration in the biosphere would need to release CO_2 to the atmosphere. Respiration is generally considered to be a function of temperature

and soil moisture, with higher rates of respiration occurring at warmer temperatures and in wetter soils. These conceptual models of respiration coincide with the observed influence of temperature on downwind CO_2 (β_{wvtemp}). Strong positive β_{wvtemp} occurs during the wet season (DJF), when precipitation is high and temperatures relatively low, and in the dry season (JJA) when precipitation is low and temperatures are relatively high (Figure 4.3).

4.5.6 Future Work

The interpretation of the analysis here is dependent on the highly idealized assumptions about the flow of the atmosphere across the Amazon basin (see Methods). It is uncertain that these relationships hold at the 5-10 day timescale over which we are applying our statistical analysis, or whether our observations are adequate to sample the complete variance of water vapor and CO2 flux into and out of the Amazon basin. To develop more confidence in the results of the statistical treatment presented here, a more in depth analysis of the atmosphere dynamics across the Amazon basin is necessary. In future work, we propose to develop a water budget across the Amazon basin using ERA-Interim water vapor, precipitation, evapotransporation, and circulation (Equation 4.4). With the full three-dimensional fields of ERA-Interim we would solve for the flux across the boundary of the Amazon basin on a 3-hourly scale to represent the influx of water vapor in the upwind region, and the exit of water vapor in the downwind region. We then plan to sample and aggregate the ERA-Interim representation of the system in the same way we do with our observations from OCO2. We can then determine whether we expect the water budget closes at the 5-10 day time scale we are applying our statistics. In addition, we will use the more complete water vapor flux from ERA-Interim to improve our estimations of flux in and out of the Amazon from OCO2 observations of total column water vapor. This future work will provide a stronger basis for our expectations for the hydrological dynamics in the Amazon basin.

4.6 Conclusion

We analyzed the newly available observations from OCO2, combined with observations of precipitation, and reanalysis of two-meter temperature to identify seasonal variations in the feedback between the ecosystem and climate in the Amazon basin. We found that, through all seasons, ecosystems appear to be limited by both cold-temperatures and water even though the Amazon basin is one of the warmest and wettest locations on Earth. Water limitation is strongest during the dry season (JJA). These observations are in agreement with a view of an Amazon basin-wide performance curve, where the positive effects of temperature on photosynthetic rates outweigh negative effects of temperature, even during particularly water limited seasons with increased atmospheric water demand. Additionally, the sensitivity of vegetation to both temperature and precipitation is the lowest in the wet season, which is consistent with the hypothesis that cloudiness is also a large constraint. The positive sensitivity of vegetation to warmer temperatures suggests that the potential exists for the Amazon ecosystem to continue absorbing carbon from the atmosphere, while providing water for precipitation in ecosystems downwind of the Amazon basin.

We found correlations between Amazon photosynthesis, and the variability in the outflow of CO_2 that are consistent with photosynthesis having a significant effect on CO_2 concentrations through absorption year round. The negative relationship between fluorescence and down wind TCWV was not consistent with photosynthesis driving increased transpiration. However, holding photosynthesis constant, temperature was strongly related to down wind TCWV during the dry season (JJA), suggesting that transpiration may be more strongly driven by variation in vapor pressure deficit, rather than photosynthesis.

Our analysis is suggestive of the sensitivity of Amazon photosynthesis to climate, and effects of Amazon photosynthesis on downwind CO_2, and possibly TCWV. However, to strengthen the analysis and inference a number of follow on analyses need to be performed. (1) Include shortwave radiation in the estimation of the sensitivity of fluorescence to climate, and the sensitivity of the atmosphere to fluorescence, particularly for TCWV for shortwave

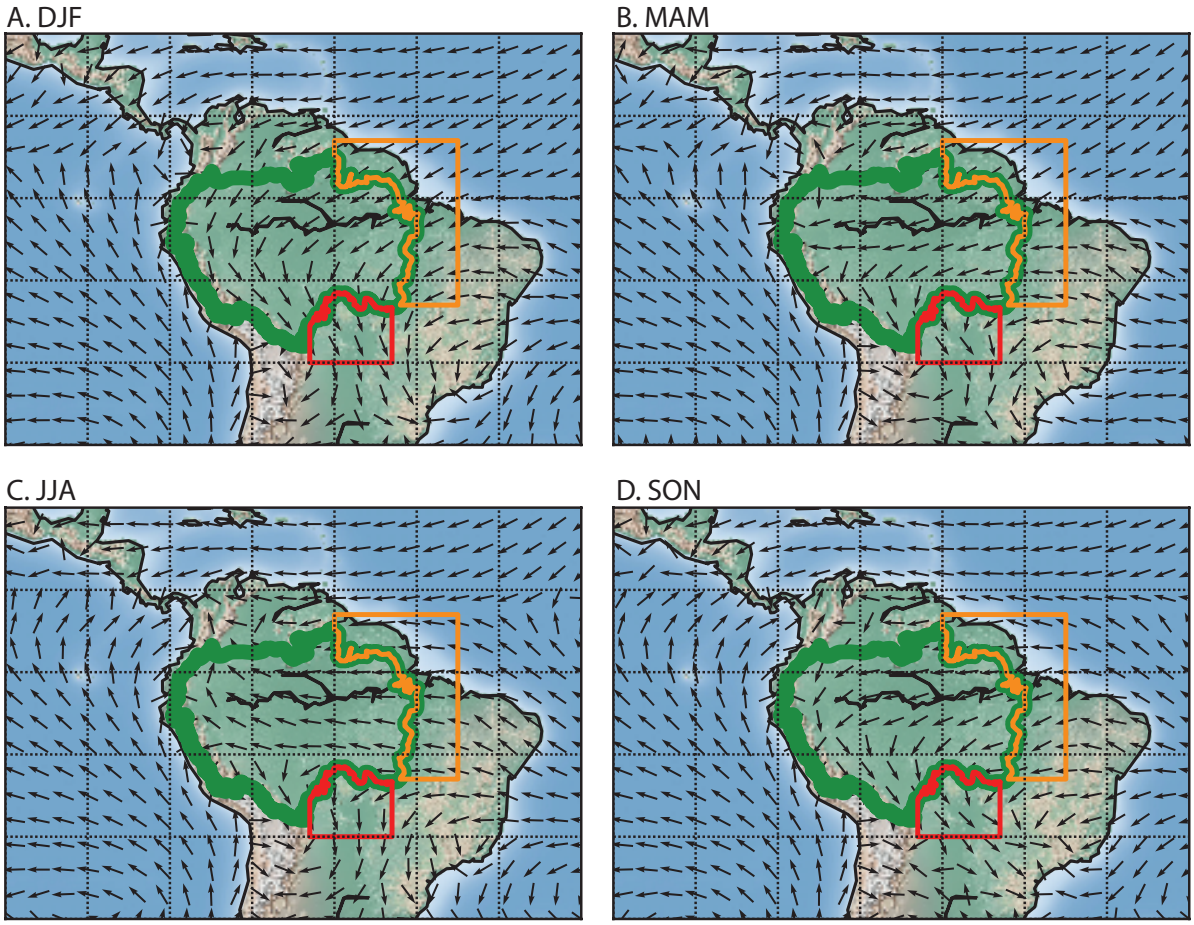

Figure 4.1: Map of study area with normalized winds (black vectors), and regions of data collection are colored outlines, upwind (orange), Amazon basin (green), downwind (red). (**A**) DJF, (**B**) MAM, (**C**) JJA, and (**D**) SON.

radiation is a potentially confounding factor. (2) More completely estimate the potential for bias from the sparse sampling of fluorescence using basin wide maps of leaf area and sunlit vegetation where OCO2 retrievals may still not be possible. (3) Use ERA-Interim to create a water budget to test the statistical analysis and improve our expectations for the statistical analysis considering the time scales being analyzed.

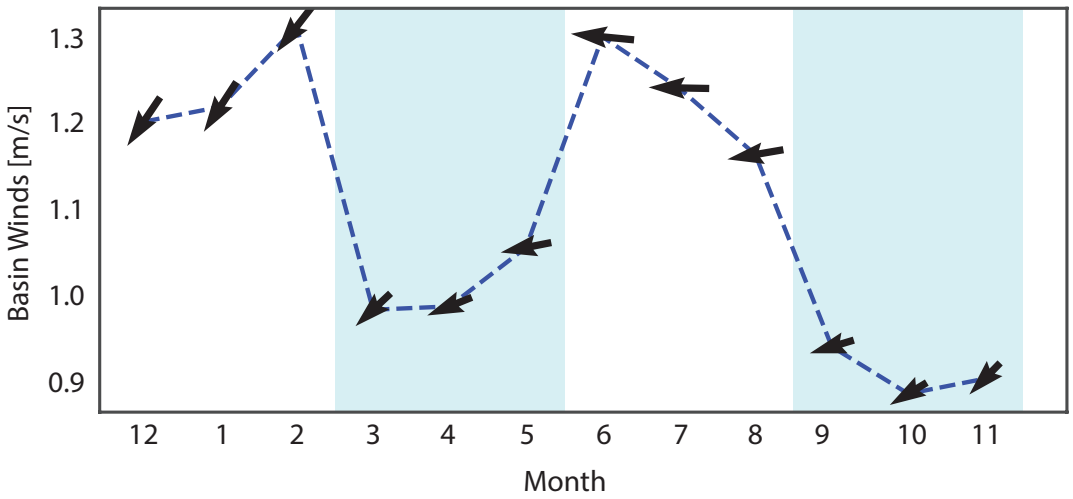

Figure 4.2: Mean winds magnitude and direction over the Amazon basin per month.

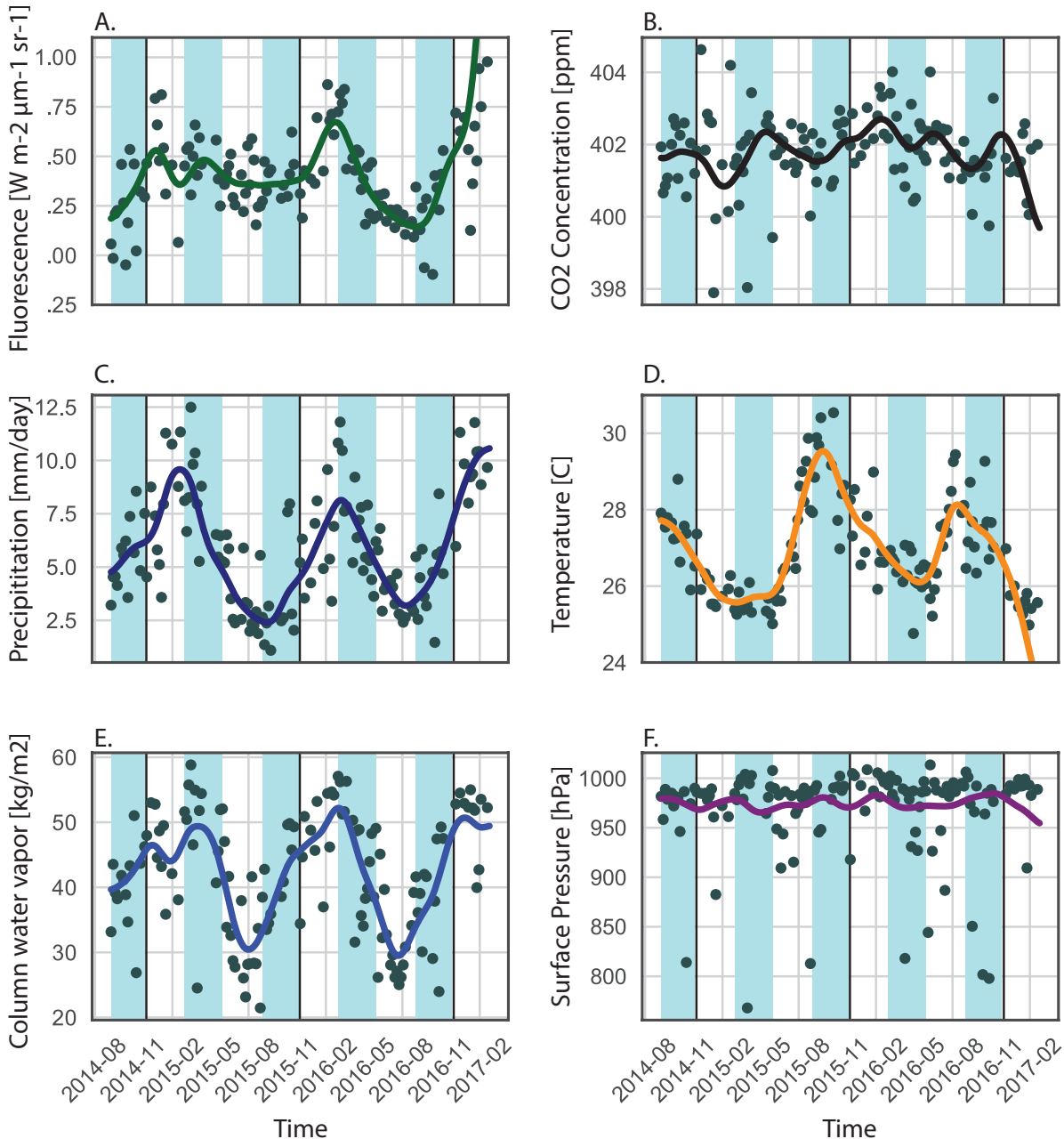

Figure 4.3: Raw observations aggregated into pentads (dots) and filtered observations (lines). Vertical black lines are breaks between years and light blue shading are seasons. (**A**) Fluorescence, (**B**) CO2, (**C**) Precipitation, (**D**) Temperature, (**E**) Total Column Water Vapor, and (**F**) OCO2 surface pressure.

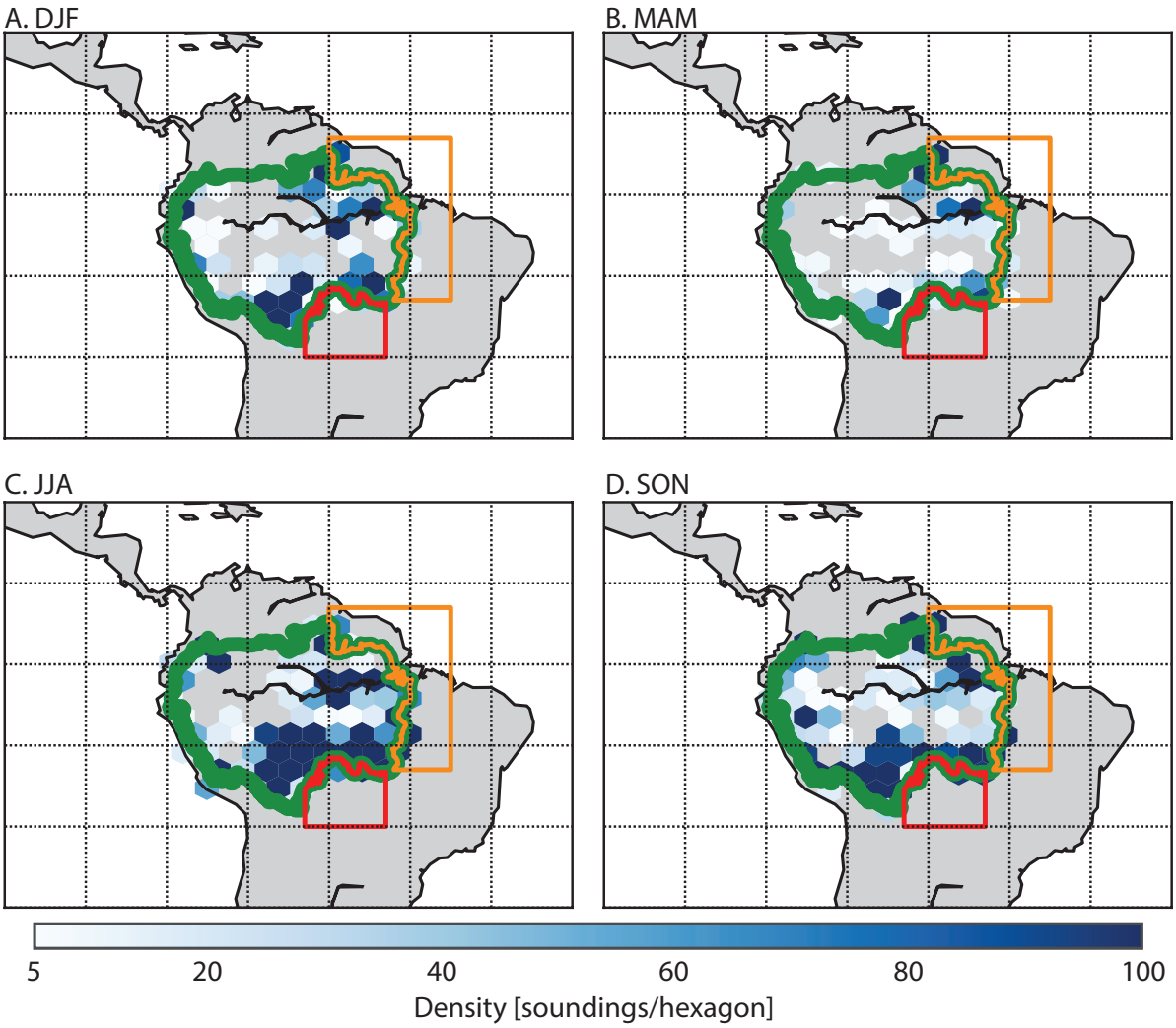

Figure 4.4: Density of observations over the Amazon basin. (**A**) DJF, (**B**) MAM, (**C**) JJA, and (**D**) SON. Regions of data collection are colored outlines, upwind (orange), Amazon basin (green), downwind (red).

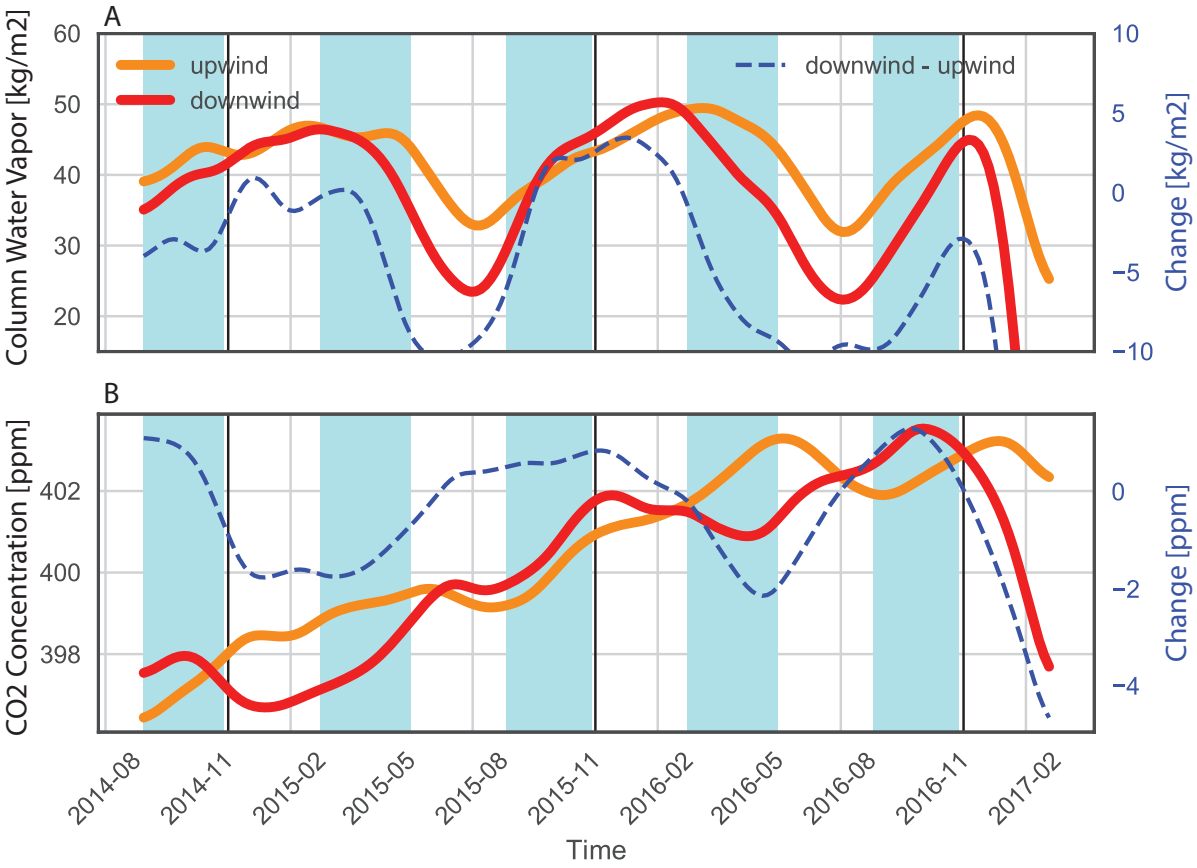

Figure 4.5: Smoothed time series of upwind (orange line) and downwind (red line) observations and the difference between them (dashed line). (**A**) Total Column Water Vapor, and (**B**) CO_2.

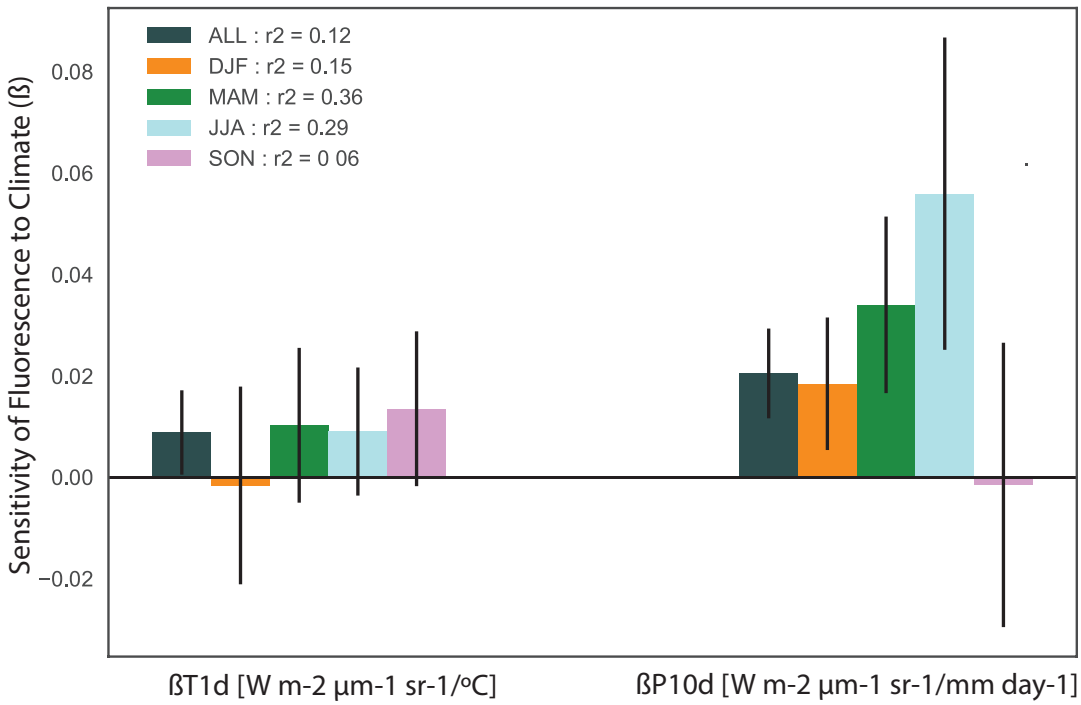

Figure 4.6: Regression coefficients (bars) of the sensitivity of fluorescence to climate for different seasons (colors). Error bars are 95% (two times the standard error). Legend reports variance explained for multi-linear model.

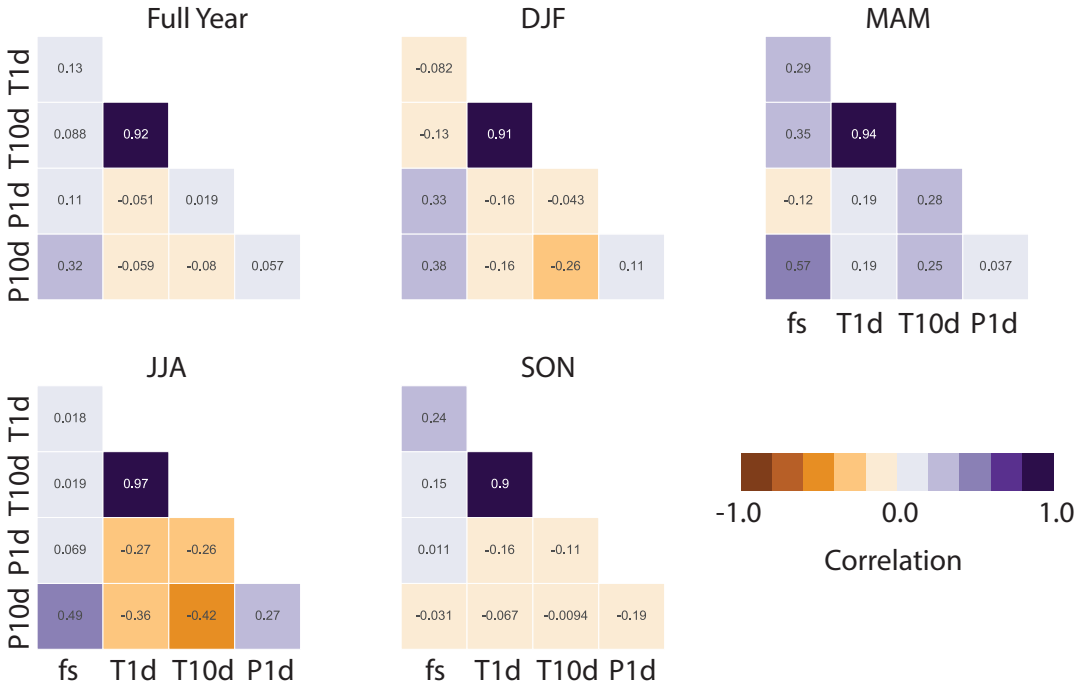

Figure 4.7: Crosscorrelation of variables considered for the multi-linear model explaining fluorescence, for the fully year, DJF, MAM, JJA, and SON.

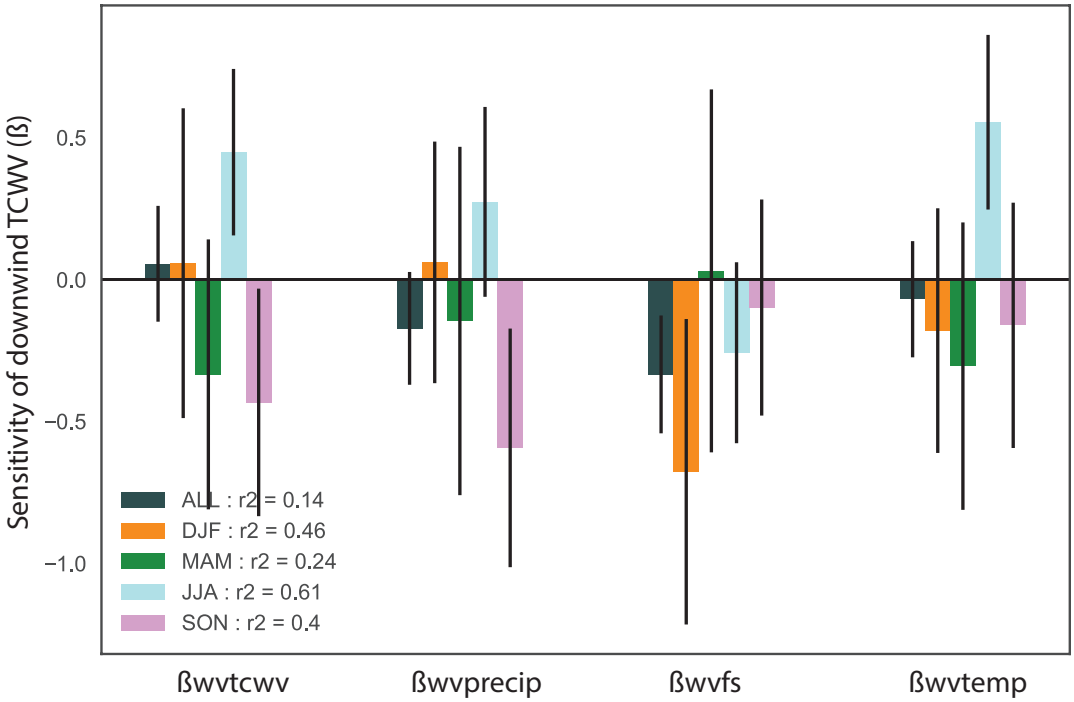

Figure 4.8: Regression coefficients (bars) of the sensitivity of downwind total column water vapor to the Amazon basin for different seasons (colors), and variables (x-axis). Error bars are 95% (two times the standard error). Legend reports variance explained for multi-linear model.

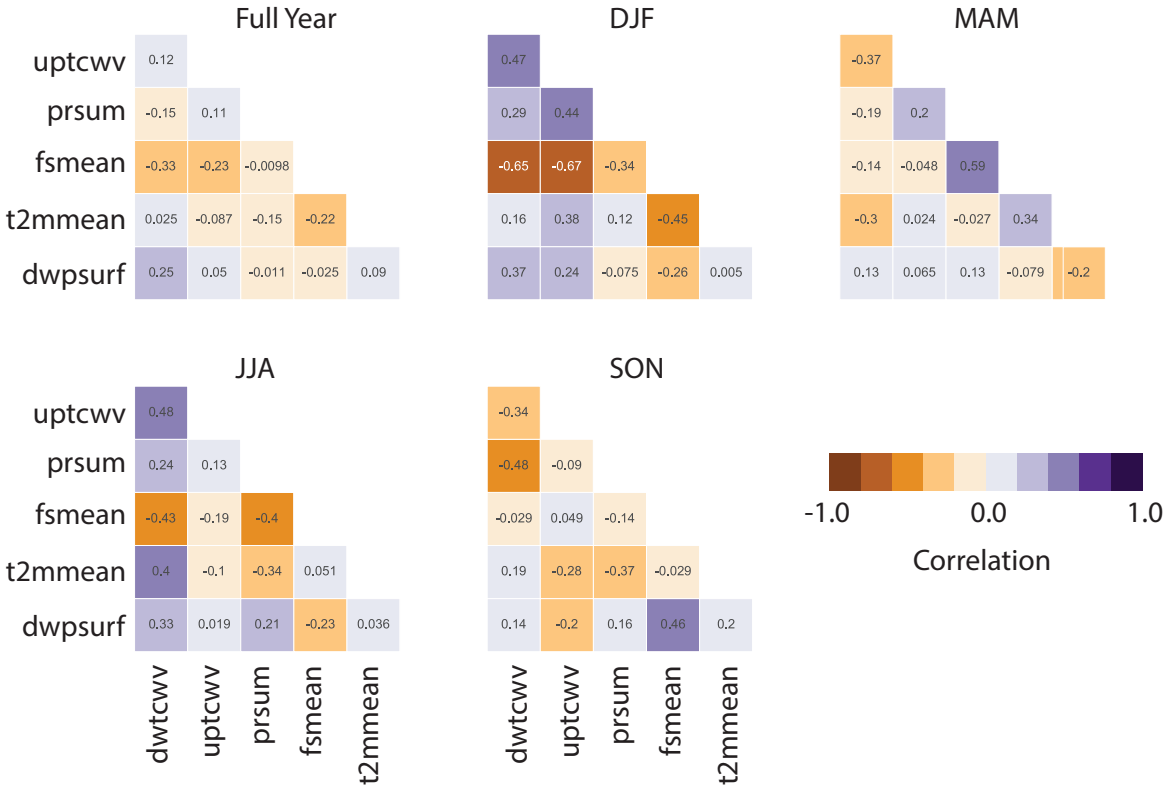

Figure 4.9: Crosscorrelation of variables considered for the multi-linear model explaining downwind total column water vapor, for the fully year, DJF, MAM, JJA, and SON.

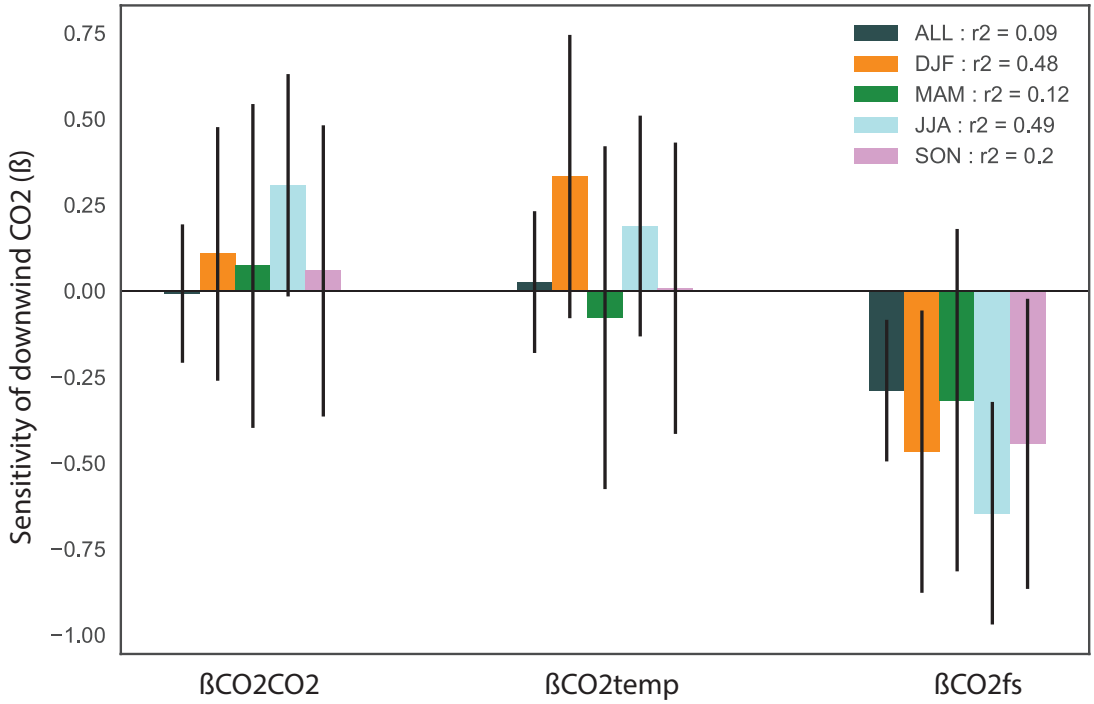

Figure 4.10: Regression coefficients (bars) of the sensitivity of downwind CO_2 concentration to the Amazon basin for different seasons (colors), and variables (x-axis). Error bars are 95% (two times the standard error). Legend reports variance explained for multi-linear model.

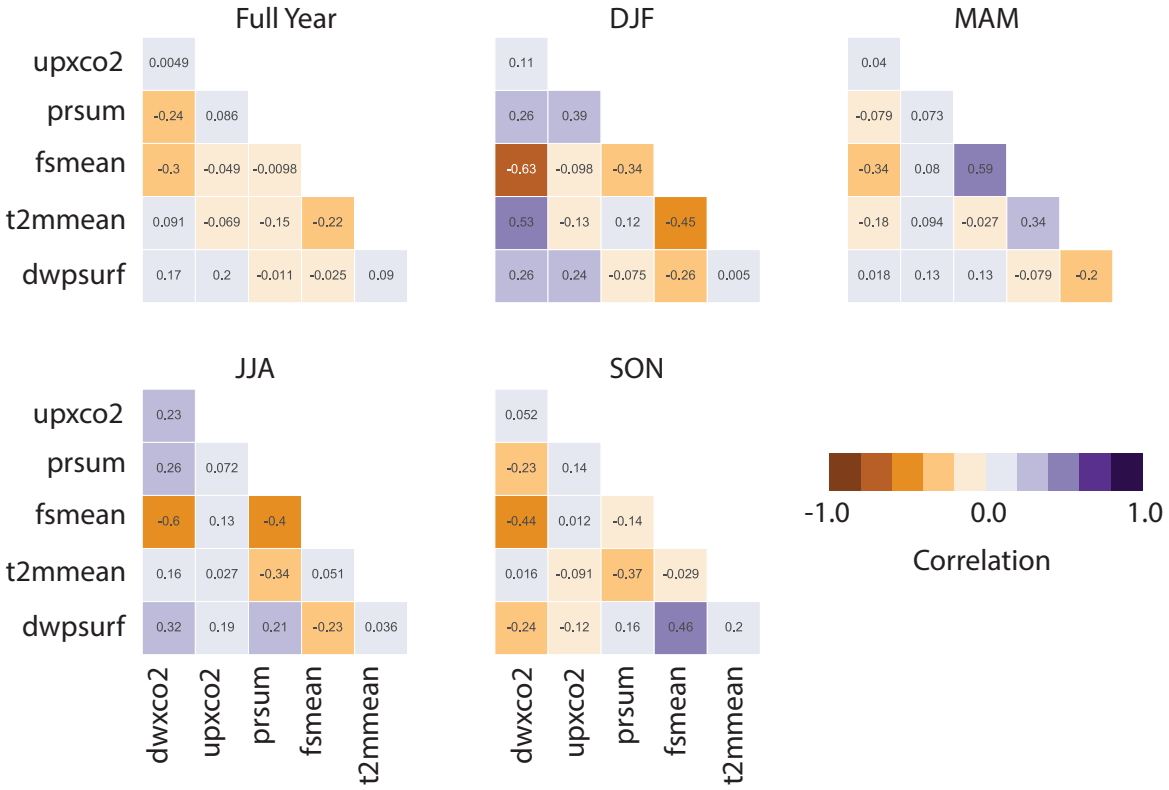

Figure 4.11: Crosscorrelation of variables considered for the multi-linear model explaining downwind CO_2, for the fully year, DJF, MAM, JJA, and SON.

BIBLIOGRAPHY

Robert F. Adler, George J. Huffman, Alfred Chang, Ralph Ferraro, Ping-Ping Xie, John Janowiak, Bruno Rudolf, Udo Schneider, Scott Curtis, David Bolvin, Arnold Gruber, Joel Susskind, Philip Arkin, and Eric Nelkin. The Version-2 Global Precipitation Climatology Project (GPCP) Monthly Precipitation Analysis (1979Present). *Journal of Hydrometeorology*, 4(6):1147–1167, December 2003. ISSN 1525-755X. doi: 10.1175/1525-7541(2003)004¡1147:TVGPCP¿2.0.CO;2. URL http://dx.doi.org/10.1175/1525-7541(2003)004<1147:TVGPCP>2.0.CO;2.

Caroline B Alden, John B Miller, Luciana V Gatti, Manuel M Gloor, Kaiyu Guan, Anna M Michalak, Ingrid T LaanLuijkx, Danielle Touma, Arlyn Andrews, and Luana S Basso. Regional atmospheric CO2 inversion reveals seasonal and geographic differences in Amazon net biome exchange. *Global Change Biology*, 2016. ISSN 1365-2486.

A. Anav, P. Friedlingstein, M. Kidston, L. Bopp, P. Ciais, P. Cox, C. Jones, M. Jung, R. Myneni, and Z. Zhu. Evaluating the Land and Ocean Components of the Global Carbon Cycle in the CMIP5 Earth System Models. *Journal of Climate*, 26(18): 6801–6843, March 2013a. ISSN 0894-8755. doi: 10.1175/JCLI-D-12-00417.1. URL http://dx.doi.org/10.1175/JCLI-D-12-00417.1.

Alessandro Anav, Guillermo Murray-Tortarolo, Pierre Friedlingstein, Stephen Sitch, Shilong Piao, and Zaichun Zhu. Evaluation of land surface models in reproducing satellite Derived leaf area index over the high-latitude northern hemisphere. Part II: Earth system models. *Remote Sensing*, 5(8):3637–3661, 2013b.

VK Arora, JF Scinocca, GJ Boer, JR Christian, KL Denman, GM Flato, VV Kharin, WG Lee, and WJ Merryfield. Carbon emission limits required to satisfy future repre-

sentative concentration pathways of greenhouse gases. *Geophysical Research Letters*, 38 (5), 2011. ISSN 1944-8007.

Gregory P. Asner, Alan R. Townsend, and Bobby H. Braswell. Satellite observation of El Nio effects on Amazon Forest phenology and productivity. *Geophysical Research Letters*, 27(7):981–984, April 2000. ISSN 1944-8007. doi: 10.1029/1999GL011113. URL http://dx.doi.org/10.1029/1999GL011113.

Owen K. Atkin and Mark G. Tjoelker. Thermal acclimation and the dynamic response of plant respiration to temperature. *Trends in Plant Science*, 8(7):343–351, July 2003. ISSN 1360-1385. doi: 10.1016/S1360-1385(03)00136-5. URL http://www.sciencedirect.com/science/article/pii/S1360138503001365.

Owen K. Atkin, Dan Bruhn, Vaughan M. Hurry, and Mark G. Tjoelker. Evans Review No. 2: The hot and the cold: unravelling the variable response of plant respiration to temperature. *Functional Plant Biology*, 32(2):87–105, 2005. URL https://doi.org/10.1071/FP03176.

A. Baccini, W. Walker, L. Carvalho, M. Farina, D. Sulla-Menashe, and R. A. Houghton. Tropical forests are a net carbon source based on aboveground measurements of gain and loss. *Science*, September 2017. doi: 10.1126/science.aam5962. URL http://science.sciencemag.org/content/early/2017/09/27/science.aam5962.abstract.

Dennis Baldocchi. Measuring fluxes of trace gases and energy between ecosystems and the atmosphere the state and future of the eddy covariance method. *Global Change Biology*, 20(12):3600–3609, December 2014. ISSN 1365-2486. doi: 10.1111/gcb.12649. URL http://dx.doi.org/10.1111/gcb.12649.

David. S. Battisti and Rosamond L. Naylor. Historical Warnings of Future Food Insecurity with Unprecedented Seasonal Heat. *Science*, 323 (5911):240–244, January 2009. doi: 10.1126/science.1164363. URL http://www.sciencemag.org/content/323/5911/240.abstract.

Christian Beer, Markus Reichstein, Enrico Tomelleri, Philippe Ciais, Martin Jung, Nuno Carvalhais, Christian Rdenbeck, M Altaf Arain, Dennis Baldocchi, and Gordon B Bonan. Terrestrial gross carbon dioxide uptake: global distribution and covariation with climate. *Science*, 329(5993):834–838, 2010. ISSN 0036-8075.

Joseph Berry and Olle Bjorkman. Photosynthetic response and adaptation to temperature in higher plants. *Annual Review of Plant Physiology*, 31(1):491–543, 1980. ISSN 0066-4294.

Celine Boisvenue and Steven W. Running. Impacts of climate change on natural forest productivity evidence since the middle of the 20th century. *Global Change Biology*, 12 (5):862–882, May 2006. ISSN 1365-2486. doi: 10.1111/j.1365-2486.2006.01134.x. URL http://dx.doi.org/10.1111/j.1365-2486.2006.01134.x.

Ben BB Booth, Chris D Jones, Mat Collins, Ian J Totterdell, Peter M Cox, Stephen Sitch, Chris Huntingford, Richard A Betts, Glen R Harris, and Jon Lloyd. High sensitivity of future global warming to land carbon cycle processes. *Environmental Research Letters*, 7 (2):024002, 2012. ISSN 1748-9326.

Rolf Borchert. Soil and Stem Water Storage Determine Phenology and Distribution of Tropical Dry Forest Trees. *Ecology*, 75(5):1437–1449, 1994. ISSN 1939-9170. doi: 10.2307/1937467. URL http://dx.doi.org/10.2307/1937467.

Elgene O. Box. Plant functional types and climate at the global scale. *Journal of Vegetation Science*, 7(3):309–320, June 1996. ISSN 1654-1103. doi: 10.2307/3236274. URL http://dx.doi.org/10.2307/3236274.

Mikhail Ivanovich Budyko. The heat balance of the earth's surface. *Soviet Geography*, 2(4): 3–13, 1961. ISSN 0038-5417.

Baozhang Chen, Guang Xu, Nicholas C. Coops, Philippe Ciais, John L. Innes, Guangyu Wang, Ranga B. Myneni, Tongli Wang, Judi Krzyzanowski, Qinglin Li, Lin Cao,

and Ying Liu. Changes in vegetation photosynthetic activity trends across the AsiaPacific region over the last three decades. *Remote Sensing of Environment*, 144 (0):28–41, March 2014. ISSN 0034-4257. doi: 10.1016/j.rse.2013.12.018. URL http://www.sciencedirect.com/science/article/pii/S0034425714000030.

Chengjin Chu, Megan Bartlett, Youshi Wang, Fangliang He, Jacob Weiner, Jrme Chave, and Lawren Sack. Does climate directly influence NPP globally? *Global Change Biology*, 22(1):12–24, January 2016. ISSN 1365-2486. doi: 10.1111/gcb.13079. URL http://dx.doi.org/10.1111/gcb.13079.

Galina Churkina and Steven W. Running. Contrasting Climatic Controls on the Estimated Productivity of Global Terrestrial Biomes. *Ecosystems*, 1(2):206–215, March 1998. ISSN 1432-9840. doi: 10.1007/s100219900016. URL http://dx.doi.org/10.1007/s100219900016.

DB Clark, LM Mercado, S Sitch, CD Jones, N Gedney, MJ Best, M Pryor, GG Rooney, RLH Essery, and E Blyth. The Joint UK Land Environment Simulator (JULES), model description-Part 2: carbon fluxes and vegetation dynamics. *Geoscientific Model Development*, 4(3):701, 2011. ISSN 1991-9603.

WJ Collins, Nicolas Bellouin, M Doutriaux-Boucher, N Gedney, P Halloran, T Hinton, J Hughes, CD Jones, M Joshi, and S Liddicoat. Development and evaluation of an Earth-System model-HadGEM2. *Geoscientific Model Development*, 4(4):1051, 2011. ISSN 1991-9603.

Peter M Cox. Description of the TRIFFID dynamic global vegetation model. *Hadley Centre technical note*, 24:1–16, 2001.

Peter M. Cox, David Pearson, Ben B. Booth, Pierre Friedlingstein, Chris Huntingford, Chris D. Jones, and Catherine M. Luke. Sensitivity of tropical carbon to climate change

constrained by carbon dioxide variability. *Nature*, 494(7437):341–344, February 2013. ISSN 0028-0836. doi: 10.1038/nature11882. URL http://dx.doi.org/10.1038/nature11882.

Michael E Day. Influence of temperature and leaf-to-air vapor pressure deficit on net photosynthesis and stomatal conductance in red spruce (Picea rubens). *Tree Physiology*, 20(1): 57–63, 2000. ISSN 0829-318X.

D. P. Dee, S. M. Uppala, A. J. Simmons, P. Berrisford, P. Poli, S. Kobayashi, U. Andrae, M. A. Balmaseda, G. Balsamo, P. Bauer, P. Bechtold, A. C. M. Beljaars, L. van de Berg, J. Bidlot, N. Bormann, C. Delsol, R. Dragani, M. Fuentes, A. J. Geer, L. Haimberger, S. B. Healy, H. Hersbach, E. V. Hlm, L. Isaksen, P. Kllberg, M. Khler, M. Matricardi, A. P. McNally, B. M. Monge-Sanz, J.-J. Morcrette, B.-K. Park, C. Peubey, P. de Rosnay, C. Tavolato, J.-N. Thpaut, and F. Vitart. The ERA-Interim reanalysis: configuration and performance of the data assimilation system. *Quarterly Journal of the Royal Meteorological Society*, 137(656):553–597, April 2011. ISSN 1477-870X. doi: 10.1002/qj.828. URL http://dx.doi.org/10.1002/qj.828.

Francina Dominguez, Praveen Kumar, Xin-Zhong Liang, and Mingfang Ting. Impact of Atmospheric Moisture Storage on Precipitation Recycling. *Journal of Climate*, 19(8):1513–1530, April 2006. ISSN 0894-8755. doi: 10.1175/JCLI3691.1. URL https://doi.org/10.1175/JCLI3691.1.

A Drumond, J Marengo, Tercio Ambrizzi, R Nieto, L Moreira, and L Gimeno. The role of the Amazon Basin moisture in the atmospheric branch of the hydrological cycle: a Lagrangian analysis. *Hydrology and Earth System Sciences*, 18:2577–2598, 2014. ISSN 1027-5606.

J-L Dufresne, M-A Foujols, Sbastien Denvil, Arnaud Caubel, Olivier Marti, Olivier Aumont, Yves Balkanski, Slimane Bekki, Hugo Bellenger, and Rachid Benshila. Climate change projections using the IPSL-CM5 Earth System Model: from CMIP3 to CMIP5. *Climate Dynamics*, 40(9-10):2123–2165, 2013. ISSN 0930-7575.

John P Dunne, Jasmin G John, Alistair J Adcroft, Stephen M Griffies, Robert W Hallberg, Elena Shevliakova, Ronald J Stouffer, William Cooke, Krista A Dunne, and Matthew J Harrison. GFDLs ESM2 global coupled climatecarbon earth system models. Part I: Physical formulation and baseline simulation characteristics. *Journal of Climate*, 25(19):6646–6665, 2012. ISSN 0894-8755.

B. Efron. Bootstrap Methods: Another Look at the Jackknife. *The Annals of Statistics*, 7 (1):1–26, 1979. ISSN 00905364. URL `http://www.jstor.org/stable/2958830`.

A. Eldering, P. O. Wennberg, D. Crisp, D. S. Schimel, M. R. Gunson, A. Chatterjee, J. Liu, F. M. Schwandner, Y. Sun, C. W. ODell, C. Frankenberg, T. Taylor, B. Fisher, G. B. Osterman, D. Wunch, J. Hakkarainen, J. Tamminen, and B. Weir. The Orbiting Carbon Observatory-2 early science investigations of regional carbon dioxide fluxes. *Science*, 358(6360), October 2017. doi: 10.1126/science.aam5745. URL `http://science.sciencemag.org/content/358/6360/eaam5745.abstract`.

E. A. B. Eltahir and R. L. Bras. Precipitation recycling in the Amazon basin. *Quarterly Journal of the Royal Meteorological Society*, 120(518):861–880, July 1994. ISSN 1477-870X. doi: 10.1002/qj.49712051806. URL `http://dx.doi.org/10.1002/qj.49712051806`.

S Feng and Q Fu. Expansion of global drylands under a warming climate. *Atmos. Chem. Phys*, 13(10):081–10, 2013.

Christian Frankenberg, Joshua B Fisher, John Worden, Grayson Badgley, Sassan S Saatchi, Jung-Eun Lee, Geoffrey C Toon, Andr Butz, Martin Jung, and Akihiko Kuze. New global observations of the terrestrial carbon cycle from GOSAT: Patterns of plant fluorescence with gross primary productivity. *Geophysical Research Letters*, 38(17), 2011. ISSN 1944-8007.

Christian Frankenberg, Joseph Berry, Luis Guanter, and Joanna Joiner. Remote sensing of terrestrial chlorophyll fluorescence from space. *SPIE Newsroom*, 19, 2013.

Christian Frankenberg, Chris O'Dell, Joseph Berry, Luis Guanter, Joanna Joiner, Philipp Khler, Randy Pollock, and Thomas E. Taylor. Prospects for chlorophyll fluorescence remote sensing from the Orbiting Carbon Observatory-2. *Remote Sensing of Environment*, 147:1–12, May 2014. ISSN 0034-4257. doi: 10.1016/j.rse.2014.02.007. URL http://www.sciencedirect.com/science/article/pii/S0034425714000522.

P. Friedlingstein, P. Cox, R. Betts, L. Bopp, W. von Bloh, V. Brovkin, P. Cadule, S. Doney, M. Eby, I. Fung, G. Bala, J. John, C. Jones, F. Joos, T. Kato, M. Kawamiya, W. Knorr, K. Lindsay, H. D. Matthews, T. Raddatz, P. Rayner, C. Reick, E. Roeckner, K.-G. Schnitzler, R. Schnur, K. Strassmann, A. J. Weaver, C. Yoshikawa, and N. Zeng. ClimateCarbon Cycle Feedback Analysis: Results from the C4mip Model Intercomparison. *Journal of Climate*, 19(14):3337–3353, July 2006. ISSN 0894-8755. doi: 10.1175/JCLI3800.1. URL http://dx.doi.org/10.1175/JCLI3800.1.

Pierre Friedlingstein, Malte Meinshausen, Vivek K. Arora, Chris D. Jones, Alessandro Anav, Spencer K. Liddicoat, and Reto Knutti. Uncertainties in CMIP5 Climate Projections due to Carbon Cycle Feedbacks. *Journal of Climate*, 27(2):511–526, September 2013. ISSN 0894-8755. doi: 10.1175/JCLI-D-12-00579.1. URL http://dx.doi.org/10.1175/JCLI-D-12-00579.1.

Peter R Gent, Gokhan Danabasoglu, Leo J Donner, Marika M Holland, Elizabeth C Hunke, Steve R Jayne, David M Lawrence, Richard B Neale, Philip J Rasch, and Mariana Vertenstein. The community climate system model version 4. *Journal of Climate*, 24(19):4973–4991, 2011. ISSN 0894-8755.

Bardan Ghimire, Christopher A Williams, Jeffrey Masek, Feng Gao, Zhuosen Wang, Crystal Schaaf, and Tao He. Global albedo change and radiative cooling from anthropogenic land-cover change, 1700 to 2005 based on MODIS, land-use harmonization, radiative kernels and reanalysis. *Geophysical Research Letters*, page 2014GL061671, October 2014. ISSN 1944-8007. doi: 10.1002/2014GL061671. URL http://dx.doi.org/10.1002/2014GL061671.

Marco A Giorgetta, Johann Jungclaus, Christian H Reick, Stephanie Legutke, Jrgen Bader, Michael Bttinger, Victor Brovkin, Traute Crueger, Monika Esch, and Kerstin Fieg. Climate and carbon cycle changes from 1850 to 2100 in MPIESM simulations for the Coupled Model Intercomparison Project phase 5. *Journal of Advances in Modeling Earth Systems*, 5(3): 572–597, 2013. ISSN 1942-2466.

P. Edward Glenn, R. Alfredo Huete, L. Pamela Nagler, and G. Stephen Nelson. Relationship Between Remotely-sensed Vegetation Indices, Canopy Attributes and Plant Physiological Processes: What Vegetation Indices Can and Cannot Tell Us About the Landscape. *Sensors*, 8(4), 2008. ISSN 1424-8220. doi: 10.3390/s8042136.

Samuel N. Goward, Brian Markham, Dennis G. Dye, Wayne Dulaney, and Jingli Yang. Normalized difference vegetation index measurements from the advanced very high resolution radiometer. *Remote Sensing of Environment*, 35(23):257–277, February 1991. ISSN 0034-4257. doi: 10.1016/0034-4257(91)90017-Z. URL `http://www.sciencedirect.com/science/article/pii/003442579190017Z`.

Julia K. Green, Alexandra G. Konings, Seyed Hamed Alemohammad, Joseph Berry, Dara Entekhabi, Jana Kolassa, Jung-Eun Lee, and Pierre Gentine. Regionally strong feedbacks between the atmosphere and terrestrial biosphere. *Nature Geosci*, 10(6):410–414, June 2017. ISSN 1752-0894. URL `http://dx.doi.org/10.1038/ngeo2957`.

Charles G. Grier and Steven W. Running. Leaf Area of Mature Northwestern Coniferous Forests: Relation to Site Water Balance. *Ecology*, 58(4):893–899, July 1977. ISSN 1939-9170. doi: 10.2307/1936225. URL `http://dx.doi.org/10.2307/1936225`.

Kaiyu Guan, Ming Pan, Haibin Li, Adam Wolf, Jin Wu, David Medvigy, Kelly K. Caylor, Justin Sheffield, Eric F. Wood, Yadvinder Malhi, Miaoling Liang, John S. Kimball, Scott R. Saleska, Joe Berry, Joanna Joiner, and Alexei I. Lyapustin. Photosynthetic seasonality of global tropical forests constrained by hydroclimate. *Nature Geosci*, 8(4):284–289, April 2015. ISSN 1752-0894. URL `http://dx.doi.org/10.1038/ngeo2382`.

Luis Guanter, Christian Frankenberg, Anu Dudhia, Philip E. Lewis, Jos Gmez-Dans, Akihiko Kuze, Hiroshi Suto, and Roy G. Grainger. Retrieval and global assessment of terrestrial chlorophyll fluorescence from GOSAT space measurements. *Remote Sensing of Environment*, 121:236–251, June 2012. ISSN 0034-4257. doi: 10.1016/j.rse.2012.02.006. URL http://www.sciencedirect.com/science/article/pii/S0034425712000909.

Thomas Hilker, Alexei I. Lyapustin, Compton J. Tucker, Forrest G. Hall, Ranga B. Myneni, Yujie Wang, Jian Bi, Yhasmin Mendes de Moura, and Piers J. Sellers. Vegetation dynamics and rainfall sensitivity of the Amazon. *Proceedings of the National Academy of Sciences*, 111(45):16041–16046, November 2014. doi: 10.1073/pnas.1404870111. URL http://www.pnas.org/content/111/45/16041.abstract.

Brent N. Holben. Characteristics of maximum-value composite images from temporal AVHRR data. *International Journal of Remote Sensing*, 7(11):1417–1434, November 1986. ISSN 0143-1161. doi: 10.1080/01431168608948945. URL http://dx.doi.org/10.1080/01431168608948945.

Arthur Y. Hou, Ramesh K. Kakar, Steven Neeck, Ardeshir A. Azarbarzin, Christian D. Kummerow, Masahiro Kojima, Riko Oki, Kenji Nakamura, and Toshio Iguchi. The Global Precipitation Measurement Mission. *Bulletin of the American Meteorological Society*, 95 (5):701–722, September 2013. ISSN 0003-0007. doi: 10.1175/BAMS-D-13-00164.1. URL https://doi.org/10.1175/BAMS-D-13-00164.1.

Stephan Hoyer and Joe Hamman. Xarray: nd labeled arrays and datasets in Python. *Journal of Open Research Software*, 5(1), 2017. ISSN 2049-9647.

A Huete, K Didan, T Miura, E.P Rodriguez, X Gao, and L.G Ferreira. Overview of the radiometric and biophysical performance of the MODIS vegetation indices. *The Moderate Resolution Imaging Spectroradiometer (MODIS): a new generation of Land Surface Monitoring*, 83(12):195–213, November 2002. ISSN 0034-4257. doi: 10.1016/S0034-4257(02)00096-2. URL http://www.sciencedirect.com/science/article/pii/S0034425702000962.

T Iversen, Mats Bentsen, Ingo Bethke, JB Debernard, A Kirkevg, Seland, Helge Drange, JE Kristjansson, Iselin Medhaug, and M Sand. The Norwegian earth system model, NorESM1-M-part 2: Climate response and scenario projections. *Geoscientific Model Development*, 6(2):389, 2013. ISSN 1991-9603.

J. D. Hunter. Matplotlib: A 2d Graphics Environment. *Computing in Science & Engineering*, 9(3):90–95, June 2007. ISSN 1521-9615. doi: 10.1109/MCSE.2007.55.

Scott Jasechko, Zachary D. Sharp, John J. Gibson, S. Jean Birks, Yi Yi, and Peter J. Fawcett. Terrestrial water fluxes dominated by transpiration. *Nature*, 496(7445):347–350, April 2013. ISSN 0028-0836. URL `http://dx.doi.org/10.1038/nature11983`.

D. Ji, L. Wang, J. Feng, Q. Wu, H. Cheng, Q. Zhang, J. Yang, W. Dong, Y. Dai, D. Gong, R.-H. Zhang, X. Wang, J. Liu, J. C. Moore, D. Chen, and M. Zhou. Description and basic evaluation of Beijing Normal University Earth System Model (BNU-ESM) version 1. *Geosci. Model Dev.*, 7(5):2039–2064, September 2014. ISSN 1991-9603. doi: 10.5194/gmd-7-2039-2014. URL `https://www.geosci-model-dev.net/7/2039/2014/`.

Duoying Ji and Yongjiu Dai. The common land model (CoLM) technical guide. *GCESS, Beijing Normal University, Beijing, China*, 2010.

JinJun Ji, Mei Huang, and KeRang Li. Prediction of carbon exchanges between China terrestrial ecosystem and atmosphere in 21st century. *Science in China Series D: Earth Sciences*, 51(6):885–898, 2008. ISSN 1006-9313.

William M. Jolly, Ramakrishna Nemani, and Steven W. Running. A generalized, bioclimatic index to predict foliar phenology in response to climate. *Global Change Biology*, 11 (4):619–632, April 2005. ISSN 1365-2486. doi: 10.1111/j.1365-2486.2005.00930.x. URL `http://dx.doi.org/10.1111/j.1365-2486.2005.00930.x`.

P Jones and I Harris. University of East Anglia Climatic Research Unit, CRU TS3. 21: Climatic Research Unit (CRU) Time-Series (TS) Version 3.21 of High Resolution Grid-

ded Data of Month-by-month Variation in Climate (Jan. 1901Dec. 2012). *NCAS British Atmospheric Data Centre*, 2013.

Martin Jung, Markus Reichstein, Hank A. Margolis, Alessandro Cescatti, Andrew D. Richardson, M. Altaf Arain, Almut Arneth, Christian Bernhofer, Damien Bonal, Jiquan Chen, Damiano Gianelle, Nadine Gobron, Gerald Kiely, Werner Kutsch, Gitta Lasslop, Beverly E. Law, Anders Lindroth, Lutz Merbold, Leonardo Montagnani, Eddy J. Moors, Dario Papale, Matteo Sottocornola, Francesco Vaccari, and Christopher Williams. Global patterns of land-atmosphere fluxes of carbon dioxide, latent heat, and sensible heat derived from eddy covariance, satellite, and meteorological observations. *Journal of Geophysical Research: Biogeosciences*, 116(G3):n/a–n/a, September 2011. ISSN 2156-2202. doi: 10.1029/2010JG001566. URL `http://dx.doi.org/10.1029/2010JG001566`.

Wolfgang Knorr. Annual and interannual CO2 exchanges of the terrestrial biosphere: Processbased simulations and uncertainties. *Global Ecology and Biogeography*, 9(3):225–252, 2000. ISSN 1466-8238.

Markus Kottek, Jrgen Grieser, Christoph Beck, Bruno Rudolf, and Franz Rubel. World map of the Koppen-Geiger climate classification updated. *Meteorologische Zeitschrift*, 15(3): 259–264, 2006. ISSN 0941-2948.

Charles D. Koven. Boreal carbon loss due to poleward shift in low-carbon ecosystems. *Nature Geosci*, 6(6):452–456, June 2013. ISSN 1752-0894. URL `http://dx.doi.org/10.1038/ngeo1801`.

Gerhard Krinner, Nicolas Viovy, Nathalie de NobletDucoudr, Jrme Oge, Jan Polcher, Pierre Friedlingstein, Philippe Ciais, Stephen Sitch, and I Colin Prentice. A dynamic global vegetation model for studies of the coupled atmospherebiosphere system. *Global Biogeochemical Cycles*, 19(1), 2005. ISSN 1944-9224.

David M Lawrence, Keith W Oleson, Mark G Flanner, Peter E Thornton, Sean C Swenson,

Peter J Lawrence, Xubin Zeng, ZongLiang Yang, Samuel Levis, and Koichi Sakaguchi. Parameterization improvements and functional and structural advances in version 4 of the Community Land Model. *Journal of Advances in Modeling Earth Systems*, 3(1), 2011. ISSN 1942-2466.

C. Le Qur, R. Moriarty, R. M. Andrew, J. G. Canadell, S. Sitch, J. I. Korsbakken, P. Friedlingstein, G. P. Peters, R. J. Andres, T. A. Boden, R. A. Houghton, J. I. House, R. F. Keeling, P. Tans, A. Arneth, D. C. E. Bakker, L. Barbero, L. Bopp, J. Chang, F. Chevallier, L. P. Chini, P. Ciais, M. Fader, R. A. Feely, T. Gkritzalis, I. Harris, J. Hauck, T. Ilyina, A. K. Jain, E. Kato, V. Kitidis, K. Klein Goldewijk, C. Koven, P. Landschtzer, S. K. Lauvset, N. Lefvre, A. Lenton, I. D. Lima, N. Metzl, F. Millero, D. R. Munro, A. Murata, J. E. M. S. Nabel, S. Nakaoka, Y. Nojiri, K. O'Brien, A. Olsen, T. Ono, F. F. Prez, B. Pfeil, D. Pierrot, B. Poulter, G. Rehder, C. Rdenbeck, S. Saito, U. Schuster, J. Schwinger, R. Sfrian, T. Steinhoff, B. D. Stocker, A. J. Sutton, T. Takahashi, B. Tilbrook, I. T. van der Laan-Luijkx, G. R. van der Werf, S. van Heuven, D. Vandemark, N. Viovy, A. Wiltshire, S. Zaehle, and N. Zeng. Global Carbon Budget 2015. *Earth Syst. Sci. Data*, 7(2):349–396, December 2015. ISSN 1866-3516. doi: 10.5194/essd-7-349-2015. URL `https://www.earth-syst-sci-data.net/7/349/2015/`.

Harald Lejens and Hans kland. Characteristics of northern hemisphere blocking as determined from a long time series of observational data. *Tellus A: Dynamic Meteorology and Oceanography*, 35(5):350–362, January 1983. ISSN null. doi: 10.3402/tellusa.v35i5.11446. URL `http://www.tandfonline.com/doi/abs/10.3402/tellusa.v35i5.11446`.

S. Levis. Modeling vegetation and land use in models of the Earth System. *Wiley Interdisciplinary Reviews: Climate Change*, 2010.

Yang Liu, Ronggao Liu, and Jing M. Chen. Retrospective retrieval of long-term consistent global leaf area index (19812011) from combined AVHRR and MODIS data. *Journal of*

Geophysical Research: Biogeosciences, 117(G4):n/a–n/a, December 2012. ISSN 2156-2202. doi: 10.1029/2012JG002084. URL http://dx.doi.org/10.1029/2012JG002084.

Yongwen Liu, Tao Wang, Mengtian Huang, Yitong Yao, Philippe Ciais, and Shilong Piao. Changes in interannual climate sensitivities of terrestrial carbon fluxes during the 21st century predicted by CMIP5 Earth System Models. *Journal of Geophysical Research: Biogeosciences*, 121(3):903–918, March 2016. ISSN 2169-8961. doi: 10.1002/2015JG003124. URL http://dx.doi.org/10.1002/2015JG003124.

Yongwen Liu, Shilong Piao, Xu Lian, Philippe Ciais, and W. Kolby Smith. Seasonal Responses of Terrestrial Carbon Cycle to Climate Variations in CMIP5 Models: Evaluation and Projection. *Journal of Climate*, 30(16):6481–6503, May 2017. ISSN 0894-8755. doi: 10.1175/JCLI-D-16-0555.1. URL https://doi.org/10.1175/JCLI-D-16-0555.1.

Danica L. Lombardozzi, Gordon B. Bonan, Nicholas G. Smith, Jeffrey S. Dukes, and Rosie A. Fisher. Temperature acclimation of photosynthesis and respiration: A key uncertainty in the carbon cycle-climate feedback. *Geophysical Research Letters*, 42 (20):8624–8631, October 2015. ISSN 1944-8007. doi: 10.1002/2015GL065934. URL http://dx.doi.org/10.1002/2015GL065934.

Nicole S Lovenduski and Gordon B Bonan. Reducing uncertainty in projections of terrestrial carbon uptake. *Environmental Research Letters*, 12(4):044020, 2017. ISSN 1748-9326.

A. E. Lugo, S. L. Brown, R. Dodson, T. S. Smith, and H. H. Shugart. The Holdridge life zones of the conterminous United States in relation to ecosystem mapping. *Journal of Biogeography*, 26(5):1025–1038, September 1999. ISSN 1365-2699. doi: 10.1046/j.1365-2699.1999.00329.x. URL http://dx.doi.org/10.1046/j.1365-2699.1999.00329.x.

Y. Q. Luo, J. T. Randerson, G. Abramowitz, C. Bacour, E. Blyth, N. Carvalhais, P. Ciais, D. Dalmonech, J. B. Fisher, R. Fisher, P. Friedlingstein, K. Hibbard, F. Hoffman, D. Huntzinger, C. D. Jones, C. Koven, D. Lawrence, D. J. Li, M. Mahecha, S. L. Niu,

R. Norby, S. L. Piao, X. Qi, P. Peylin, I. C. Prentice, W. Riley, M. Reichstein, C. Schwalm, Y. P. Wang, J. Y. Xia, S. Zaehle, and X. H. Zhou. A framework for benchmarking land models. *Biogeosciences*, 9(10):3857–3874, 2012. doi: 10.5194/bg-9-3857-2012. URL http://www.biogeosciences.net/9/3857/2012/.

Natalie Mahowald, Fiona Lo, Yun Zheng, Laura Harrison, Chris Funk, Danica Lombardozzi, and Christine Goodale. Projections of leaf area index in earth system models. *Earth System Dynamics*, 7:211–229, 2016.

Yadvinder Malhi, Luiz E. O. C. Arago, David Galbraith, Chris Huntingford, Rosie Fisher, Przemyslaw Zelazowski, Stephen Sitch, Carol McSweeney, and Patrick Meir. Exploring the likelihood and mechanism of a climate-change-induced dieback of the Amazon rainforest. *Proceedings of the National Academy of Sciences*, February 2009. doi: 10.1073/pnas.0804619106. URL http://www.pnas.org/content/early/2009/02/12/0804619106.abstract.

Jose Antonio MARengo. On the hydrological cycle of the Amazon Basin: A historical review and current state-of-the-art. *Revista Brasileira de Meteorologia*, 21(3):1–19, 2006.

Martin G. De Kauwe, Trevor F. Keenan, Belinda E. Medlyn, I. Colin Prentice, and Cesar Terrer. Satellite based estimates underestimate the effect of CO2 fertilization on net primary productivity. *Nature Clim. Change*, 6(10):892–893, October 2016. ISSN 1758-678X. URL http://dx.doi.org/10.1038/nclimate3105.

Nathan G. McDowell. Mechanisms Linking Drought, Hydraulics, Carbon Metabolism, and Vegetation Mortality. *Plant Physiology*, 155 (3):1051–1059, March 2011. doi: 10.1104/pp.110.170704. URL http://www.plantphysiol.org/content/155/3/1051.short.

Wes McKinney. Data Structures for Statistical Computing in Python. In Stfan van der Walt

and Jarrod Millman, editors, *Proceedings of the 9th Python in Science Conference*, pages 51 – 56, 2010.

Anna L. Merrifield and Shang-Ping Xie. Summer U.S. Surface Air Temperature Variability: Controlling Factors and AMIP Simulation Biases. *Journal of Climate*, 29 (14):5123–5139, April 2016. ISSN 0894-8755. doi: 10.1175/JCLI-D-15-0705.1. URL https://doi.org/10.1175/JCLI-D-15-0705.1.

Marc J. Metzger, Robert G. H. Bunce, Rob H. G. Jongman, Roger Sayre, Antonio Trabucco, and Robert Zomer. A high-resolution bioclimate map of the world: a unifying framework for global biodiversity research and monitoring. *Global Ecology and Biogeography*, 22(5):630–638, May 2013. ISSN 1466-8238. doi: 10.1111/geb.12022. URL http://dx.doi.org/10.1111/geb.12022.

Qiaozhen Mu, Faith Ann Heinsch, Maosheng Zhao, and Steven W Running. Development of a global evapotranspiration algorithm based on MODIS and global meteorology data. *Remote sensing of Environment*, 111(4):519–536, 2007. ISSN 0034-4257.

R.B. Myneni, F.G. Hall, P.J. Sellers, and A.L. Marshak. The interpretation of spectral vegetation indexes. *Geoscience and Remote Sensing, IEEE Transactions on*, 33(2):481–486, March 1995. ISSN 0196-2892. doi: 10.1109/36.377948.

R.B Myneni, S Hoffman, Y Knyazikhin, J.L Privette, J Glassy, Y Tian, Y Wang, X Song, Y Zhang, G.R Smith, A Lotsch, M Friedl, J.T Morisette, P Votava, R.R Nemani, and S.W Running. Global products of vegetation leaf area and fraction absorbed PAR from year one of MODIS data. *The Moderate Resolution Imaging Spectroradiometer (MODIS): a new generation of Land Surface Monitoring*, 83(12):214–231, November 2002. ISSN 0034-4257. doi: 10.1016/S0034-4257(02)00074-3. URL http://www.sciencedirect.com/science/article/pii/S0034425702000743.

Robert R. Nelson, David Crisp, Lesley E. Ott, and Christopher W. O'Dell. High-accuracy

measurements of total column water vapor from the Orbiting Carbon Observatory-2. *Geophysical Research Letters*, 43(23):12,261–12,269, December 2016. ISSN 1944-8007. doi: 10.1002/2016GL071200. URL http://dx.doi.org/10.1002/2016GL071200.

R. R. Nemani, C. D. Keeling, H. Hashimoto, W. M. Jolly, S. C. Piper, C. J. Tucker, R. B. Myneni, and S. W. Running. Climate-driven increases in global terrestrial net primary production from 1982 to 1999. *Science*, 300(5625):1560–1563, 2003.

Keith W Oleson, David M Lawrence, B Gordon, Mark G Flanner, Erik Kluzek, J Peter, Samuel Levis, Sean C Swenson, E Thornton, and Johannes Feddema. Technical description of version 4.0 of the Community Land Model (CLM). 2010.

Robert M. Obrien. A Caution Regarding Rules of Thumb for Variance Inflation Factors. *Quality & Quantity*, 41(5):673–690, 2007. ISSN 1573-7845. doi: 10.1007/s11135-006-9018-6. URL http://dx.doi.org/10.1007/s11135-006-9018-6.

Nicholas C. Parazoo, Kevin Bowman, Christian Frankenberg, Jung-Eun Lee, Joshua B. Fisher, John Worden, Dylan B. A. Jones, Joseph Berry, G. James Collatz, Ian T. Baker, Martin Jung, Junjie Liu, Gregory Osterman, Chris O'Dell, Athena Sparks, Andre Butz, Sandrine Guerlet, Yukio Yoshida, Huilin Chen, and Christoph Gerbig. Interpreting seasonal changes in the carbon balance of southern Amazonia using measurements of XCO2 and chlorophyll fluorescence from GOSAT. *Geophysical Research Letters*, 40(11):2829–2833, June 2013. ISSN 1944-8007. doi: 10.1002/grl.50452. URL http://dx.doi.org/10.1002/grl.50452.

Fabian Pedregosa, Gal Varoquaux, Alexandre Gramfort, Vincent Michel, Bertrand Thirion, Olivier Grisel, Mathieu Blondel, Peter Prettenhofer, Ron Weiss, and Vincent Dubourg. Scikit-learn: Machine learning in Python. *Journal of Machine Learning Research*, 12(Oct): 2825–2830, 2011.

M. C. Peel, B. L. Finlayson, and T. A. McMahon. Updated world map of the

Kppen-Geiger climate classification. *Hydrol. Earth Syst. Sci. Discuss.*, 4(2):439–473, March 2007a. ISSN 1812-2116. doi: 10.5194/hessd-4-439-2007. URL http://www.hydrol-earth-syst-sci-discuss.net/4/439/2007/.

M. C. Peel, B. L. Finlayson, and T. A. McMahon. Updated world map of the Kppen-Geiger climate classification. *Hydrol. Earth Syst. Sci.*, 11(5):1633–1644, October 2007b. ISSN 1607-7938. doi: 10.5194/hess-11-1633-2007. URL http://www.hydrol-earth-syst-sci.net/11/1633/2007/.

Shilong Piao, Philippe Ciais, Pierre Friedlingstein, Nathalie de Noblet-Ducoudr, Patricia Cadule, Nicolas Viovy, and Tao Wang. Spatiotemporal patterns of terrestrial carbon cycle during the 20th century. *Global Biogeochemical Cycles*, 23(4): n/a–n/a, December 2009. ISSN 1944-9224. doi: 10.1029/2008GB003339. URL http://dx.doi.org/10.1029/2008GB003339.

Shilong Piao, Huijuan Nan, Chris Huntingford, Philippe Ciais, Pierre Friedlingstein, Stephen Sitch, Shushi Peng, Anders Ahlstrm, Josep G Canadell, and Nan Cong. Evidence for a weakening relationship between interannual temperature variability and northern vegetation activity. *Nature communications*, 5, 2014.

Jorge E. Pinzon and Compton J. Tucker. A Non-Stationary 19812012 AVHRR NDVI3g Time Series. *Remote Sensing*, 6(8):6929–6960, 2014. ISSN 2072-4292. doi: 10.3390/rs6086929. URL http://www.mdpi.com/2072-4292/6/8/6929.

Albert Porcar-Castell, Esa Tyystjrvi, Jon Atherton, Christiaan van der Tol, Jaume Flexas, Erhard E. Pfndel, Jose Moreno, Christian Frankenberg, and Joseph A. Berry. Linking chlorophyll a fluorescence to photosynthesis for remote sensing applications: mechanisms and challenges. *Journal of Experimental Botany*, 65(15):4065–4095, August 2014. ISSN 0022-0957. doi: 10.1093/jxb/eru191. URL http://dx.doi.org/10.1093/jxb/eru191.

Gregory R. Quetin and Abigail L. S. Swann. Empirically Derived Sensitivity of Vegetation to

Climate across Global Gradients of Temperature and Precipitation. *Journal of Climate*, 30(15):5835–5849, April 2017. ISSN 0894-8755. doi: 10.1175/JCLI-D-16-0829.1. URL https://doi.org/10.1175/JCLI-D-16-0829.1.

Rashid Rafique, Fang Zhao, Rogier de Jong, Ning Zeng, and R. Ghassem Asrar. Global and Regional Variability and Change in Terrestrial Ecosystems Net Primary Production and NDVI: A Model-Data Comparison. *Remote Sensing*, 8(3), 2016. ISSN 2072-4292. doi: 10.3390/rs8030177.

Andrew D. Richardson, T. Andy Black, Philippe Ciais, Nicolas Delbart, Mark A. Friedl, Nadine Gobron, David Y. Hollinger, Werner L. Kutsch, Bernard Longdoz, Sebastiaan Luyssaert, Mirco Migliavacca, Leonardo Montagnani, J. William Munger, Eddy Moors, Shilong Piao, Corinna Rebmann, Markus Reichstein, Nobuko Saigusa, Enrico Tomelleri, Rodrigo Vargas, and Andrej Varlagin. Influence of spring and autumn phenological transitions on forest ecosystem productivity. *Philosophical Transactions of the Royal Society B: Biological Sciences*, 365(1555):3227, September 2010. doi: 10.1098/rstb.2010.0102. URL http://rstb.royalsocietypublishing.org/content/365/1555/3227.abstract.

Andrew D. Richardson, Trevor F. Keenan, Mirco Migliavacca, Youngryel Ryu, Oliver Sonnentag, and Michael Toomey. Climate change, phenology, and phenological control of vegetation feedbacks to the climate system. *Agricultural and Forest Meteorology*, 169(0): 156–173, February 2013. ISSN 0168-1923. doi: 10.1016/j.agrformet.2012.09.012. URL http://www.sciencedirect.com/science/article/pii/S0168192312002869.

Franz Rubel and Markus Kottek. Observed and projected climate shifts 19012100 depicted by world maps of the Koppen-Geiger climate classification. *Meteorologische Zeitschrift*, 19 (2):135–141, 2010. ISSN 0941-2948.

Steven W. Running, Ramakrishna R. Nemani, Faith Ann Heinsch, Maosheng Zhao, Matt Reeves, and Hirofumi Hashimoto. A Continuous Satellite-Derived Measure of Global Terrestrial Primary Production. *BioScience*, 54(6):547–560,

June 2004. doi: 10.1641/0006-3568(2004)054[0547:ACSMOG]2.0.CO;2. URL http://bioscience.oxfordjournals.org/content/54/6/547.abstract.

S. van der Walt, S. C. Colbert, and G. Varoquaux. The NumPy Array: A Structure for Efficient Numerical Computation. *Computing in Science & Engineering*, 13(2):22–30, April 2011. ISSN 1521-9615. doi: 10.1109/MCSE.2011.37.

Sassan S. Saatchi, Nancy L. Harris, Sandra Brown, Michael Lefsky, Edward T. A. Mitchard, William Salas, Brian R. Zutta, Wolfgang Buermann, Simon L. Lewis, Stephen Hagen, Silvia Petrova, Lee White, Miles Silman, and Alexandra Morel. Benchmark map of forest carbon stocks in tropical regions across three continents. *Proceedings of the National Academy of Sciences*, 108(24):9899–9904, June 2011. doi: 10.1073/pnas.1019576108. URL http://www.pnas.org/content/108/24/9899.abstract.

Hisashi Sato, Akihiko Itoh, and Takashi Kohyama. SEIBDGVM: A new Dynamic Global Vegetation Model using a spatially explicit individual-based approach. *Ecological Modelling*, 200(3):279–307, 2007. ISSN 0304-3800.

Prakki Satyamurty, Claudia Priscila Wanzeler da Costa, and Antonio Ocimar Manzi. Moisture source for the Amazon Basin: a study of contrasting years. *Theoretical and Applied Climatology*, 111(1):195–209, January 2013. ISSN 1434-4483. doi: 10.1007/s00704-012-0637-7. URL https://doi.org/10.1007/s00704-012-0637-7.

David Schimel, Ryan Pavlick, Joshua B. Fisher, Gregory P. Asner, Sassan Saatchi, Philip Townsend, Charles Miller, Christian Frankenberg, Kathy Hibbard, and Peter Cox. Observing terrestrial ecosystems and the carbon cycle from space. *Global Change Biology*, pages n/a–n/a, 2014. ISSN 1365-2486. doi: 10.1111/gcb.12822. URL http://dx.doi.org/10.1111/gcb.12822.

William H. Schlesinger and Scott Jasechko. Transpiration in the global water cycle. *Agricultural and Forest Meteorology*, 189190(0):115–117, June

2014. ISSN 0168-1923. doi: 10.1016/j.agrformet.2014.01.011. URL http://www.sciencedirect.com/science/article/pii/S0168192314000203.

JMO Scurlock. Worldwide historical estimates of leaf area index, 1932-2000. Technical report, ORNL Oak Ridge National Laboratory (US), 2002.

Alistair W. R. Seddon, Marc Macias-Fauria, Peter R. Long, David Benz, and Kathy J. Willis. Sensitivity of global terrestrial ecosystems to climate variability. *Nature*, advance online publication, February 2016. ISSN 1476-4687. URL http://dx.doi.org/10.1038/nature16986.

Pu Shao, Xubin Zeng, Koichi Sakaguchi, Russell K. Monson, and Xiaodong Zeng. Terrestrial Carbon Cycle: Climate Relations in Eight CMIP5 Earth System Models. *Journal of Climate*, 26(22):8744–8764, July 2013. ISSN 0894-8755. doi: 10.1175/JCLI-D-12-00831.1. URL http://dx.doi.org/10.1175/JCLI-D-12-00831.1.

Marc Simard, Naiara Pinto, Joshua B. Fisher, and Alessandro Baccini. Mapping forest canopy height globally with spaceborne lidar. *Journal of Geophysical Research: Biogeosciences*, 116(G4):G04021, December 2011. ISSN 2156-2202. doi: 10.1029/2011JG001708. URL http://dx.doi.org/10.1029/2011JG001708.

G. Louis Smith, Anne C. Wilber, Shashi K. Gupta, and Paul W. Stackhouse. Surface Radiation Budget and Climate Classification. *Journal of Climate*, 15(10):1175–1188, May 2002. ISSN 0894-8755. doi: 10.1175/1520-0442(2002)015¡1175:SRBACC¿2.0.CO;2. URL http://dx.doi.org/10.1175/1520-0442(2002)015<1175:SRBACC>2.0.CO;2.

G.L. Smith, K.J. Priestley, N.G. Loeb, B.A. Wielicki, T.P. Charlock, P. Minnis, D.R. Doelling, and D.A. Rutan. Clouds and Earth Radiant Energy System (CERES), a review: Past, present and future. *Advances in Space Research*, 48 (2):254–263, July 2011. ISSN 0273-1177. doi: 10.1016/j.asr.2011.03.009. URL http://www.sciencedirect.com/science/article/pii/S0273117711001700.

Nicholas G Smith and Jeffrey S Dukes. Plant respiration and photosynthesis in global-scale models: incorporating acclimation to temperature and CO2. *Global Change Biology*, 19 (1):45–63, January 2013. ISSN 1365-2486. doi: 10.1111/j.1365-2486.2012.02797.x. URL http://dx.doi.org/10.1111/j.1365-2486.2012.02797.x.

Nicholas G. Smith, Danica Lombardozzi, Ahmed Tawfik, Gordon Bonan, and Jeffrey S. Dukes. Biophysical consequences of photosynthetic temperature acclimation for climate. *Journal of Advances in Modeling Earth Systems*, 9(1):536–547, March 2017. ISSN 1942-2466. doi: 10.1002/2016MS000732. URL http://dx.doi.org/10.1002/2016MS000732.

R Solano, K Didan, A Jacobson, and A Huete. MODIS vegetation indices (MOD13) C5 users guide. *Versin*, 2:2010, 2010.

Douglas G Sprugel, Michael G Ryan, JR Brooks, KA Vogt, and Timothy A Martin. Respiration from the organ level to the stand. *Resource physiology of conifers*, pages 255–299, 1995.

Y. Sun, C. Frankenberg, J. D. Wood, D. S. Schimel, M. Jung, L. Guanter, D. T. Drewry, M. Verma, A. Porcar-Castell, T. J. Griffis, L. Gu, T. S. Magney, P. Khler, B. Evans, and K. Yuen. OCO-2 advances photosynthesis observation from space via solar-induced chlorophyll fluorescence. *Science*, 358(6360), October 2017. doi: 10.1126/science.aam5747. URL http://science.sciencemag.org/content/358/6360/eaam5747.abstract.

Abigail L. S. Swann, Inez Y. Fung, and John C. H. Chiang. Mid-latitude afforestation shifts general circulation and tropical precipitation. *Proceedings of the National Academy of Sciences*, 109(3):712–716, January 2012. doi: 10.1073/pnas.1116706108. URL http://www.pnas.org/content/109/3/712.abstract.

Abigail L. S. Swann, Forrest M. Hoffman, Charles D. Koven, and James T. Randerson. Plant responses to increasing CO2 reduce estimates of climate impacts on drought severity. *Proceedings of the National Academy of Sciences*,

113(36):10019–10024, September 2016. doi: 10.1073/pnas.1604581113. URL http://www.pnas.org/content/113/36/10019.abstract.

Matias Takala, Kari Luojus, Jouni Pulliainen, Chris Derksen, Juha Lemmetyinen, Juha-Petri Krn, Jarkko Koskinen, and Bojan Bojkov. Estimating northern hemisphere snow water equivalent for climate research through assimilation of space-borne radiometer data and ground-based measurements. *Remote Sensing of Environment*, 115(12): 3517–3529, December 2011. ISSN 0034-4257. doi: 10.1016/j.rse.2011.08.014. URL http://www.sciencedirect.com/science/article/pii/S0034425711003166.

Karl E. Taylor, Ronald J. Stouffer, and Gerald A. Meehl. An Overview of CMIP5 and the Experiment Design. *Bulletin of the American Meteorological Society*, 93(4): 485–498, October 2011. ISSN 0003-0007. doi: 10.1175/BAMS-D-11-00094.1. URL http://dx.doi.org/10.1175/BAMS-D-11-00094.1.

R. J. van der Ent and H. H. G. Savenije. Length and time scales of atmospheric moisture recycling. *Atmos. Chem. Phys.*, 11(5):1853–1863, March 2011. ISSN 1680-7324. doi: 10.5194/acp-11-1853-2011. URL https://www.atmos-chem-phys.net/11/1853/2011/.

Rudi J. van der Ent, Hubert H. G. Savenije, Bettina Schaefli, and Susan C. Steele-Dunne. Origin and fate of atmospheric moisture over continents. *Water Resources Research*, 46: W09525, September 2010.

DL Verseghy, NA McFarlane, and M Lazare. CLASSA Canadian land surface scheme for GCMs, II. Vegetation model and coupled runs. *International Journal of Climatology*, 13 (4):347–370, 1993. ISSN 1097-0088.

Xuhui Wang, Shilong Piao, Philippe Ciais, Pierre Friedlingstein, Ranga B. Myneni, Peter Cox, Martin Heimann, John Miller, Shushi Peng, Tao Wang, Hui Yang, and Anping Chen. A two-fold increase of carbon cycle sensitivity to tropical temperature

variations. *Nature*, advance online publication, January 2014. ISSN 1476-4687. URL http://dx.doi.org/10.1038/nature12915.

S Watanabe, T Hajima, K Sudo, T Nagashima, T Takemura, H Okajima, T Nozawa, H Kawase, M Abe, and T Yokohata. MIROC-ESM: model description and basic results of CMIP5-20c3m experiments. *Geoscientific Model Development Discussions*, 4(2): 1063–1128, 2011. ISSN 1991-9611.

Danielle A. Way and Wataru Yamori. Thermal acclimation of photosynthesis: on the importance of adjusting our definitions and accounting for thermal acclimation of respiration. *Photosynthesis Research*, 119(1):89–100, February 2014. ISSN 1573-5079. doi: 10.1007/s11120-013-9873-7. URL https://doi.org/10.1007/s11120-013-9873-7.

Robert H Whittaker. Classification of natural communities. *The Botanical Review*, 28(1): 1–239, 1962. ISSN 0006-8101.

Robert Harding Whittaker. Communities and ecosystems. *Communities and ecosystems.*, 1970.

D.S. Wilks. The stippling shows statistically significant gridpoints: How Research Results are Routinely Overstated and Over-interpreted, and What to Do About It. *Bulletin of the American Meteorological Society*, 2016. ISSN 0003-0007. doi: 10.1175/BAMS-D-15-00267.1. URL http://dx.doi.org/10.1175/BAMS-D-15-00267.1.

John W. Williams, Stephen T. Jackson, and John E. Kutzbacht. Projected distributions of novel and disappearing climates by 2100 AD. *Proceedings of the National Academy of Sciences of the United States of America*, 104(14):5738–5742, April 2007.

Donghai Wu, Xiang Zhao, Shunlin Liang, Tao Zhou, Kaicheng Huang, Bijian Tang, and Wenqian Zhao. Time-lag effects of global vegetation responses to climate change. *Global Change Biology*, 21(9):3520–3531, September 2015. ISSN 1365-2486. doi: 10.1111/gcb.12945. URL http://dx.doi.org/10.1111/gcb.12945.

Tongwen Wu, Weiping Li, Jinjun Ji, Xiaoge Xin, Laurent Li, Zaizhi Wang, Yanwu Zhang, Jianglong Li, Fang Zhang, and Min Wei. Global carbon budgets simulated by the Beijing Climate Center Climate System Model for the last century. *Journal of Geophysical Research: Atmospheres*, 118(10):4326–4347, 2013. ISSN 2169-8996.

Jingfeng Xiao, Qianlai Zhuang, Beverly E. Law, Dennis D. Baldocchi, Jiquan Chen, Andrew D. Richardson, Jerry M. Melillo, Kenneth J. Davis, David Y. Hollinger, Sonia Wharton, Ram Oren, Asko Noormets, Marc L. Fischer, Shashi B. Verma, David R. Cook, Ge Sun, Steve McNulty, Steven C. Wofsy, Paul V. Bolstad, Sean P. Burns, Peter S. Curtis, Bert G. Drake, Matthias Falk, David R. Foster, Lianhong Gu, Julian L. Hadley, Gabriel G. Katul, Marcy Litvak, Siyan Ma, Timothy A. Martin, Roser Matamala, Tilden P. Meyers, Russell K. Monson, J. William Munger, Walter C. Oechel, U. Kyaw Tha Paw, Hans Peter Schmid, Russell L. Scott, Gregory Starr, Andrew E. Suyker, and Margaret S. Torn. Assessing net ecosystem carbon exchange of U.S. terrestrial ecosystems by integrating eddy covariance flux measurements and satellite observations. *Agricultural and Forest Meteorology*, 151(1):60–69, January 2011. ISSN 0168-1923. doi: 10.1016/j.agrformet.2010.09.002. URL `http://www.sciencedirect.com/science/article/pii/S0168192310002479`.

Zhiqiang Xiao, Shunlin Liang, Jindi Wang, Ping Chen, Xuejun Yin, Liqiang Zhang, and Jinling Song. Use of general regression neural networks for generating the GLASS leaf area index product from time-series MODIS surface reflectance. *Geoscience and Remote Sensing, IEEE Transactions on*, 52(1):209–223, 2014. ISSN 0196-2892.

Guang Xu, Huifang Zhang, Baozhang Chen, Hairong Zhang, John L Innes, Guangyu Wang, Jianwu Yan, Yonghong Zheng, Zaichun Zhu, and Ranga B Myneni. Changes in Vegetation Growth Dynamics and Relations with Climate over Chinas Landmass from 1982 to 2011. *Remote Sensing*, 6(4):3263–3283, 2014.

Wataru Yamori, Kouki Hikosaka, and Danielle A. Way. Temperature response of photosynthesis in C3, C4, and CAM plants: temperature acclimation and temperature adap-

tation. *Photosynthesis Research*, 119(1):101–117, February 2014. ISSN 1573-5079. doi: 10.1007/s11120-013-9874-6. URL https://doi.org/10.1007/s11120-013-9874-6.

Miao Yu, Guiling Wang, and Haishan Chen. Quantifying the impacts of land surface schemes and dynamic vegetation on the model dependency of projected changes in surface energy and water budgets. *Journal of Advances in Modeling Earth Systems*, 8(1):370–386, March 2016. ISSN 1942-2466. doi: 10.1002/2015MS000492. URL http://dx.doi.org/10.1002/2015MS000492.

Taiping Zhang, Paul W Stackhouse, Shashi K Gupta, Stephen J Cox, J Colleen Mikovitz, and Laura M Hinkelman. The validation of the GEWEX SRB surface shortwave flux data products using BSRN measurements: A systematic quality control, production and application approach. *Journal of Quantitative Spectroscopy and Radiative Transfer*, 122: 127–140, 2013. ISSN 0022-4073.

L. Zhou, R. K. Kaufmann, Y. Tian, R. B. Myneni, and C. J. Tucker. Relation between interannual variations in satellite measures of northern forest greenness and climate between 1982 and 1999. *Journal of Geophysical Research: Atmospheres*, 108 (D1):4004, January 2003. ISSN 2156-2202. doi: 10.1029/2002JD002510. URL http://dx.doi.org/10.1029/2002JD002510.

Liming Zhou, Compton J. Tucker, Robert K. Kaufmann, Daniel Slayback, Nikolay V. Shabanov, and Ranga B. Myneni. Variations in northern vegetation activity inferred from satellite data of vegetation index during 1981 to 1999. *Journal of Geophysical Research: Atmospheres*, 106(D17):20069–20083, September 2001. ISSN 2156-2202. doi: 10.1029/2000JD000115. URL http://dx.doi.org/10.1029/2000JD000115.

Zaichun Zhu, Jian Bi, Yaozhong Pan, Sangram Ganguly, Alessandro Anav, Liang Xu, Arindam Samanta, Shilong Piao, Ramakrishna R Nemani, and Ranga B Myneni. Global data sets of vegetation leaf area index (LAI) 3g and Fraction of Photosynthetically Active Radiation (FPAR) 3g derived from Global Inventory Modeling and Mapping Studies

(GIMMS) Normalized Difference Vegetation Index (NDVI3g) for the period 1981 to 2011. *Remote Sensing*, 5(2):927–948, 2013.

Zaichun Zhu, Shilong Piao, Ranga B. Myneni, Mengtian Huang, Zhenzhong Zeng, Josep G. Canadell, Philippe Ciais, Stephen Sitch, Pierre Friedlingstein, Almut Arneth, Chunxiang Cao, Lei Cheng, Etsushi Kato, Charles Koven, Yue Li, Xu Lian, Yongwen Liu, Ronggao Liu, Jiafu Mao, Yaozhong Pan, Shushi Peng, Josep Penuelas, Benjamin Poulter, Thomas A. M. Pugh, Benjamin D. Stocker, Nicolas Viovy, Xuhui Wang, Yingping Wang, Zhiqiang Xiao, Hui Yang, Sonke Zaehle, and Ning Zeng. Greening of the Earth and its drivers. *Nature Clim. Change*, advance online publication, April 2016. ISSN 1758-6798. URL `http://dx.doi.org/10.1038/nclimate3004`.

[A]

Appendix A

UNCERTAINTY ANALYSIS IN LINEAR REGRESSION, BINNING AND DATASETS

To establish the uncertainty and robustness of the analysis of ecological climate interaction across climate space we performed four experiments: a monte-carlo bootstrap uncertainty estimate (Section A.0.1), an experiment using the shorter time series available from MODIS NDVI (Section A.0.2), an experiment with the CRU TS3.21 dataset representing statistically upscaled station observations of the environment (Section A.0.3), and an experiment omitting grid points with strong interannual correlation between precipitation and temperature (Section A.0.4) (Figures 2.4 and A1). Results generally show low uncertainty in the sign of β outside of the transition area and the hot-wet region, and they are qualitatively consistent using MODIS NDVI and CRU TS3.21 in place of NDVI3g and the combination of ERA-Interim and GPCP, as well as when points of high correlation are omitted. Methodology and specific differences are discussed below.

A.0.1 Estimating Uncertainty of β in Time and Climate Space

To estimate the uncertainty in the regression coefficient values (β), we used a Boot-Strap Monte Carlo technique, similar to Method 2 discussed in Efron, 1979, was used in combination with the regression at each grid point [Efron, 1979] (Figure 2.1). We performed 10,000 regressions by randomly drawing 8-year time series from the total 16-year dataset. The mean of these 10,000 β values is reported as the sensitivity of vegetation (Figure 2.3). The resulting distributions of sensitivity are combined with the uncertainties from the bins to determine 95% bounds on the uncertainty (Figure 2.4).

To aggregate patterns of the β across climate space, each geospatial point was assigned

a bin dictated by its climatological mean annual temperature and precipitation. There are 178 bins, each 1.8 °C by 186.5 mm/year, bins with less than 10 points were ignored (Figure 2.2, Figure 2.1A and 2.1B). We include all 10,000 vegetation sensitivities calculated as part of the temporal Monte Carlo for all spatial points falling in a given bin. We do a further Monte Carlo sampling of this set by selecting randomly from the 10,000 point temporal distribution of β for half of the spatial points in each bin. From this selection we calculate an area-weighted mean for that bin 10,000 times resulting in a distribution of bin-mean β. The area-weighted mean of the distribution of β within a bin is then reported as the β for that bin and the range is used to determine the 95% bounds as the error bars (Figure 2.4).

The uncertainty analysis includes the contributions of both the uncertainty in the regression (i.e. the consistency of the ecological climate interaction across time) and the uncertainty in each bin (i.e. the consistency in the ecological climate interaction in any particular climate bin). The uncertainty in sign for β_{TEMP} is strongest in the hot-wet climates and along the sloping transitions from positive β_{TEMP} to negative β_{TEMP}. In comparison, the uncertainty in β_{PRECIP} also shows the sloping transition line and is particularly low for climate regions below precipitation values of 1500 mm/year. Again, the hot-wet climate regions are particularly uncertain. The aggregated patterns of uncertainty show similar patterns to those of the mean β values, suggesting that the consistency of β generally follows the strength of β. This uncertainty appears to be a function of climate as well. The differences in the analysis due to using different vegetation indices and environmental datasets also primarily occur in regions where the temporal and binning uncertainty are highest. This correlation is to be expected if the patterns of the analysis done with different datasets are approximately the same as the original analysis, as the sign and amplitude is more likely to change where the analysis was uncertain in the first place.

A.0.2 Analysis with MODIS NDVI

As noted above there are multiple other remotely sensed vegetation indices, as well as multiple corrections to the NDVI vegetation index [Hilker et al., 2014, Solano et al., 2010, Holben,

1986]. To test the robustness of the observed patterns to our choice in NDVI product, we compared the newer MODIS NDVI observations which are available from (2003 - 2015) with the overlapping portion (2003 - 2011) of NDVI3g with complete years. Qualitatively these analyses are very similar to those of the original analysis using NDVI3g from 1997 - 2012 (Figure A1 final two columns). Hot-dry climates have negative β_{TEMP} and positive β_{PRECIP} (greening when cooler and wetter), the cold regions show positive β_{TEMP} and negative β_{PRECIP} (greening when warmer and drier), there is evidence of the sloped optimums ($\beta = 0$) and the hot-wet climates show a mix of both β_{TEMP} and β_{PRECIP}, but are predominantly greener when warmer and drier. We observe a few notable differences. Firstly, the MODIS NDVI results have generally stronger sensitivities (Figure A1B and A1E). This result follows from the observations that the seasonal cycle of MODIS NDVI is stronger than that of NDVI3g, which would lead us to expect that the interannual variation would also be stronger [Huete et al., 2002]. Secondly, the cold region shows many more points where there is a greening during wetter years (Figure A1B and A1E). However, the location of the change from generally negative β_{PRECIP} to positive β_{PRECIP} is preserved, particularly in drier climates. This is not entirely the case for β_{TEMP}, at lower rain levels there is a clear transition zone, but at the wetter/warmer end of this transition zone the region of greening when cooler has expanded. It is not completely unexpected that there would be instability in this region, as it is the least certain in our original analysis, and the 2003 - 2011 time window shows some encroachment of greener when cooler and wetter even in the shortened NDVI3g analysis (Figure 2.4A and 2.4B, Figure A1C, A1F, A1I, compares 2nd and 3rd columns).

A.0.3 Analysis with other Environmental Data

To ascertain the robustness of the analysis to choice of environmental data sets we used alternate environmental data from CRU TS3.21. We performed the regressions over the same time period 1997 - 2012 with CRU TS3.21 temperature and precipitation and NDVI3g vegetation index (Figure A1A, A1D, A1G). CRU TS3.21 was chosen because it uses a different method to derive global gridded datasets of temperature and precipitation. Rather than a

reanalysis product (such as ERA-Interim) or a combination of gauge and remote sensing observations (such as GPCP), CRU TS3.21 is a statistically upscaled gridded product based on station data. Station coverage is relatively dense over North America and Europe and particularly sparse over the tropical South America and Africa. Our results using CRU TS3.21 show that the analysis using a different environmental dataset is qualitatively similar and continues to support our results and discussion (Compare Figure 2.3A, Figure 2.3B, and Figure 2.5A with Figure A1A, A1D, A1G).

A.0.4 Temperature and Precipitation Correlation

The predictor variables of interannual temperature and precipitation used in the linear regression are often collinear in nature. Where there is particularly strong correlation, there is the possibility that a multilinear regression will not do a good job of separating the variation explained by each predictor variable. To address this concern we ran a test by omitting points from our analysis that have higher correlation coefficients (> 0.6 correlation). We find nearly no change to our analysis and no changes to our overall interpretation and discussion of the results. We determine that pixels with high correlations between temperature and precipitation do not appear to have undue influence on the aggregated pattern discussed in the manuscript.

Our omission of pixels with correlations above 0.6 (36% shared variance) is conservative per the statistical literature where it is suggested that correlation coefficients of up to 0.77 (60% shared variance) can be linearly separated and even some suggestion that values as high as a correlation coefficient of 0.89 (80% shared variance) are acceptable [Obrien, 2007]. Only a small portion of the global area analyzed exceeds a correlation coefficient between precipitation and temperature of 0.6.

A.0.5 Variability Across Aridity Datasets

Vegetation health and productivity is driven by a balance of the supply and demand of water in many environments. Aridity is a measurement of the dryness of an environment

that takes both the supply of water (Precipitation (P)) and the demand for water (Potential Evapotranspiration (PET)) into account. Potential Evapotranspiration can be calculated in a number of ways based on net radiation (Equation 2) [Budyko, 1961], empirical temperature based relationships (CRU TS3.21) and a more complete Penman-Monteith approach that treats the complete surface energy budget (MODIS PET, GLDAS PET) [Smith et al., 2011, Jones and Harris, 2013, Mu et al., 2007, Feng and Fu, 2013]. We investigated a number of observationaly-derived products of PET to use in combination with precipitation from GPCP to create an aridity index of P/PET. We found that the absolute values of aridity (P/PET) were highly variable, due to different estimates of PET, but that the slopes of the contours binned across precipitation and temperature were relatively stable (Figure A2A). From this we conclude that our comparisons of the slope of the optimal lines ($\beta = 0$) with contours of P/PET are robust, but that the actual values of P/PET at which changes in ecological-climate interaction change are unknown due to uncertain global estimates of PET (Figure 2.7). For our comparison we chose the simplest of the PET estimates that depends only on the net downward shortwave radiation [Budyko, 1961]. Using observations from CERES-SYN, we calculated PET in order to calculate P/PET to compare with β (Figure A2B) (Equation A.1).

$$PET = \frac{S_w}{L_v \rho_w} \tag{A.1}$$

PET is calculated as the amount of water that the energy available in the net downward shortwave radiation (S_w) could possibly evaporate by dividing it by the latent heat of vapor (L_v) and the density of water (ρ_w).

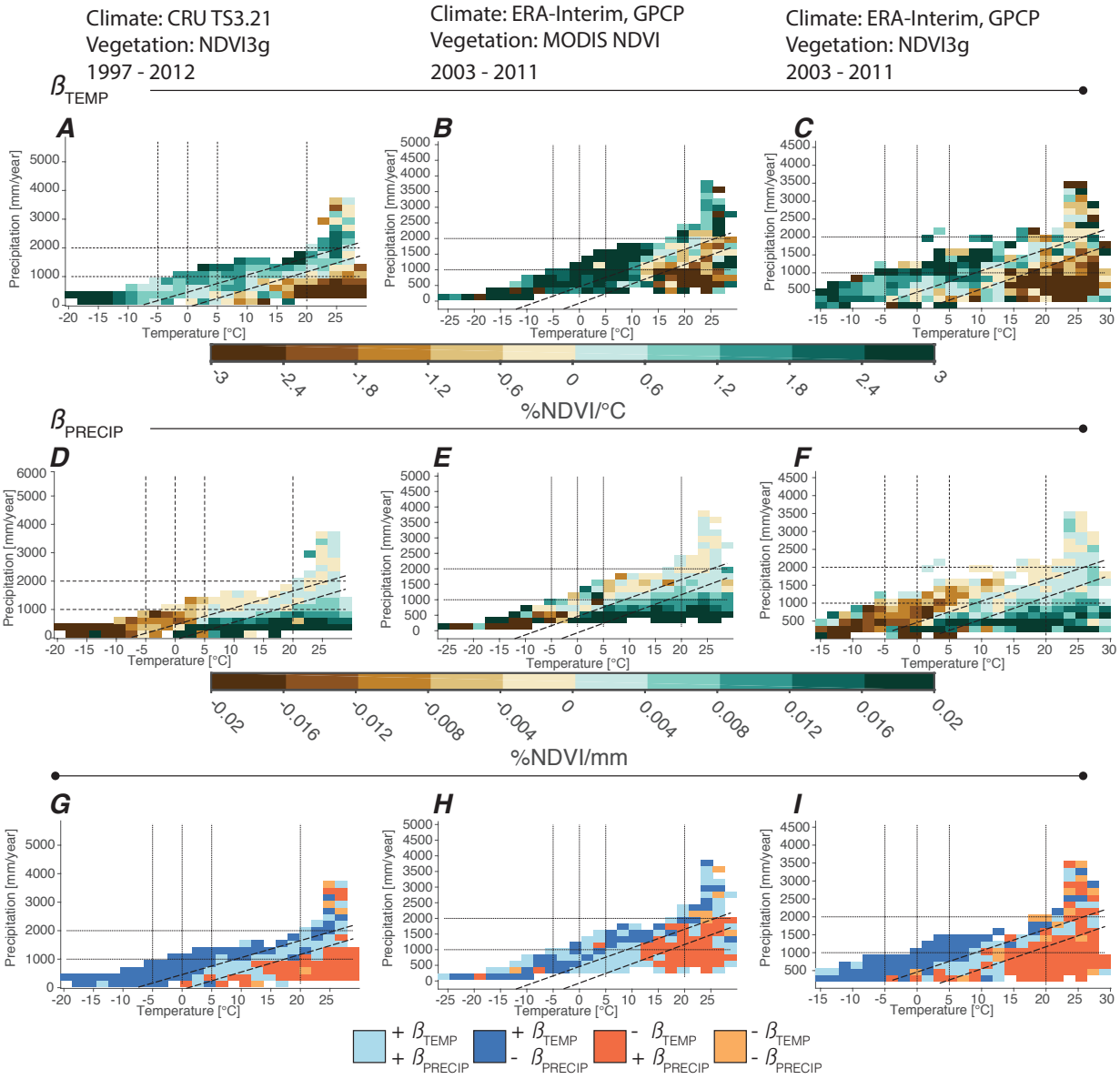

Figure A.1: Binned sensitivity of vegetation to annually averaged (Row 1**A, B, C**) temperature (β_{TEMP}), (Row 2, **D, E, F**) precipitation (β_{PRECIP}) calculated from robust regressions, and (Row 3, **G, H, I**) the combinations of the signs of the regression coefficients. Coloring as in Figure 2.3 and Figure 2.5. Columns represent the same analysis with either (Column 1: A,D,G) different environmental data (CRU TS3.21), (Column 2: B,E,H) different observations of NDVI (MODIS) over a different time period of 2003 - 2011, or (Column 3: C,F,I) the same data as the original but over the different time period of 2003 - 2011 as in column 2.

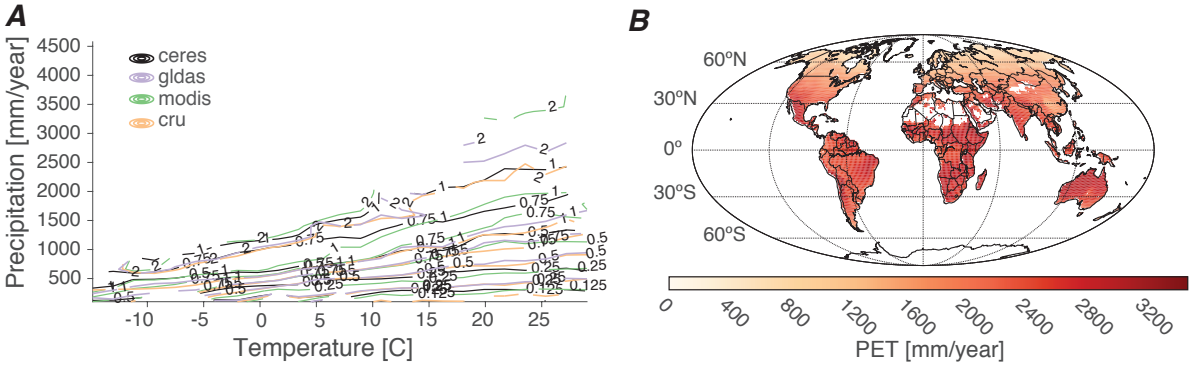

Figure A.2: **(A)** Contours of binned longterm means of multiple datasets of potential evapotranspiration. Binned values are contoured at values as in Holdridge Life Zones chart and displayed in temperature and precipitation climate space. **(B)** map of mean PET from 2001 - 2012 created from CERES-SYN net shortwave downward surface radiation. Colors are in mm/year of potential evapotranspiration.

VITA

Gregory Ross Quetin is originally from Santa Barbara, California where he attended elementary school and high school. Though from Santa Barbara, he has always had a special place in his heart for the Pacific Northwest where he spent most summers and ultimately attended college at the University of Washington studying Aeronautical and Astronautical Engineering. After college Gregory accepted a job as an engineer at the NASA Jet Propulsion Laboratory building instruments and participating in field campaigns ranging from hurricane research, to mapping of tropical forest, to research and development on astronomical telescopes. After graduate school at the University of Washington Gregory intends to continue is research regarding the carbon cycle and Earth's climate. Career aspirations include apply climate science to city design, becoming an astronaut, and being active in finding solutions for global warming.